



UNIVERSIDAD NACIONAL DE COLOMBIA

Reformulation of the Action and Phase Jump Method to Obtain Magnetic Errors in the LHC

Alba Carolina García Bonilla

Universidad Nacional de Colombia
Facultad de Ciencias, Departamento de Física
Bogotá D.C., Colombia
Año 2015

Reformulation of the Action and Phase Jump Method to Obtain Magnetic Errors in the LHC

Alba Carolina García Bonilla

Tesis presentada como requisito parcial para optar al título de:
Doctor en Ciencias - Física

Director:
(Ph.D.) Javier Fernando Cardona

Línea de Investigación:
Física de Haces de Partículas a Altas Energías
Grupo de Investigación:
Física de Aceleradores

Universidad Nacional de Colombia, Sede Bogotá.
Facultad de Ciencias, Departamento de Física
Bogotá, Colombia
Año 2015

To the tree that did not die

We said that the laws of nature
are approximate ...: how can the
results of an experiment be wrong?
Only by being inaccurate.

R. Feynman.
1918-1988

Acknowledgment

For the motivation to setting up this project through the fellowship *Beca a Estudiantes Sobresalientes de Posgrado*, I acknowledge *Vicerrectoria Académica* at *Universidad Nacional de Colombia*.

Three-fourths of the results in this dissertation are made possible thanks to the support of the Foundation, *Fundación Para la Promoción de la Investigación y la Tecnología* FPIT to whom I acknowledge.

The unknowns have also an important role for the development of this dissertation, thanks to them: To my parents for their support and for let me time to do this.

To the opportunity to change my eye-view about this dissertation by providing the flight tickets and the accommodation expenses through the program *Programa Nacional de Internacionalización del Conocimiento 2013-2015*, I acknowledge *Universidad Nacional de Colombia* and its dependencies involved in the *Sede Bogotá* campus.

Besides the support I mentioned, I am grateful for the *immaterial* part of this dissertation.

Most of the experimental points of view and the LHC simulator used during this dissertation is thanks to the people at CERN. Specially, I recognize their help during my stay at CERN. Thank you to R. Tomas and the OMC team presented from 04-17-2015 to 05-15-2015 at CERN.

And last but not least, I acknowledge the Director of this project, prof. JF Cardona at the *Universidad Nacional de Colombia*, for his patience and the topics developed in this project, and I acknowledge the Committee members who approved this dissertation on 04-29-2016.

Thanks a lot!

Abstract

In this dissertation a reformulation of the Action and Phase Jump Method (APJ) is presented using both simulated and experimental LHC orbits. The LHC is the accelerator able to create proton-proton collisions with the highest energy in a laboratory. The APJ is a technique to measure magnetic errors and the stated reformulation consists in to eliminate the central BPM measurement and to include the phase advances of the triplets' quadrupoles. New theoretical equations are introduced and a comparison with the previous formulation is developed. The results includes the design and study of digital filters to reduce noise. It is found that the new formulation is better in specific occasions and that the best filter is always a combination. For instance, σK_1 is reduced in experimental orbits from 7.41 to $2.48 \times 10^{-7} m^{-2}$ using the reformulation compared to the previous APJ. Those orbits are obtained using an AC Dipole and its effect is discussed. Also, a study of the alternative methods is presented and magnetic errors are obtained which are compared with APJ results.

Keywords: Beams in Particle Accelerators, charged-particle in accelerators, LHC, Beam optics (charged-particle beams), Circular Accelerators.

Resumen

Una reformulación del Método de Acción y Fase (APJ) es presentada, usando órbitas del LHC tanto simuladas como experimentales. El LHC es el acelerador construido en un laboratorio para alcanzar las más altas energías en colisiones protón-protón. APJ es una técnica para medir errores magnéticos y la reformulación consiste en eliminar la dependencia en la medición del BPM central y en incluir los avances de fase en los cuadrupolos. Se presentan las nuevas ecuaciones teóricas y una comparación con las anteriores. Los resultados incluyen el diseño y estudio de filtros digitales para reducir ruido. Se encuentra que la reformulación es mejor en ocasiones específicas, y que el mejor filtro es siempre una combinación. Por ejemplo, σK_1 disminuye en órbitas experimentales de 7.41 a $2.48 \times 10^{-7} m^{-2}$, usando la nueva formulación comparada con la anterior. Estas órbitas son obtenidas usando un dipolo AC y su efecto es discutido. También, un estudio de los métodos alternativos es presentado y errores magnéticos son obtenidos, los cuales son comparados con los resultados de APJ.

Palabras claves: Haces en Aceleradores de partículas, partículas cargadas en aceleradores, LHC, óptica del haz en aceleradores, Aceleradores circulares

Contents

Acknowledgment	vii
Abstract	ix
List of symbols	xii
1. Introduction	1
2. Statement of the Problem	4
3. Basic Concepts and the LHC	7
3.1. Description of the motion in a Storage Ring	7
3.2. Basic Accelerator Physics Concepts	11
3.3. The LHC or Large Hadron Collider	15
3.3.1. The LHC Triplets	17
4. The Action and Phase Jump Method (APJ) and AC Dipole Effect	20
4.1. Theoretical Description of the APJ	21
4.2. APJ in Accelerators	28
4.3. The AC Dipole Effect	31
5. Design of a Digital Filter to Reduce Noise in LHC Orbits	37
5.1. The Band-Pass Filter	37
5.2. Signal to Noise Ratio for the Band-Pass Filter	42
5.3. Different Ways to Reduce Noise in the Orbits by applying Digital Filters. . .	44
6. Reformulation of the APJ, and Orbits Analysis	47
6.1. Theoretical Equations Removing the Central BPM Dependency	47
6.2. Theoretical Equations Including Different Phase Advances at the Quadrupoles Triplets	53
6.3. Comparison Reformulation and Old Formulation using Ideal Orbits	57
6.4. Comparison Reformulation and Old Formulation using Noised Orbits	64
7. Methods used for Linear Corrections of Magnetic Errors in the LHC	73
7.1. Resonance Driving Terms Method	73

7.2. Segment-by-Segment Method	80
7.2.1. Results using SBS and RDT with Simulated Orbits	81
8. Analysis of Experimental LHC Orbits	86
8.1. Comparison New and Old APJ Formulation with 2010's Orbits	86
8.2. Magnetic Error Measurements using APJ with 2015's Orbits	92
8.3. Magnetic Error Measurements using SbS with 2015's Orbits	102
8.4. Summary of Results from the Different Methods with 2015's Orbits	106
9. Conclusion and Future Direction	116
9.1. Conclusions	116
9.2. Future Direction	118
A. The Best A1,B1,B1 Combination	120
B. APJ on Uniform Noised Orbits	125
B.1. Best Combinations of Filters for the Simulation with Uniform Noise.	130
References	139

List of symbols

This section contains the main Symbols and Abbreviations used during this dissertation.

Symbols in Latin Letters

Symbol	Name/Definition	SI Units
s	Longitudinal component of the particle position	m
x	Horizontal component of the particle position	m
y	Vertical component of the particle position	m
K_{1s}	Skew magnetic multipolar component for quadrupoles	m^{-2}
A_1	Skew magnetic multipolar component for quadrupoles	m^{-2}
A_1	Skew Magnetic Error or Gradient Error	m^{-2}
K_1	Normal multipolar component for quadrupoles	m^{-2}
B_1	Normal multipolar component for quadrupoles	m^{-2}
B_1	Normal quadrupole Error or Gradient Error	m^{-2}
A_1, B_1, B_1	Magnetic Error Combination of two Normal and one Skew errors	

Symbols in Greek Letters

Symbol	Name/Definition	SI Units
β	One of the Courant-Snyder Parameters	m
β^*	β -function at the collision point	m
$\frac{\Delta\beta}{\beta}$	Beta-Beating	

Abbreviations/Acronyms

Abbreviation/Acronym	Meaning
APJ	Action and Phase Jump Method
APJ	Action and Phase Method
APJ	Action and Phase
IP	Interaction Point for the particle collision
IR	Insertion Region
LHC	Large Hadron Collider
New	Results obtained using the Reformulation
Old	Results obtained using the previous APJ formulation
RDT	Resonance Driving Terms Method
SBS	Segment-by-Segment Method
SbS	Segment-by-Segment Method and CERN software
w/o	without
sim.	LHC Simulation (ideal orbits)
noi.	LHC Simulation and noise (random number) included

1. Introduction

To study the basic components of the matter, accelerators like the LHC are constructed. The basic components of the matter which constitute all the things we see every day includes people, plants, rocks and animals. In fact a proton is one of the particles that all such things have in common and its mass is less than 1.7×10^{-27} Kg. In particular in the LHC, to understand the interaction between the basic components of the matter, collisions between protons at high energy are carried out every 25×10^{-9} s. Those protons are kept in the circular ring of the LHC using magnetic fields from more than a thousand magnets.

To fulfill a collision point as accurately as possible, one of the goals during the LHC commissioning is to reduce the magnetic errors. This is because the magnetic devices cannot be built to have only one component in a plane without disturbing other planes, especially at the edges, therefore there are always more components presented than the expected ones. Also, during the installation and working processes of the magnets, a couple of problems could be presented: fabrication defects on their materials and a deviation from their design position along the ring. These situations cause a beam quality loss or a large uncertainty in the measurement of the particles position and hence in the determination of the collision point.

The magnetic errors are found according to the multipolar expansion of the magnetic field, and one of the biggest contributions comes from linear components. Hence, one of the major problems when doing the commissioning of an accelerator is to identify and correct the linear components of the magnetic errors.

One of the methods used to localize, to measure, and to correct magnetic errors is the Action and Phase Jump (APJ) Method Analysis. It is based on the theoretical principle of preservation of the Action and Phase variables in absence of a magnetic error. This method had been successfully tested in RHIC using closed-orbit data from experiments [1] and its theoretical development is fully presented in [2]. The corrections are made locally and specially at the Interaction Regions (IR) of an accelerator.

Preliminary analyses on turn-by-turn (TBT) orbits at the LHC show promising results ([3] and [4]), although one of the initial difficulties to apply the Action and Phase Jump (APJ) analysis to LHC orbits was the high level of noise present in the BPM measurements. The

noise is due to the wide bandwidth of the LHC BPMs and the availability of only one *bunch* to perform the optical measurements. On the other hand, the unprecedented number of turns for LHC allows us to use all sort of filters.

This dissertation have the aim of reformulating the Action and Phase Jump (APJ) Method in order to obtain and estimate the magnetic errors presented at the LHC or *Large Hadron Collider*. The specific purposes are:

1. To reformulate the APJ method in order to dismiss (i.e. eliminate) the BPM dependency presented at the insertion region of the LHC.
2. To study the effect on the magnetic error estimation using turn-by-turn data orbits generated by an AC Dipole. This study is from the both points of view, the simulations and the experiments. Optionally, to compare the magnetic errors estimation using closed orbits and turn-by-turn data.
3. To reformulate the APJ method to include the possibility of having different phase advances at the quadrupoles triplets.
4. To explore the possible ways to reduce the noise of the orbit data presented at the LHC by testing digital filters.
5. To study the alternative methods to estimate the magnetic errors at the LHC.

In this document, the most relevant results for each purpose are presented. Their corresponding development are in several parts along this dissertation, but their main discussions are in the Chapters or Sections 6.1, 4.3, 6.2, 5 and 7, respectively.

Additionally, some theoretical developments for the APJ is presented in the first part of this dissertation in Section 4.1 and the results obtained when analyzing experimental data are presented in Chapter 8. The previous concepts for the understanding of this dissertation are briefly explained in Chapter 3, including some aspects of the LHC.

The procedure followed to achieve the goals were in general: to obtain the theoretical equations of the reformulation, and then use the LHC simulator in MAD-x [5] to implement the corresponding simulations to corroborate the relations obtained from the theory. After the validation of the calculations, to use the APJ software to analyze the data from LHC experiments. Also, to use the software developed in the LHC for the Linear Corrections to estimate magnetic errors using the same orbits that the APJ, for comparison.

In this way, along this dissertation, the above listed factors are investigated to establish their influence in the uncertainty of the measurements when analyzing the LHC data. Also,

when comparing the results with the measurements given by the other techniques directly used in the LHC, a more confidence in the corrections obtained is reached. Even further, this investigation of the magnetic errors once the corresponding corrections are performed at the accelerator, in this case the LHC, implies that the set of specific parameters which are imposed during the creation of the accelerator, called design parameters, are closer to the actual measured parameters, and a major control of the beams is achieved.

2. Statement of the Problem

In Physics one of the biggest questions to answer is how the elementary particles interact to build all the things we see, including ourselves, rocks, plants and animals. Even more, this basic question leads us to prove and to study theories about the origin of the universe.

To answer those questions the first instants of the universe are recreated all over again and again inside a machine called accelerator. A huge number of repetitions is necessary to acquire enough statistics to account as many different outcomes as possible. Although many outcomes are expected, all of them are taken from the same initial conditions.

Those initial conditions are controlled in the accelerator, and among others these are: the luminosity of the beam, the beam-size, the expected collision point, the beam stability.

For instance, as presented by the CERN news on 2011, the Luminosity¹ measurement of the LHC is reaching the value it is expected to have by the date, an integrated luminosity larger than 1 fb^{-12} [7] (The reported Integrated Luminosity up to July/2011 is, at ATLAS 2522 pb^{-1} , at CMS 2438 pb^{-1} , at LHCb 732 pb^{-1} and at ALICE 3.8 pb^{-1} [8]). Nevertheless, this is less than the 2% of the expected Luminosity of the machine for an ultimate proton-proton collision run, which is 131 fb^{-1} [9]; so the question is how the luminosity is increasing by the time.

Picking up some numbers, it is expected to have 2808 bunches, of 1.7×10^{11} particles each, spacing by 25 ns, in order to obtain a luminosity is $2.3 \times 10^{34} \text{ cm}^{-2} \text{ s}^{-1}$ at ATLAS and CMS (with a configuration of $\beta^* = 0.5 \text{ m}$ at the collision point) [10] and by May 2011, there were 1092 bunches for a peak luminosity reached of $1.25 \times 10^{33} \text{ cm}^{-2} \text{ s}^{-1}$ [7]. One can state that by increasing the number of bunches from 1092 to 2808, it would be enough to increase the luminosity. Probably it is correct; the problem is that having more particles inside the accelerator without having the control of the beam is dangerous for the machine. ³.

¹The Luminosity is a measure of the probability to obtain particle encounters in a head on collision of two beams [6]

²One inverse femto barn equates to around 70×10^{12} collisions

³For a nominal bunch intensity and 25 bunches in the LHC the energy stored per beam is 1 MJ. This energy could produce a serious damage outside the beam pipe, since only 1 MJ of energy is enough to melt 2 Kg of copper [11], the material used (a $75 \mu\text{m}$ layer of Cooper [12]) to reduce the amount of reflected photons from the expected collisions.

From a beam optics point of view, the machine is designed to reach their maximum luminosity (approx. $10^{34} \text{ cm}^{-2}\text{s}^{-1}$) under specific design parameters. Failure of having the actual parameters close to the designed ones implies, among others, that the expected luminosity values are not going to be reached.

Therefore it is necessary not only to measure the actual parameters but also to be able to arrange the beam to be close to its designed characteristics. By estimating the location and the value of the magnetic errors, an arrangement to the beam properties close to the design values, can be done.

This dissertation is related with the *puesta a punto* or *fine tuning* of the beam at the LHC, by using the Action and Phase Jump Method to measure the linear magnetic errors. The hypothesis of this dissertation is that the uncertainty of the magnetic errors measurement can be improved, by exploring the below facts.

Although the APJ method is already a successful technique, there are factors that need to be reviewed to establish a decrease in the uncertainty of the magnetic errors measurements.

When the APJ method is used to estimate the magnetic errors in a storage ring, it is mandatory to use the trajectory information obtained by many BPMs located at both sides outside the interaction region (IR⁴) and an only one BPM inside the region. Therefore, it is clear that the uncertainty on the magnetic error is strongly affected by the single measurement at the IR. Hence it is needed to study what happen with the magnetic error if the dependency on the BPM located at the interaction region is removed.

Also, in the LHC the turn-by-turn data taking by the BPMs is obtained after the use of an AC Dipole to generate the oscillations [13]. Up to the beginning of this dissertation the tested simulations using the APJ method were used closed orbit and single orbit using a kicker or a dipole corrector to generate the oscillations. Therefore it is necessary to simulate the process with the new settings, this is, to generate the oscillations on the beam trajectory using an AC Dipole or taking it into account, to collect the turn-by-turn data and then take the average of selected orbits to obtain a single orbit in order to apply the method. An important part of this process is the selection of the orbits. The question to answer here is, which is the actual effect of the AC Dipole on the orbits? Using the AC Dipole to generate the orbits is more or less precise to calculate the magnetic errors in LHC using the APJ method.

On the other hand, a main component of the interaction region is the triplets, which are

⁴IR stands for Insertion region in the LHC, but it also corresponds to the interaction region, in this document interaction and insertion regions are consider synonyms

used to decrease the beam size. The β -functions are usually large there, therefore the phase advance difference is almost null along the quadrupoles belonged to the triplets. The APJ method was derive assuming that those quadrupoles have the same phase advance (Appendix B [14]) but in the LHC there are configurations where this assumption is not always valid. The question that arise to answer is how the inclusion of the quadrupole phase advances affects the calculation of the magnetic error.

The APJ method had been successfully tested using experimental data for a single orbit measurements. Unfortunately in the LHC the single orbit data is characterized for having a lot noise, refer to [4] or [3]. The causes of the noise in the LHC are attributed to BPMs bandwidth (compare with the RHIC BPMs where the APJ method was successfully tested, the bandwidth of the LHC BPMs is larger) and to the fact that in the development of this dissertation the optics measurements are made with a single bunch of particles in the beam. Therefore, it is desirable to try a digital filter on the beam position measurements in order to decrease the noise of the signals keeping the appropriate magnetic error measurements.

Moreover, it is always desirable to compare the results using alternative methods. Therefore it is necessary to include in the analysis for this dissertation a comparative study with the available beam-based methods at LHC, for the same type of discussed magnetic errors, the linear magnetic errors.

3. Basic Concepts and the LHC

Before start discussing in this dissertation how the measurements or the estimation of the magnetic errors are made in accelerators like the LHC, this chapter introduces the concepts and definitions that are pertinent to clarify first. Also, a brief description of the LHC is included.

3.1. Description of the motion in a Storage Ring

The devices used in accelerators produce electric fields as well as magnetic fields, all of them having a free charge region close to the apparatus axis ($\rho_{free} = 0$). The design of these devices is in a way that the beam can cross them freely and during a time which the fields are time independent ($\frac{\partial \vec{E}}{\partial t} = 0$ and $\frac{\partial \vec{B}}{\partial t} = 0$). During the particles journey, the beam-pipe is under vacuum and the current produced by the charges (in the beam) are comparative small and do not affect the fields around them [15].

In particular for a storage ring, the particle is kept at a fixed energy and its acceleration process is considered complete. This is the case as well for the LHC configuration when the optical measurements to obtain the magnetic errors are performed. Therefore, in the Maxwell equations, the assumptions are $\vec{J} = 0$, $\vec{E}_{ind} = 0$ and $\vec{B}_{ind} = 0$, and the simple representation obtained is:

$$\begin{aligned}\nabla \times \vec{E} &= 0 & \nabla \cdot \vec{E} &= 0 \\ \nabla \times \vec{B} &= 0 & \nabla \cdot \vec{B} &= 0\end{aligned}\tag{3-1}$$

The mathematical ways to express the fields that follow that type of equations are:

$$\begin{aligned}\vec{E} &= -\nabla\Phi \\ \vec{B} &= -\nabla V\end{aligned}\tag{3-2}$$

where Φ and V are scalar functions. And, in this case, there is a symmetry in the equations and there is not a mathematical difference in which field is choosed to solve the equations. Depending on the accelerator sector in which the particle is traveling, i.e. the particle position along the accelerator, their motion will be determinated by the electric or the magnetic field.

In the case of the magnetic errors measurements, the interested theory is when the particle is travelling under the influence of just the magnetic field presented. Therefore, the mathematical equation to solve is a kind of the Laplace equation but for a magnetic potential. Using the fact that the beam travels in a cylindrical tube, it is convenient to express the space in cylindrical coordinates. If the longitudinal axis in the cylindrical coordinates is written as s instead of z :

$$\begin{aligned} \nabla^2 V &= 0 \\ \frac{\partial^2 V}{\partial r^2} + \frac{1}{r} \frac{\partial V}{\partial r} + \frac{1}{r^2} \frac{\partial^2 V}{\partial \phi^2} + \frac{\partial^2 V}{\partial s^2} &= 0 \end{aligned} \quad (3-3)$$

where s represents the axis of the direction of motion along the accelerator while x and y are the transverse coordinates.

The ansatz for this differential equation is [16]:

$$V(r, \phi, s) = -\frac{p}{e} \sum_{n>0} \frac{1}{n!} A_n(s) r^n e^{in\phi} = -\frac{p}{e} \sum_{n>0} \frac{1}{n!} A_n(s) (x + iy)^n \quad (3-4)$$

where the expression at the right corresponds to the ansatz when it is written in Cartesian coordinates x and y , where n is the multipolar index and A_n is the corresponding coefficient which in general is a number that depends also on the longitudinal position. The factor $p/e = B\rho$ is called the beam rigidity and is the ratio between the momentum and the electric charge of the beam.

After replacing this solution in the Laplace equation it is obtain that the ansatz is valid for each order n separately (not only the sum is solution of the equation). This scalar function is related with the Hamiltonian of the motion and after all with the dynamics of a particle in the storage ring.

For a particle, or in general for a beam, the Hamiltonian of the motion is usually expressed in terms of the phase-space coordinates; this allows to exploit the analysis of linear and nonlinear betatron motion, using the fact that the motion is periodic [6]. The relation is [17]:

$$\mathcal{H}(x, p_x, y, p_y; s) = \frac{e}{p_0} \frac{p_x^2 + p_y^2}{2} + \frac{1}{\rho^2} \frac{x^2}{2} + k_1 \left(-\frac{x^2}{2} + \frac{y^2}{2} \right) - \Re \left\{ \sum_{n=3}^{\infty} \frac{1}{n!} (b_n + ia_n) (x + iy)^n \right\} \quad (3-5)$$

where $p_x = dx/ds$ and $p_y = dy/ds$ are the transverse momentum components in the phase space, for a beam of total momentum p_0 , ρ is the curvature radius, x and y are the transverse

coordinates, k_1 is a quadrupole gradient, b_n and a_n are the normal and skew component of the magnetic field as related with A_n as stated in the following paragraphs. The variables depend on the longitudinal position s , these are: $p_x = p_x(s)$, $p_y = p_y(s)$, $x = x(s)$, $y = y(s)$, $\rho = \rho(s)$, $k_1 = k_1(s)$.

Theoretical Description of the Magnets

As mentioned above, the magnets in the accelerator are located in a space without charges and currents, therefore the rotational of the magnetic field goes to zero, and the field follows equations (3-1).

The Normal and Skew components of the magnetic field are given by:

$$b_n = \frac{1}{B\rho} \frac{\partial^{n-1} B_y}{\partial x^{n-1}} \quad \text{and} \quad a_n = \frac{1}{B\rho} \frac{\partial^{n-1} B_x}{\partial x^{n-1}} \quad (3-6)$$

where B_x and B_y are the transverse components of the magnetic field.

In accelerator physics, two conventions for the magnetic field multipolar components have been adopted. These result from the fact that the indices for the multipolar components coefficients differs from the indices for the positions [18]:

$$B(z) = B_y + \mathbf{i}B_x = \sum_{n=0}^{\infty} [B_n + \mathbf{i}A_n] \left(\frac{s}{R_{ref}} \right)^n \quad \text{U.S. Conv.} \quad (3-7)$$

$$B(z) = B_y + \mathbf{i}B_x = \sum_{n=1}^{\infty} [B_n + \mathbf{i}A_n] \left(\frac{s}{R_{ref}} \right)^{n-1} \quad \text{European Conv.} \quad (3-8)$$

where R_{ref} is a normalization constant, common for the components and obtained according to potential ansatz (equation (3-4)).

Hence, in the previous expressions the **normal** components are denoted by B_n while the **skew** components are denoted by A_n . These new multipolar components notation is also related to the previous one:

$$\begin{aligned} B_n &= \frac{q}{p} b_n \\ A_n &= \frac{q}{p} a_n \end{aligned} \quad (3-9)$$

The magnets are built to have the main components alignment to the expected corresponding magnetic field. In general the skew magnet have a rotation of $\pi/(2n)$, where n is the order of the multipole. In this dissertation the notation will be given by the U.S. Convention.

Examples of the magnetic field expressions for the different multipoles can be found in sec 3.1.5 of [16] (3rd Edition). Some of the expressions are below with the convention adopted for this dissertation.

Dipole

The magnetic field component for a normal quadrupole is:

$$\frac{B_x}{B_\rho} = 0 \quad (3-10)$$

$$\frac{B_y}{B_\rho} = k_x \quad (3-11)$$

$$(3-12)$$

where k_x is the constant term of the magnetic potential.

Quadrupole

The magnetic field component for a normal quadrupole is:

$$\frac{B_x}{B_\rho} = -kx \quad (3-13)$$

$$\frac{B_y}{B_\rho} = ky \quad (3-14)$$

$$(3-15)$$

where k is the gradient of the magnet.

Skew quadrupole

This is a normal quadrupole field with a rotation of 45° around its symmetric axis.

$$\frac{B_x}{B_\rho} = k'y \quad (3-16)$$

$$\frac{B_y}{B_\rho} = k'x \quad (3-17)$$

$$(3-18)$$

where k' is the gradient of the magnet.

Skew Sextupole

This is a normal sextupole field with a rotation of 30° around its symmetric axis.

$$\frac{B_x}{R_\rho} = -m xy \quad (3-19)$$

$$\frac{B_y}{R_\rho} = -\frac{1}{2}m(x^2 - y^2) \quad (3-20)$$

$$(3-21)$$

where m is the second gradient of the magnet defined as $m = \frac{\partial B_{ny}}{\partial x} |_{x,y=0}$.

Magnetic Errors

The magnetic field errors on the accelerators are divided in two categories: Linear errors and non-linear errors. The linear magnetic errors correspond with fields of order zero and one, while the non-linear errors are fields of order two and more. These errors alter the dynamics of the particle in the accelerator.

During the beam commissioning is important to detect the linear errors because they have the biggest contribution in the reduction of the beam lifetime and dynamical aperture [6]. In general the equations using only linear magnetic fields are directly solved (as the harmonic oscillation problem), while including non-linear fields the equations of motion are solved using perturbation theory. Refer to chapter 3 of [6] (2nd Edition) for a detail explanation of the effect of Linear magnetic imperfections.

3.2. Basic Accelerator Physics Concepts

The Coordinate System

In an accelerator, just to refine the coordinates mentioned in the previous section, the axis along the direction of the particles advances around the accelerator, along the tube, is called the longitudinal axis, while its perpendicular plane is called the transverse plane, [19]. The notation of the coordinate system in an instant along the the accelerator, used in this disseration, is (s, x, y) where y is the coordinate in the vertical axis of the transverse plane and x is the coordinate in the horizontal axis.

Courant Snyder Parameters

The trajectory of the beam along an accelerator is described by several parameters. The traditional system to describe the beam motion is the set $\{\beta, \psi, s\}$, where s is the coordinate in the direction of the motion, β is a function of the amplitude of the motion, and ψ is the phase advance (in the phase space) expressing as:

$$\psi_z(s) = \int_0^s \frac{ds}{\beta_z(s)} \quad (3-22)$$

where the variable z stands for any of the transverse coordinates x or y .

To simplify the expressions of the dynamics representation, it is usual to use the Courant Snyder Parameters (β, γ, α) , which are defined as:

$$\beta = \beta(s) = \text{amplitude} \quad (3-23)$$

$$\alpha = \alpha(s) = -\frac{1}{2} \frac{d\beta}{ds} \quad (3-24)$$

$$\gamma = \gamma(s) = \frac{1 + \alpha^2}{\beta} \quad (3-25)$$

Betatron oscillations

Every time a particle passes by the magnets in a storage ring, it is expected to receive the appropriate deviation on their trajectory to complete their designed journey inside the ring. Because the magnets are not perfect, the beam change the expected trajectory and an oscillation is produced. If the oscillation is produced in the transverse plane it is called *Betatron oscillation*.

In addition, *kickers* or dipole correctors or AC Dipoles, are used to excite oscillations in the transverse plane of the beam orbit along the accelerator. These oscillations are also called *Betatron oscillations* and from them the information to describe the orbit that the particles follow is obtained.

Tune

The number of oscillations the particles do per cycle (one revolution) is defined as the Tune. The oscillation can be determined for each axis separately; hence the tune can be defined for each axis. The oscillations produced in the transversal plane are the same betatron oscillations, and in this case, the tune can be expressed in terms of the Courant Snyder parameters as:

$$Q_x = \frac{1}{2\pi} \oint \frac{ds}{\beta_x(s)} \quad \text{and} \quad Q_y = \frac{1}{2\pi} \oint \frac{ds}{\beta_y(s)} \quad (3-26)$$

here the integral is along the ring from s to $s + C$, being C the circumference of the ring.

The tune is a real number, its integer part is usually given as a reference and its decimal part is the main information. The notation used for this quantity is Q or ν . [20].

Hills Equation and the Action and Phase Parameters

The Hamiltonian that describes the motion of a particle in a storage ring equation (3-5) implies that the equation of motion (especially for linear terms) can be expressed as

$$\frac{d^2u}{ds^2} = -k(s) u \quad (3-27)$$

where the variable u , represents any of the transversal coordinates x or y , and $k(s)$ is a periodic function $k(s + C) = k(s)$, according to the circumference of the ring C [21].

The function $k(s)$ has a different representation given by the magnetic element involved. For example, in the horizontal case, if one want to describe the particle motion crossing a normal quadrupole $k(s) = eg/p$, where e is the charge of the beam, p its momentum and g the gradient of the quadrupole; while, in the case of a dipole $k(s) = 1/\rho^2$, where ρ is the bending radius of the dipole field.

The equation of motion in the transverse plane, equation (3-27), is called the Hill's equation. The solution of this equation is of the type

$$u = u(\psi, \beta, s) = a\sqrt{\beta_u(s)} \cos(\psi_u(s) + \epsilon_u) \quad (3-28)$$

where $\psi_u(s) = \int_0^s \frac{ds}{\beta_u(s)}$ is define as before. In terms of the Action and Phase variables (J, δ)

$$u = u(J, \delta, s) = \sqrt{2J_0\beta_u(s)} \sin(\psi_u(s) - \delta_0) \quad (3-29)$$

where the action and angle variables has a null subscript to denote that they are constants throughout the motion.

Taylor Map

In accelerators the trajectory of the beam can be represented theoretically using different formalisms. The relation that converts the coordinates from an initial point to a final point, using polynomials functions of the initial point, is called a Taylor Map [22]

In the case of linear contributions the equation of motion can solve exactly and the Taylor Map takes its simple form as a Matrix, and usually it is called the Transportation Matrix. In the non-linear case the representation is more complex. In general the convenient way to express the Taylor Map is using the *Lie Operator*.

By definition the exponential Lie Operator implies [23]:

$$e^{i\mathcal{L}}g = g + [f, g] + \frac{1}{2}[f, [f, g]] + \dots \quad (3-30)$$

where g and f are differentiable functions and $[f, g] = \sum_j \left(\frac{\partial f}{\partial q_j} \frac{\partial g}{\partial p_j} - \frac{\partial f}{\partial p_j} \frac{\partial g}{\partial q_j} \right)$, is the Poisson bracket.

Transformation Matrix

As discussed above, the linear motion inside the accelerator can be represented as a transformation from the initial to the final coordinates. For two longitudinal points of the accelerator, x_1 and x_2 is possible to express:

$$\begin{pmatrix} x_2 \\ x'_2 \end{pmatrix} = M \begin{pmatrix} x_1 \\ x'_1 \end{pmatrix} \quad (3-31)$$

where $x' = dx/ds$ for each of the two longitudinal points of the accelerator.

Each point of the accelerator is represented by the Courant-Snyder parameters, and for each transversal plane:

$$M = \begin{pmatrix} \sqrt{\frac{\beta_1}{\beta_2}} (\cos \psi_{12} + \alpha_1 \sin \psi_{12}) & \sqrt{\beta_1 \beta_2} \sin \psi_{12} \\ \frac{\alpha_1 - \alpha_2}{\sqrt{\beta_1 \beta_2}} \cos \psi_{12} - \frac{1 + \alpha_1 \alpha_2}{\sqrt{\beta_1 \beta_2}} \sin \psi_{12} & \sqrt{\frac{\beta_1}{\beta_2}} (\cos \psi_{12} - \alpha_2 \sin \psi_{12}) \end{pmatrix} \quad (3-32)$$

is called the *Transfer or Transformation Matrix* from the point $x_1 = x(s_1)$ to $x_2 = x(s_2)$.

In base of this representation, every piece of the accelerator can be model as a Transformation Matrix. In particular the magnets can be represented by matrices in analogy with the lens matrices in optics. Refer to Appendix C.2 of [16] 3rd Edition for the representation of the different type of magnets.

Beam Position Monitors

The control of the beam is made from the measurement of the beam position made by the Beam Position Monitors (BPMs). These devices are located in the beam pipe of the accelerator and are composed by two or four conductor plates. They are built to follow one of these two types of configurations: an electrostatic (equivalent as a current generator) or a magneto-static (equivalent to a voltage generator with a series inductor) [6].

Every time the beam passed by the BPM, induced charges are produced in their plates, with an electric charge corresponding to the beam charge. This charge can be transmitted from the plates to a low impedance circuit to be measured or the charges can produced an induced voltage that can be measure on a high impedance port (as a capacitance) between the electrode (where the charge is collected) and the surrounding vacuum chamber.

In general, the electric charge is stored to determine the beam position as u :

$$u \approx \frac{w}{2} \frac{\Delta}{\Sigma} \quad (3-33)$$

where $\frac{w}{2}$ is the effective width of the BPM, $\Delta = U_+ - U_-$, $\Sigma = U_+ + U_-$, and U_+ and U_- are according with the configuration, the current or the voltage at the each BPM electrode. The BPMs are also known (in the old school) as pickup electrodes or PUEs [6].

In the LHC (Run I) there is a total of 1032 BPMs installed. Those BPMs are of two kinds: Buttons or Strip-Lines. The difference between those comes from the shape of the plate they have and the precision that they reach [12].

3.3. The LHC or Large Hadron Collider

In a Ring with a circumference of approximately 27000 m, located in French and Swiss territory, is installed the *Large Hadron Collider* or LHC. This machine reach the highest energies for proton-proton collision, in a laboratory constructed and designed by humans. It includes the most recent advances on particle detectors in four points along itself, in those, there are located the experiments ALICE, CMS, ATLAS and LHCb, where collaborations from different nations are jointed to design, adjust, operate and maintain the equipment and also to do analysis of the data from the collisions.

This machine was built with the aim to study the Higgs particle, the dark matter and the dark energy [12]. For this, the first instants of the Universe are reproduced in a safe way. The LHC started its operation in 2008 and later in 2012 it was announced that *CERN experiments observe (a) particle consistent with (a) long-sought Higgs boson* [24]. Recently, this year on May 14th, 2015, the experimental mass of the Higgs Boson is determined to be $m_H = 125.09 \pm 0.21$ (stat) ± 0.11 (syst) GeV [25], which favors the theories close to the Standard Model, and leads to the path to more detailed studies on its behavior.

The discovery of the Standard Higgs Boson was made using proton-proton collisions with a center-of-mass energy of 7 and 8 TeV. This energy is half of the expected ultimate energy of the LHC. The corresponding data were obtained from the so called Run I of the machine. At this time, the second semester of 2015, it is running the so called Run II of the LHC.

To obtain such amount of energy in one point, the European Laboratory of Particle Physics of the CERN (the European Organization for Nuclear Research) has a chain of previous accelerators that starts to accelerate light Hydrogen Ions using two Linacs, and then protons arrive to the Booster and the PS, to finally get into the SPS and get out to the LHC with an energy of 450 GeV. In the accelerator, the particles travel in a set or package of particles

called **bunch**.

The LHC in few words is a set of two synchrotron accelerators, which accelerate the two beams of protons from 450 GeV to the expected ultimate energy of 7 TeV. The synchrotron principle corresponds to the fact that electrical fields are used to accelerate the particles, while magnetic fields are used to guide the particles in the circular trajectory along the accelerator, these fields are time dependent and they are synchronized for certain trajectory [19].

To guide, to bend, to focus, and to do the magnetic corrections in the LHC beams, there are available: the main magnets, like Dipoles and Quadrupoles, and the correctors of the lattice and orbit, which include Octupoles, Skew quadrupoles, Sextupoles, Skew sextupole, Decapoles, Skew octupoles and Dodecapoles. Kickers are used for the injection and ejection of the beam, in the dump and septum regions. Additionally, Warm magnets are presented in the RF interaction. [12].

In order to produce the proton-proton collision, two beams of protons travel in different tubes along the LHC, and only at the detectors interaction points the beams share the same beam pipe. This demands a synchronism of the beams and an appropriate calibration of each individual beam. As presented in this document, the aim of this investigation is to analyze the quality of these beams by the detection of the magnetic errors in the LHC lattice.

The LHC optics arrangement is divided in eight sectors. Four of those are where the main interaction points take place and the detectors of the main experiments ALICE, CMS, LHCb and ATLAS are located. The other four interaction sectors are the points where the maintenance of each beam is done (the momentum and betatron cleaning, the RF and the Dump). Therefore, the magnets along the LHC are distributed in Sectors or in Octants, the sectors are called 12, 23, 34, 45, 56, 67, 78 and 81, while the octants runs from 1 to 8, with a mismatch of 20 degrees from the sector. [26].

It is usual to call the straight regions of the accelerator by *IRs* of the LHC, while the regions with a strong bend are called the *Arcs* of the LHC. In this dissertation both concepts are repeatedly used.

Insertion Region

Each insertion region of the LHC is composed mainly by a **Long Straight Section** (LSS) and two **dispersion suppressor** (DS). The LSS are *the quasi-straight sections between the upstream and downstream dispersion suppressor of an insertion, including the separation/recombination dipole magnets*, see Vol 1 chapter 2 [12]. Each DS *consists of four indivi-*

dually powered quadrupole magnets which are separated by two dipole magnets, this arrange of magnets plus six more dipoles is referred to a *two missing dipole cells*; nevertheless, the term DS involves the two missing dipole cells plus one additional arc cell. The last contains two quadrupole magnets with a special powering, which allows to reach a zero dispersion at the Interaction Points.

The insertion region, according with the duty of the machine at the particular point, could be a couple of matching regions or triplets assemblies plus the separation/recombination dipoles. The last configuration is used in the insertions where the main experiments take place, in those, the triplet consists of four quadrupole magnets where the two central quadrupole magnets work as one functional entity. The regions in the LHC with Triplets are IR1, IR2, IR5 and IR8. Vol 1 chapter 2 [12].

3.3.1. The LHC Triplets

The assembly of three quadrupole magnets, used for a reduction of the optical β -functions at each Interaction Point (IP) where the two LHC beams are expected to collide, is called a **triplet**. It includes all the cryogenics necessary to keep those superconductive magnets at 1.9 K ([27]). There are two triplets in each IR, each one at each side of the IP.

In Table **3-1** the sequence of quadrupole magnets, corresponding to $n = 1$ (U.S. conv.), which belongs to triplets at LHC IR5 and IR1, is introduced. In addition, the triplets have the cryogenics and power supply systems, plus a dipole corrector in the middle of the each couple of quadrupoles denoted by Q2.

Each row in Table **3-1** corresponds to a quadrupole magnet, but there are also magnets that work as one unity, the case of magnets labeled by Q2. In the table, the first column is the name of the magnet according to the LHC nomenclature. In the second column there is the longitudinal position (*Long. Pos.*) referred to the LHC beam 1. In the third column is the type of quadrupole magnet (*Quad. Type*). In the last column labeled with (*Eti.*) is the notation used along this dissertation for the magnets.

In summary, in each region there are mainly: three normal quadrupoles, a skew quadrupole and a normal dipole magnet, for each triplet.

According to the LHC design parameters, the quadrupoles have a magnetic length of 3.4 m, with an aperture of 70 mm. The coils are NbTi Rutherford type, whose main part is composed by filaments of 6 μm under a steel base. Several layers are used to insulate the coils and all the other components, see page 5 in [12] for the material description. The actual

Name	Long. Pos. [m]	Quad. Type	Eti. Q
IP 5 Left Triplet			
MQXA.3L5	10142.81065	Normal	3L5
MQSX.3L5	10143.27915	Skew	
MQXB.B2L5	10151.22565	Normal	2L5
MQXB.A2L5	10157.72565	Normal	
MQXA.1L5	10166.81065	Normal	1L5
IP 5 Right Triplet			
MQXA.1R5	10219.11065	Normal	1R5
MQXB.A2R5	10227.32565	Normal	
MQXB.B2R5	10233.82565	Normal	2R5
MQSX.3R5	10236.49515	Skew	
MQXA.3R5	10243.11065	Normal	3R5
IP 1 Left Triplet			
MQXA.3L1	23472.40462	Normal	3L1
MQSX.3L1	23472.87312	Skew	
MQXB.B2L1	23480.81962	Normal	2L1
MQXB.A2L1	23487.31962	Normal	
MQXA.1L1	23496.40462	Normal	1L1
IP 1 Right Triplet			
MQXA.1R1	23548.70462	Normal	1R1
MQXB.A2R1	23556.91962	Normal	
MQXB.B2R1	23563.41962	Normal	2R1
MQSX.3R1	23566.08912	Skew	
MQXA.3R1	23572.70462	Normal	3R1

Table 3-1.: Quadrupole Magnets in the Triplets on the LHC regions IR5 and IR1

parameters registered at the LHC, from this type of magnets, include the fact that they can produce a maximum strength of 215 T/m, refer to [27], with the same aperture and other characteristics established in the design process of the accelerator.

4. The Action and Phase Jump Method (APJ) and AC Dipole Effect

Initially the Action and Phase Jump (APJ) method was presented as an analysis of only the Action Jump, it was in a Physics Accelerator Conference in 2001 [28]. The authors explain that the quadrupole strength can be estimate from the BPM information with a kicker located at the arc immediately before the IR or with a kicker in any previous arc different to the arc immediately before the IR. The first case scenario corresponds to a *principal strength* while the other is the *secondary strength* scenario (page 3133 [28]). A comparative study with the Closed Orbit Bump (COB) method is included.

By the next year, the method is officially named as the Action and Phase Jump Analysis. In the publication [29] of 2002, the authors mention about the APJ method that *the corrector must be chosen such that the difference of phase advance between the corrector and the IR under study is close to an odd multiple of $\pi/2$* . Also they include an analysis on the triplets' quadrupoles, giving the fact that the APJ method only can gives the total error on the triplet (it cannot distinguish the quadrupoles).

In the BNL laboratory, by 2003 at RHIC, there were experiments developed to measure the sextupole strengths, using the APJ method. They consist of set a sextupole corrector to a known strength value, and measure the orbits obtained when a particular dipole corrector changes their strength to various values in the horizontal and in the vertical plane. The difference orbits were obtained in each case as the method demands. This experiment was repeated for different sextupole strengths. The results of the sextupoles strength can be consulted in [30].

Since the APJ method was showing accurate results, the followed studies were centered in the accuracy of the method. In 2004, the reported studies were made using MAD and including quadrupole errors of 1% of a strength of $7 \times 10^{-3} m^{-1}$, the biggest difference observed for the recovery values was 3.5% [1]. In that publication an analysis using real RHIC data is also presented.

In a 2005 publication [31] there was a first attempt to use multi-turn trajectories to apply the APJ method in the SPS. They observed that using trajectories instead of closed orbit data

implies *the fact that the orbit is not always a maximum at the place where the specific sextupole is*’, producing a jump of the known sextupole locations but in different turn numbers.

Therefore, the APJ method starts to demands an update of the theory. In a 2007 article [32], J. Cardona refined the APJ method by including a better estimation of the orbit at the error location and a careful construction of the difference orbits from multi-turn orbits. The refine of the theory at the error consisted in taking into account the phase advances at the BPMs locations, leading to a recovery error of 0.04% against the original 3.5% observed. To create the better difference orbits the turns *should be chosen such that the orbit excursion at s_θ is the biggest possible*’, s_θ is the error location.

In 2009, an article in the Journal of Physical Review Special Topics - Accelerators and Beams summarizes the physical principles of the APJ technique, and converts it into a method that can be applied in any High Energy Storage Ring or Collider, refer to [2]. This publication is also the most recent publication of the APJ method in Journals.

Additionally, since 2010 there is a book about the APJ method, the one published by the LAP and titled *Action and Phase Jump Analysis on Orbit Data*, [33].

In the following, a brief theoretical description is introduced, then a review of the application of the method in different accelerators is made. And, in the last part of this chapter the analysis of the AC Dipole effect is presented.

4.1. Theoretical Description of the APJ

With the APJ method, the variables of Action (J) and Phase (δ) are measured for a main orbit around the accelerator and then three regions are identified: the region which contains the magnetic error, a region (or subsection of the accelerator) before that error region, and a region after the error region. To calculate the magnetic errors the method uses J and δ from the region before and after the error region, and one transverse position from the error region.

Theoretically, the position of the particle in each region can be obtained from the solution of the equation of Hills, and on the other hand, the magnetic error that is going to be estimated is considered as a *kick* on the particle trajectory. This last means that the change in the trajectory is perceived initially as a change only in the slope of the phase space. In the absence of magnetic errors, the Action and Phase variables are preserved along the ring.

Table 4-1 shows the theoretical representation of the beam trajectory in the phase space as described by this method when there is a magnetic error that produced a change given by the kick θ . The variables $\beta(s)$, $\psi(s)$ and $\alpha(s)$ are the Courant-Snyder parameters at the longitu-

Region	Position $z(s)$	Slope $\frac{dz(s)}{ds}$
Before the error	$\sqrt{2J_0\beta_z(s)} \sin(\psi_z(s) - \delta_0)$	$\sqrt{2J_0\gamma_z(s)} \cos(\psi_z(s) + \eta_z(s) - \delta_0)$
At the error point	$\sqrt{2J_0\beta_z(s)} \sin(\psi_z(s) - \delta_0)$	$\sqrt{2J_0\gamma_z(s)} \cos(\psi_z(s) + \eta_z(s) - \delta_0)$ $+ \theta_z$
After the error	$\sqrt{2J_0\beta_z(s)} \sin(\psi_z(s) - \delta_0) +$ $+ \theta_z \sqrt{\beta_z(s)\beta_z(s_\theta)} \sin(\psi_z(s) - \psi_z(s_\theta))$ or $\sqrt{2J_1\beta_z(s)} \sin(\psi_z(s) - \delta_1)$	

Table 4-1.: Trajectory Equations described by the Action and Phase Method. Variable z represents the x or y Axis while $\eta_z(s) = \arctan[\alpha_z(s)]$, as mentioned in [2].

dinal position s where the equations are evaluated, while J_n and δ_n are the Action and Phase variables, for the regions before $n = 0$ and after $n = 1$ the magnetic error region, respectively.

To obtain the trajectory after the error, one can use the Transfer Matrix, equation (3-32), from the longitudinal position of the magnetic error s_θ to a any position s . The final equation of trajectory can be expressed also as a simple solution of the equation of motion, in the same way as the trajectory before the error

$$z(s) = \sqrt{2J_1\beta_z(s)} \sin(\psi_z(s) - \delta_1) = \sqrt{2J_1\beta_s} \sin(\psi_s - \delta_1) \quad (4-1)$$

if the new action and phase values J_1 and δ_1 are represented as equations (9) and (10) from [2]. The procedure to obtain those variables and the *kick* is as follows:

From equations (7) and (8) of the same paper [2], which is the expression for the position after the error reported in here in the previous Table 4-1, third row and second column, an expansion of the trigonometric functions is performed. Then the coefficients of the $\sin \psi_s$ and $\cos \psi_s$ functions are equalized and the below couple of equations can be inferred

$$\begin{aligned} \sqrt{2J_0\beta_s} \cos \delta_0 + \theta_z \sqrt{\beta_s\beta_{s\theta}} \cos \psi_{s\theta} &= \sqrt{2J_1\beta_s} \cos \delta_1 \\ \sqrt{2J_0\beta_s} \sin \delta_0 + \theta_z \sqrt{\beta_s\beta_{s\theta}} \sin \psi_{s\theta} &= \sqrt{2J_1\beta_s} \sin \delta_1 \end{aligned} \quad (4-2)$$

Therefore, to obtain the phase after the error, equations (4-2) can be arranged together as:

$$\tan \delta_1 = \frac{\sqrt{2J_0} \sin \delta_0 + \theta_z \sqrt{\beta_{s\theta}} \sin \psi_{s\theta}}{\sqrt{2J_0} \cos \delta_0 + \theta_z \sqrt{\beta_{s\theta}} \cos \psi_{s\theta}} \quad (4-3)$$

To find the Action J after the kick error, in terms of only the variables before the error, one can use again the couple of equations (4-2) and the identity $\cos^2 \delta_1 + \sin^2 \delta_1 = 1$. The new

expression depends on the Action and Phase variables for the region before the magnetic error and the kick. The relation is:

$$J_1 = J_0 + \frac{\theta^2 \beta_{s\theta}}{2} + \sqrt{2J_0 \beta_{s\theta}} \theta_z \cos(\psi_{s\theta} - \delta_0) \quad (4-4)$$

A practical result of this theory and the base of the magnetic error measurement is to get the magnetic kick from the action and phase variables. This can be done with these steps: to multiply the first relation, of the couple of equations (4-2), by $\cos \delta_0$, and to multiply the second relation by $\sin \delta_0$; then, to add the results of the preceding steps; and finally to replace the factor $\theta_z \cos(\psi_{s\theta} - \delta_0)$ in terms of the action given by equation (4-4). These end up in the following relation

$$\sqrt{2J_0 \beta_s} + \sqrt{\beta_s \beta_{s\theta}} \left(\frac{J_1 - J_0 - \theta_z^2 \beta_{s\theta} / 2}{\sqrt{2J_0 \beta_{s\theta}}} \right) = \sqrt{2J_1 \beta_s} \cos(\delta_1 - \delta_0) \quad (4-5)$$

and solving for the kick value in magnitude

$$\theta_z = \sqrt{\frac{2J_0 + 2J_1 - 4\sqrt{J_0 J_1} \cos(\delta_1 - \delta_0)}{\beta_{s\theta}}} \quad (4-6)$$

This kick, or magnetic kick error, in terms of the magnetic field *can have contributions from any magnetic field component- dipole, quadrupole, skew quadrupole, sextupole, et cetera* [2]. To identify the type of component, the multipolar expansion of the magnetic field as discussed in the previous chapter is used.

Each kick, horizontal θ_x or vertical θ_y cause a deviation of the trajectory of the particles. If the trajectory is represented by the transversal coordinates x and y , at certain point s_θ , the kick values are the (corrected) equations (19) and (20) in paper [2], these are:

$$\begin{aligned} \theta_x &= B_0 - xB_1 + yA_1 + 2xyA_2 + B_2(-x^2 + y^2) + \dots \\ \theta_y &= A_0 + xA_1 + yB_1 + 2xyB_2 + A_2(x^2 - y^2) + \dots \end{aligned} \quad (4-7)$$

where A_n and B_n are the skew and normal magnetic strength of the multipole field, respectively.

Measurement of Magnetic Errors

To measure the magnetic errors using the Action and Phase Jump method, a change in the closed orbit is necessary. This change is obtained by using a dipole corrector or a kicker that exaggerates the betatron oscillations, even more, recent measurements are made from the betatron oscillations produced by an AC Dipole. Then, a single-turn trajectory of the closed orbit is recorded, also multiple turns of the beam with different positions can be recorded in each BPMs to then obtain a single turn, or even just the first-turn is recorded.

In fact, the experiments carried out at RHIC, consisted in changing the strength of a dipole corrector keeping the other variables with a constant value. The results showed that the APJ method, with the equations as described above are useful to the measurement of magnetic errors. For details in the accuracy and precision of the method and more, refer to [33] or [2] and the others mentioned at the beginning of this chapter.

A *difference orbit* is created from the measure BPM data, and it is the trajectory information that is going to be used to apply the technique. In the majority of cases, the difference orbit is the closed orbit change obtained when the orbit, generate with the kicker, is subtracted by a *baseline orbit* and the baseline orbit is the measurement orbit when the dipole corrector or the kicker is off.

From the measurements obtained in the BPMs, in particular from two adjacent BPMs (i and $i + 1$) on the same region, the Action and Phase variables can be inferred to be (as equations (13) and (14) in [2]):

$$J = \frac{z_{i+1}^2/\beta_{i+1} + z_i^2/\beta_i}{2 \sin^2(\psi_{i+1} - \psi_i)} - \frac{z_{i+1}z_i \cos(\psi_{i+1} - \psi_i)}{\sqrt{\beta_{i+1}\beta_i} \sin^2(\psi_{i+1} - \psi_i)} \quad (4-8)$$

$$\tan \delta = \frac{(z_i/\sqrt{\beta_i}) \sin \psi_{i+1} - (z_{i+1}/\sqrt{\beta_{i+1}}) \sin \psi_i}{(z_i/\sqrt{\beta_i}) \cos \psi_i - (z_{i+1}/\sqrt{\beta_{i+1}}) \cos \psi_{i+1}} \quad (4-9)$$

where z stands for any of the transverse coordinates x or y , while β and ψ are the Courant-Snyder parameters at the adjacent locations. These transverse positions are measured using the BPMs.

In this way, from every two adjacent BPMs, the Action and Phase values can be obtained, and at the same time, the average of the variables are determined for each region. This last means that the values of J_0 , J_1 , δ_0 and δ_1 are obtained as the average of the values measured for the corresponding region, with label 0 for region before the magnetic error and label 1 after the error.

Afterwards, the strength of the kick error θ can be estimated using equation (4-6) for each difference orbit. The corresponding magnetic strength can be inferred from the θ_u vs. u plots, for each transversal coordinate $u = x$ or $u = y$, using equations (4-7) up to the interested order. The values for the variables J_n , δ_n in equation (4-6) are generally obtained as the average of the individual measurements in the arc before (J_0 , δ_0) and after (J_1 , δ_1) the error region.

For the linear case, the magnetic error measurement can be obtained directly from the equations if the transverse position at the magnetic error is known. When there is only one magnetic error, the measurement in one of the BPM measurements is used as the error

position if the BPM is closed enough to the quadrupole with the magnetic error. If the BPM is far, the estimation of the position is made using equation (2) in [32], which is:

$$z(s) = \sqrt{\frac{\beta_z(s_0)}{\beta_z(s_{BPM})}} \frac{\sin(\psi(s_0) - \delta_0)}{\sin(\psi(s_{BPM}) - \delta_0)} z(s_{BPM}) \quad (4-10)$$

where the measurement at the closest BPM $z(s_{BPM})$ is included, and generally this BPM belongs to the error region and is connected in the middle of the triplets. In this dissertation, this BPM measurement is removed from the equations, as explained in the next chapter.

In addition, in the case of linear errors, when there is more than one magnetic error, the concept of equivalent error have been introduced, see [14]. New variables are proposed to obtain the total magnetic errors using a couple of orbits (1 and 2), these are (equation (5.28) in [14]):

$$\begin{aligned} B_1^{tx} &= \frac{y_1\theta_2^x - y_2\theta_1^x}{-x_2y_1 + x_1y_2} \\ B_1^{ty} &= \frac{x_1\theta_2^y - x_2\theta_1^y}{-x_2y_1 + x_1y_2} \\ A_1^t &= \frac{x_1\theta_2^x - x_2\theta_1^x}{-x_2y_1 + x_1y_2} \end{aligned} \quad (4-11)$$

where θ_i^z are the kicks obtained from the actions and phases, using equation (4-6), for each orbit $i = \{1, 2\}$ independently, while z_i are the error position estimations given by (4-10). The variables B_1^{tx} , B_1^{ty} and A_1^t are the total equivalent linear normal quadrupole component in plane X, the total equivalent linear normal quadrupole component in plane Y and the total equivalent skew quadrupole component, respectively.

However, not all the orbits from the accelerator are suitable to measure the magnetic errors, using the Action and Phase Jump method. Four types of orbits from the turn-by-turn are chosen, with the condition to have a maximum and/or minimum for the amplitude, in both transverse planes, at the longitudinal position where the magnetic errors are measured. [34].

At the beginning of 2011, in [4], for the first time it is presented a validation of the APJ Method applied to the LHC, the authors established that the best way to reduce the noise in the LHC data is doing a selection of orbits by establishing a phase range. The selected orbit is therefore taken as the average of many orbits.

Four selected orbits are then reported to be useful to obtain the magnetic errors using the Action and Phase Jump method for turn-by-turn orbits in the LHC, as presented in [3], and it is how in this dissertation the results are obtained, unless something different is mentioned.

Each main orbit is selected according to a reference phase advance in each transverse plane, given by the region where the magnetic errors are located. Each main orbit is a sum of the orbits that have a similar phase to reference value in each plane, in this way the 4-type orbits are called: "maxmax", "minmax", "maxmin" and "minmin". Those names corresponds to the characteristic of the orbit, where the three first letters are given by the condition at the plane X, while the next three letters are given by the condition at the plane Y; the letters "max" and "min" mean that the orbit has a maximum of amplitude or a minimum of amplitude at the error location, respectively.

To obtain the magnetic errors in the LHC, it can be shown that the effect of having magnetic errors in all the quadrupoles from both triplets, at one IR, in other words, to have magnetic errors at the quadrupoles located in left and in the right from the collision point, can be summarized in having two normal quadrupole errors and one skew quadrupole error ([3], [34], and the Appendix A in this dissertation).

According to [3], all the normal quadrupole errors presented in the triplets can be corrected if only the strength of two magnets are changed (equation (3) in [3], and discussed further in this section, equation (6-18)), by a quantity that depends on the total equivalent errors B_1^{tx} and B_1^{ty} and the β -functions. Meanwhile to correct the skew quadrupole errors, according to [3], it is enough to change the strength in one of the skew corrector by the amount of $-A_1^t/L$ where L is the length of the corrector used and A_1 is the measured value from all the skew quadrupole components, and is given by 4-11.

In general, it is assumed that the magnetic errors are given by the contribution from each magnet, individually. In this way, for each quadrupole i there is a deviation in the orbit given by $\theta_{z,i}$, which at the same time can be expressed as a function of magnetic multipolar components given by equations (19) and (29) from [2] as follows:

$$\begin{aligned}\theta_x &= B_0 - B_1x(s^\varepsilon) + A_1y(s^\varepsilon) + 2A_2x(s^\varepsilon)y(s^\varepsilon) + B_2[-x^2(s^\varepsilon) + y^2(s^\varepsilon)] + \dots \\ \theta_y &= A_0 + A_1x(s^\varepsilon) + B_1y(s^\varepsilon) + 2B_2x(s^\varepsilon)y(s^\varepsilon) + A_2[x^2(s^\varepsilon) - y^2(s^\varepsilon)] + \dots\end{aligned}\quad (4-12)$$

where the transverse positions are given by $z(s^\varepsilon) = \sqrt{2J_0\beta_{z,\varepsilon}} \sin(\psi_{z,\varepsilon} - \delta_0)$, which depends only of the Action and Phase measured at the region before the error, and of the Courant-Snyder parameters obtained from the model of the accelerator, β_z, ψ_z at the longitudinal position of the error denoted by s^ε , for each transverse plane $z = \{x, y\}$.

In case of just one normal quadrupole magnetic error, B_1 , the equations are reduced to $\theta_x = -B_1x(s^\varepsilon)$ and $\theta_y = B_1y(s^\varepsilon)$. A study for this case, when orbits include noise, was developed during this dissertation [35]. Results show that there is a better accuracy in one plane than in the other, but for a quick result in the measurements this approach can be

useful.

Higher Accuracy using the Integrals

In 2011, there is a publication on Conference Proceedings [3] in which the authors state that *the effects of normal quadrupole errors in the triplet can be suppressed by changing the strengths of two quadrupoles of the triplet according to the values B_1^{tx} and B_1^{ty}* , where B_1^{tx} and B_1^{ty} are the equivalent magnetic strength of triplet in each transverse plane. The corresponding change in the quadrupoles strength is given by:

$$\begin{aligned}\Delta k_1(Q_1) &= \frac{B_1^{ty} \beta_y(s_*) \int_{Q_2} \beta_x ds - B_1^{tx} \beta_x(s_*) \int_{Q_2} \beta_y ds}{\int_{Q_1} \beta_x ds \int_{Q_2} \beta_y ds - \int_{Q_2} \beta_x ds \int_{Q_1} \beta_y ds} \\ \Delta k_1(Q_2) &= \frac{B_1^{tx} \beta_x(s_*) \int_{Q_1} \beta_y ds - B_1^{ty} \beta_y(s_*) \int_{Q_1} \beta_x ds}{\int_{Q_1} \beta_x ds \int_{Q_2} \beta_y ds - \int_{Q_2} \beta_x ds \int_{Q_1} \beta_y ds}\end{aligned}\quad (4-13)$$

where s_* is the position of the skew quadrupole corrector of the triplet.

The first contribution from this dissertation is to obtain the integrals $\int_Q \beta ds$ in a more automatically way and for all the quadrupoles at the LHC, not only for the β -function at Beam 1, but also for Beam 2.

Furthermore, one of the improvements introduced, for the magnetic error estimation, is to include the β -function integral when the measurement of the skew quadrupole is done, though its variation is not as larger as for the normal quadrupole errors.

For both cases, the normal quadrupole errors and the skew quadrupole errors, the numerical way to obtain the integrals is using the *Simpson's Rule* (as presented in [36]) for 5000 divisions of each quadrupole.

In Table 4-2, it is shown the results when applied the integrals and the case without integrals, for the particular magnetic errors. The results are obtained for each beam independently. In the table the Relative Error is reported, it is given by the simulated value K_s and the recovery value using the Action and Phase Method K , $Error = \Delta = \left| \frac{K_s - K}{K_s} \right| \cdot 100\%$.

Taking into account the integrals of those skew quadrupoles, a slightly higher accuracy is reached, just about 0.1% better compare to the case of obtaining the magnetic errors without the integrals. Nevertheless, for the normal quadrupoles the accuracy of the measurements increases by about 5%.

Table 4-2.: Relative Errors for the Recovery of Magnetic Errors using the Old Formulation

sim. $\beta^* = 2.0 m$	$\Delta K_1(Q2L)$ [%]	$\Delta K_1(Q2R)$ [%]	$\Delta K_{1s}(MQSL5)$ [%]
Beam 1			
WITH INTEGRALS	0.163	0.663	0.524
WITHOUT INTEGRALS	5.862	4.644	0.589
Beam 2			
WITH INTEGRALS	0.248	0.619	0.323
WITHOUT INTEGRALS	5.959	4.688	0.387

These values were obtained using the formulation as described above, called here **Old**, for 2000 orbits turn-by-turn. In the simulator three errors were installed in the same optics used to analyze the 2010's orbits, and the quadrupoles where the errors were installed are the same used to analyze the orbits as explain in the following chapter and along this dissertation.

4.2. APJ in Accelerators

Using experimental data, the Action and Phase Jump have been tested at different laboratories, as mentioned at the beginning of this chapter. A summary of the reported studies is presented in Table 4-3, so far the accelerators used to do the measurements are RHIC, SPS and LHC. An excellent reading about the results from RHIC and the Action and Phase method is in [33].

Nevertheless, the majority of measurements were made using a closed orbit or with a kicker to generate the betatron motion of the orbits. In the table, turn-by-turn† means than the measurements were made by using the data of multiple turns. As mentioned above from the turn-by-turn orbits a single orbit is obtained to apply the APJ method, in fact, 4-type orbits are generally used. In [3] author show an example of the characteristics of the orbits, they explain that *One of these orbits ... has a maximum excursion of the horizontal position of the beam at the right triplet .. while the vertical position is minimum at the same place. The other kinds of orbits correspond to the combinations: maximum in the horizontal plane while the vertical is maximum, minimum in the horizontal plane while the vertical is maximum and minimum in the horizontal plane while the vertical is minimum.*

Also, at the beginning of 2011 for the first time it is presented a validation of the APJ Method applied to the LHC [4]. It is important to notice that the simulations performed for the LHC lattice confirmed the accuracy of the APJ method for the magnetic error measurement in High Energy colliders. Using an orbit corrector (a kicker), the normal quadrupole error or gradient error accuracy reported from the simulations was of the 0.01% with an uncertainty of 1.53% in the LHC. In the middle of 2011, as presented in Table **4-3**, there is a publication on Conference Proceedings [3] about a comparison of the APJ method with the Segment-by-Segment Technique (SBST).

In this dissertation analysis from turn-by-turn orbits are presented. The orbits are obtained using simulations and the LHC. The experimental data analyzed is from 2010, the same reported in [3] but in here with a different configuration, and also using orbits from recent experiments in 2015. The results for the simulations are reported in here and in Chapter 6 while the results and discussion for the experimental data is reported in Chapter 8.

Table 4-3.: Studies using the Action and Phase Jump method reported at Accelerator Conferences up to 2011.

Accelerator	Oscillator generator	Type of Orbit	Magnetic Field under study at IR	Type of field	Comparative study with	Year of publication
RHIC	kicker	Difference orbit	Mea. quadrupole cor.	linear	COB	2001 [28]
RHIC	dipole cor.	Difference orbit	Mea. skew quadrupole cor.	linear	APJ & COB	2002 [29]
RHIC and SPS	dipole cor.	Difference orbit	Mea. Sextupole strength	non-linear	n.a.	2003 [30]
RHIC			Sim. Gradient Mea. Quad. Mea. Skew quadrupole	linear linear	n.a. n.a.	2004 [1]
SPS and RHIC	h-kicker	Multiturn trajectory Closed orbits	Mea. Sextupole Sim. Sextupole	non-linear	n.a.	2005 [31]
RHIC			Sim. and Mea. Skew quad.	linear	Old APJ	2007 [32]
LHC	kicker	difference orbits	Sim. quad. noise	linear	n.a.	2011 [4]
LHC	AC-Dipole	turn-by-turn†	quadrupoles	linear	SBST	2011 [3]

Mea. stands for Measurement, *n.a.* stands for non-applied, *cor.* magnet corrector, *Sim.* stands for simulation

4.3. The AC Dipole Effect

Various techniques are available to measure the lattice errors and/or the nonlinearities in accelerators. Those can be classified in three categories, according with the type of perturbation used: Orbit Bump, Energy Change, and Dipole Kick; as described in Chapter 10 of [23]. What it is important to point out is that there are cases where the application of the technique ends up in the destruction of the beam, as in the case of APJ method (which can be classified inside the Dipole Kick techniques).

Actually, the not-destructive cases are only the Orbit Bump Techniques and the techniques that use an AC Dipole to generate the betatron-oscillations. Nowadays the APJ method is applied to experimental orbits generated by an AC Dipole in the LHC.

An AC Dipole is a dipolar magnet in where the magnetic field changes with time, this is similar to say that the dipole is connected to an AC power supply. The expected change in the magnetic field is just the enough amount to the beam to complete the accelerator journey without further distortions on its trajectory i.e. the effect is to keep the beam in its ideal trajectory eternally. In the LHC, to generate the orbits turn-by-turn, an AC dipole for each beam was installed [37], for Run II an update to the AC Dipole was made to be able to take 6600 consecutive turns instead of just 2000 turns.

AC Dipole Theoretical Description

The dipole which is used to create oscillations without disturbing the orbits is called an AC Dipole. A dipolar field corresponds with a magnetic field with a multipolar component of order zero.

In the Hamiltonian of a particle in an accelerator, the inclusion of an AC Dipole adds the term:

$$H_{0,dipole} = -\delta(s, t)x \quad (4-14)$$

The kick produced by an AC Dipole is represented in a linear Hamiltonian as:

$$H_{dipo} = -f(s, t) \quad \text{with} \quad f(s, t) = \frac{BL}{B_0\rho} \delta_{Dirac}(s - s_D) \cos(2\pi Q_D t + \psi_0) \quad (4-15)$$

where BL is the integrated field amplitude of the magnet, $(B_0\rho)$ is the rigidity of the beam, Q_D and ψ_0 are the tune and the initial phase of the AC dipole, and δ is the Dirac Delta function (refer to page 1 on [38]).

AC Dipole Simulation

For this dissertation, the simulation of the AC dipole was performed using the MAD-X files from CERN, where the AC Dipole has been constructed through the transfer matrix, which components are:

$$M_{21} = \frac{2(\cos(2\pi Q_{x,d}) - \cos(2\pi Q_x))}{\beta_{x,ac} \sin(2\pi Q_x)} \text{ for the horizontal plane,} \quad (4-16)$$

$$M_{43} = \frac{2(\cos(2\pi Q_{y,d}) - \cos(2\pi Q_y))}{\beta_{y,ac} \sin(2\pi Q_y)} \text{ for the vertical plane} \quad (4-17)$$

and the other terms to a corresponding identity matrix. The quantities Q_{xd} and Q_{yd} are the new tunes, which are reached by the accelerator due to the AC dipole effect; Q_x and Q_y are the accelerator tunes without the AC Dipole; $\beta_{x,ac}$ and $\beta_{y,ac}$ are the Courant-Snyder parameters where the AC Dipole was installed.

After running the LHC simulator, it was found that this new element changes the obtained values for the Action and the Phase variables. This is explained by the fact that the effect of the AC Dipole is also to change, by a small amount, the expected Courant-Snyder parameters from the new accelerator model. This change in the parameters is described in [39].

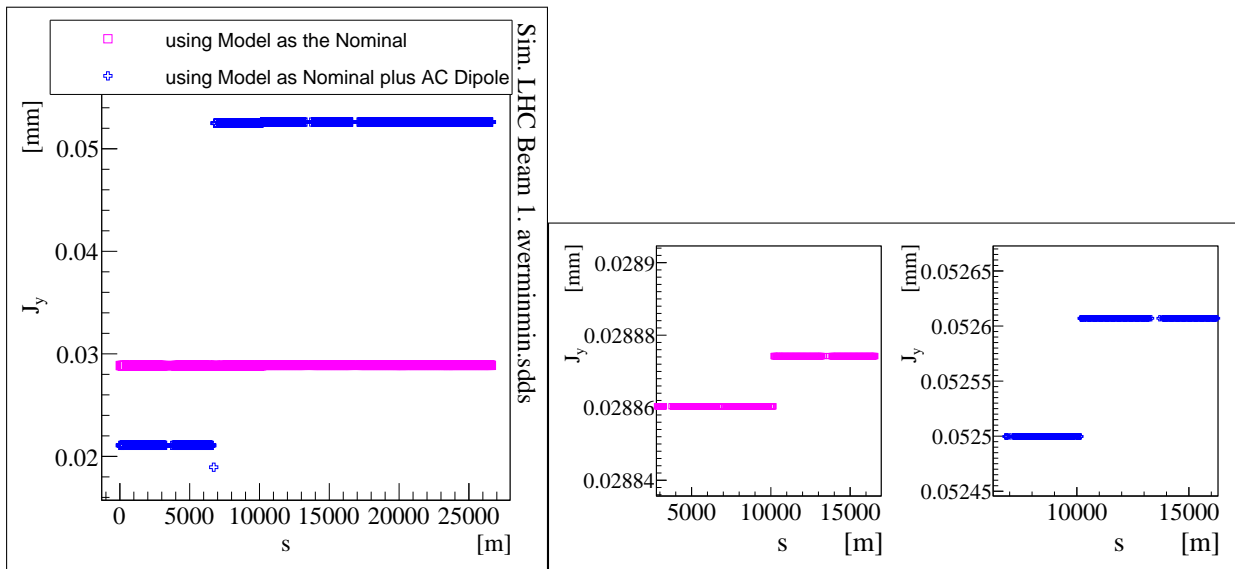


Figure 4-1.: Action in Y-axis (J_y) along the LHC. Simulation with presence of an AC Dipole at 6707.354433 m, and a magnetic error at 10158 m. Squared dots are obtained taking the model as the nominal one, while Crosses dots are obtained taking the model as the nominal in the presence of the AC Dipole, a close-up of each case is presented in the subfigures at the right.

Figures 4-1 and 4-2 show that the values of the Action and Phase along the accelerator, when a magnetic error K_1 is introduced and taking or not taking into account an AC Dipole, with the configuration described above. In the plots both cases are plotted, the case without the AC Dipole is the one with the model taking as the Nominal model of the accelerator (magenta squares) while the other is when the model is taken as the Nominal plus the AC Dipole (blue crosses). The fractional nominal tunes in the simulator are 0.28 and 0.31, in planes X and Y, respectively, while taking into account the AC Dipole effect are 0.31 and 0.22 to finally have 0.28 and 0.31.

In the graphs for the Action, Figure 4-1, the jump closer to 7000 m corresponds to the effect of the AC Dipole (installed at 6707.354433 m, which is at $(1.583/2)$ m from MKQA.6L4.B1 with a 0.0 m length), while the jump closer to 10000 m, almost unseen when using the nominal model plus the AC dipole, corresponds to the longitudinal position where the magnetic error was installed. A close-up of these last jumps is in the subfigures (at the right).

In the graphs for the Phase, Figure 4-2, it is observed directly the two jumps, given by the AC Dipole and the magnetic error for the model taked as the nominal case (squared dots). In the same scale the jump from the magnetic error close to 10000 m is easy to identify for any of the two studied cases, although the jump produced by the AC Dipole is much more notorious.

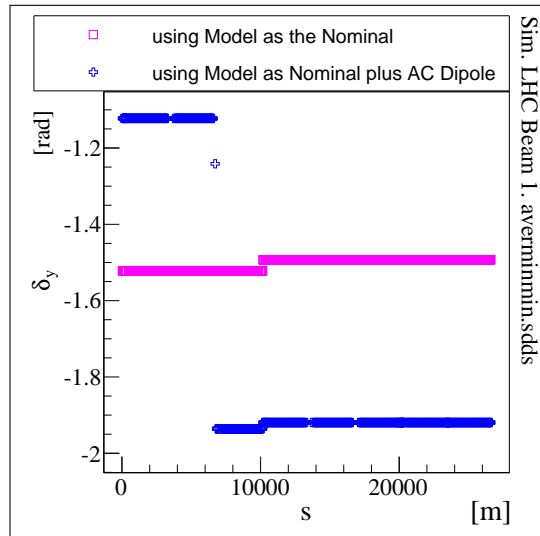


Figure 4-2.: Phase in Y-axis along the LHC. Simulation with presence of an AC Dipole at 6707.354433 m, and a magnetic error at 10158 m. Squared dots are obtained taking the model as the nominal one, while Crosses dots are obtained taking the model as the nominal in the presence of the AC Dipole.

From the average of J and δ in each region, before and after the error, it was obtained

that the magnetic error is $0.000100000020 \text{ m}^{-1}$ when the model is taken as the nominal and $9.99999411 \times 10^{-5} \text{ m}^{-1}$ when the model is taken as the nominal plus the AC Dipole. The magnetic error was installed with a strength of 0.00010 m^{-1} using the thin lens approximation with a length of zero at BPMS.2L5.B1 (at 13297.76023 m). The simulation was performed using MAD-X ([5]) with the V6.5 sequence and the injection mode with $\beta^* = 2 \text{ m}$ for Beam 1 of the LHC.

Therefore, although the values for Action and Phase are different for the corresponding analysis with just the Nominal model or including the AC Dipole, the recovery value is the same within 7 significant figures. From this, it is inferred that there is not a significant change in the relative error of the measurement when using the model that includes the AC Dipole or the model that does not.

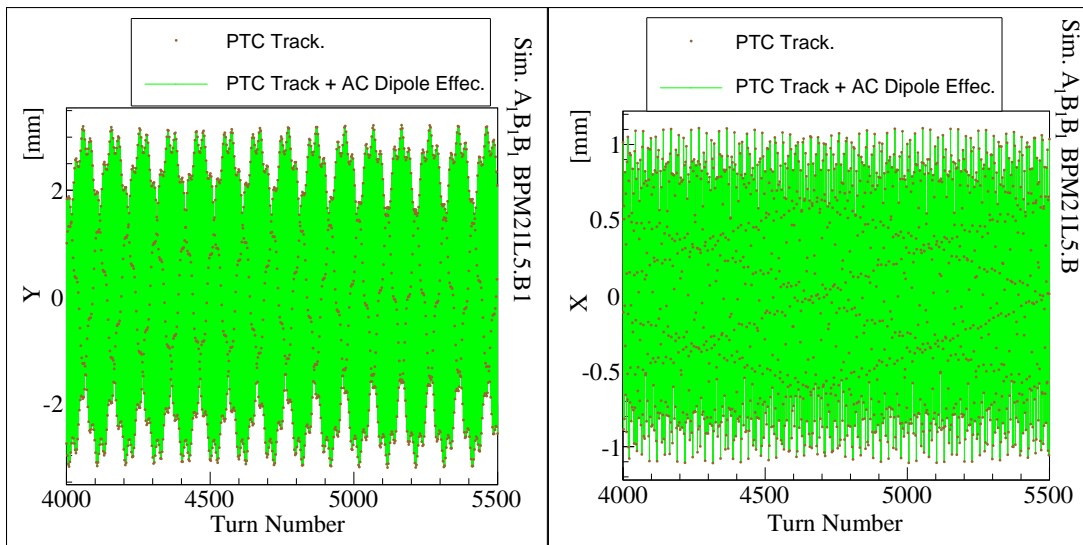


Figure 4-3.: Trajectories after many turns in a specific location in the LHC with and without the effect of an AC Dipole (at 6707.354433 m). The AC Dipole does not influence the simulated trajectory and this is valid for the all ring. For this case, the start position is $(x, y) = (0.0001 \text{ m}, 0.0001 \text{ m})$ and the three magnetic errors are located close to 10000 m (IR5).

The AC Dipole, as presented in the next subsection, just guarantee that the beam keeps stable after many turns. In the simulator to obtain the several turns without losing the general amplitude, the module PTC [40] is used, and it gives the particle track at any chosen accelerator element. For instance, Figure 4-3 shows the trajectories observed from turn 4000 to more than 5000 in the simulator; two cases are plotted, when the trajectory takes, and not takes, into account the AC Dipole effect. To keep the same tune values given by the AC Dipole in the analysis of the simulated orbits, two ways were obtained, one by adding the line

MKQA.6L4.B1, HKICK := Θ_{21} , VKICK := Θ_{43} ; , with the parameters of the AC Dipole, before calling the module PTC in the LHC simulator, or by doing a matching at the tunes using the MATCH command in MAD-x, this last is the implemented way for this dissertation.

From the above, it is shown that for the method of Action and Phase, it is not relevant how the orbits turn-by-turn are generated, provided that the generator of the turns is far from the place where the magnetic errors are measured. Even more, the magnetic errors can be obtained despite changes in the Courant-Snyder parameters, as the caused by an AC Dipole (a detailed description of the AC Dipole effects are in [39]).

If the simulations does not count the AC Dipole effect, the trajectories would be always less than 2000 orbits followed by a total decrease of the amplitude for the transverse trajectories, but it is not the case. Therefore, for the rest of the dissertation it is understood that the simulated orbits are generated taking into account the AC Dipole effect.

AC Dipole to Generate Orbits at LHC

To add experimental evidence in this discussion of the AC Dipole effect, Figure 4-4 presents the trajectory of Beam 1 from a particular part of a LHC Experiment. This is a screen of the GUI Window that was obtained during the Experiment, courtesy of the OMC Team at CERN.

At the top of Figure 4-4 are the measured positions at the transverse plane X, while at the bottom are the measurements for plane Y. The system used to kick in each transverse plane is different. The horizontal trajectories were excited using a *kicker* while the betatron oscillations in the vertical plane were obtained using an *AC Dipole* (installed close to MKQA.6L4).

The most important observation is that, due to the decoherence effect the amplitude of the orbit is drastically reduced (from 3 mm to less than 1mm) after 2000 turns, when the *kicker* is used to excite the orbits. In contrast, the orbits kicked by the *AC Dipole* remains with the expected amplitude (of almost 5 mm) along the time of more than 5000 turns.

All the LHC data for the magnetic corrections are taken using the AC Dipole as the creator of the multiple turn-by-turn orbits.

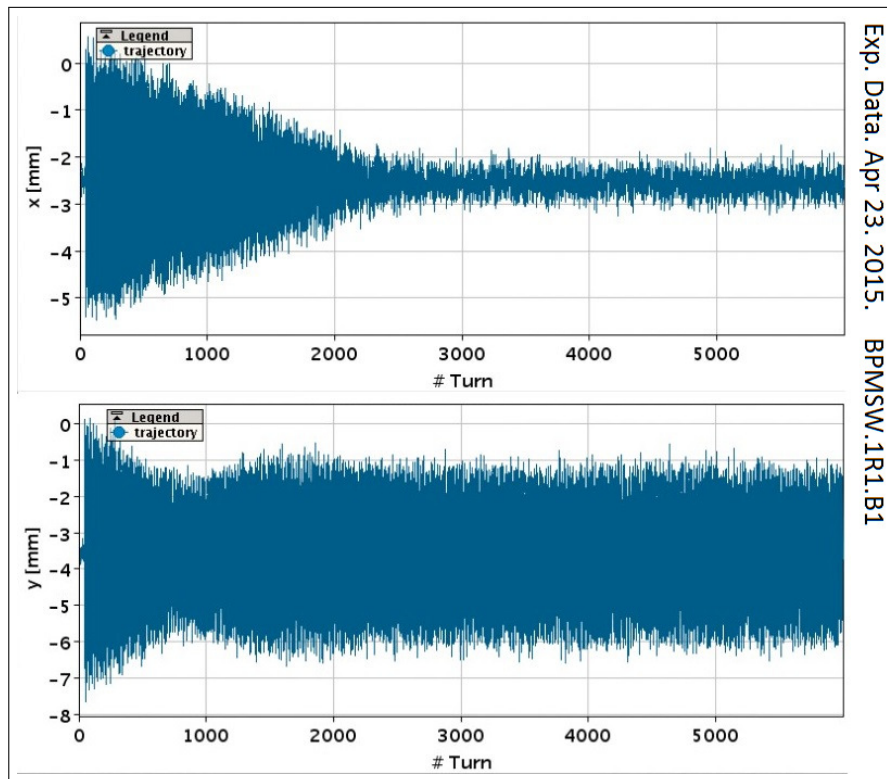


Figure 4-4.: Betatron oscillations, for Beam 1, excited by a different system in each plane. Part of a LHC Experiment performed in Apr 23th, 2015.

5. Design of a Digital Filter to Reduce Noise in LHC Orbits

The first step in the development of this dissertation is the design of a Digital Filter which can be useful to reduce noise in the LHC orbits.

The Large Hadron Collider (LHC), as mentioned earlier, is a machine designed to have two beams of particles, which encounter each other in 4 different points around a ring of 26.7 *Km*. The LHC system is capable to have 2808 bunches in each beam. To perform this task, the Beam Position Monitors (BPMs) have a wide bandwidth to account RF frequencies of 400.8 MHz. [12]

A requirement for the optical measurements is that each beam has to be with a single bunch. Therefore, with the wide bandwidth of the BPMs, the measurements has a considerable amount of noise compare to previous trials of APJ in accelerators.

On the other hand, the thousands of available orbits at the LHC leads us to apply all sort of digital filters. Several trials were performed with the problem that the characteristic jump for the Action and Phase along the accelerator, in the presence of magnetic errors, is lost.

In this chapter a *Band-pass* Filter, specially designed during this dissertation, is presented. The signal-to-noise ratio is also included for its characterization. Results of the magnetic error measurement using the filter for the simulation of two magnetic errors, one B_1 and one A_1 are included. This filter have already been presented at a Conference [41] and the plots and most of the paragraphs are extracted from there.

Also, in the last part of the chapter the different ways to reduce noise studied in this dissertation are presented and its corresponding tools are described.

5.1. The Band-Pass Filter

For a fixed longitudinal position, one way to consider a sampling of the LHC TBT data is taking the basic unit as 1 turn. Therefore the signal to be filtered is the data recorded at

one of the BPMs; the frequency is given, in rad/turn or simply rad. The transverse beam position after n turns, in terms of the Action (J) and Phase (δ), is:

$$z(n) = \sqrt{2J\beta_{BPM}} \sin(\psi_{BPM} + 2\pi Q_z n - \delta) \quad (5-1)$$

where the total phase advance have been replaced, and the measurements of β and ψ are the beam β -function and phase advance at the BPM location, Q_z is the accelerator tune, for each transverse plane $z = \{x, y\}$.

These transverse positions turn-by-turn constitute a discrete signal, when taken in a fixed point along the accelerator. In principle, this signal can be filtered.

From the available filters, the band-pass filter was chosen, because it reduces the noise without damaging the magnetic errors recovery. In this study, the filter was implemented using directly PYTHON functions, although trials were also made with own built transfer functions. The implementation is as a second order filter, with Butterworth coefficients and the double run function given in [42].

Also previous trials showed that the best results are obtained using a band-pass filter with two bands, each band centered on the transverse tunes ν_x and ν_y (a 99% uncertainty is reached if only one tune band is used without noise when the using thin magnetic errors), both bands with the same bandwidth.

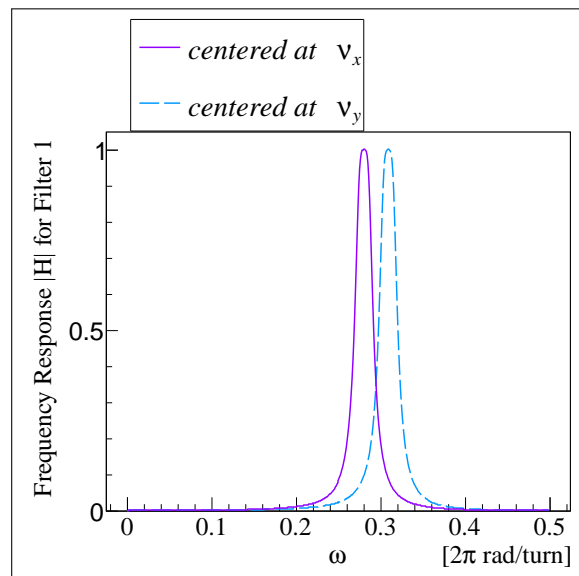


Figure 5-1.: Frequency Response for the Dual Band-pass Filter. It is designed to have its bands at the frequencies 0.2805 and 0.309.

The filtered signal is the addition of the signals obtained with the two single band-pass filters, whose frequency response looks like Figure 5-1, and in case of overlapping, the addition of the filtered signals is followed by the subtraction of the corresponding overlapping band-pass signal.

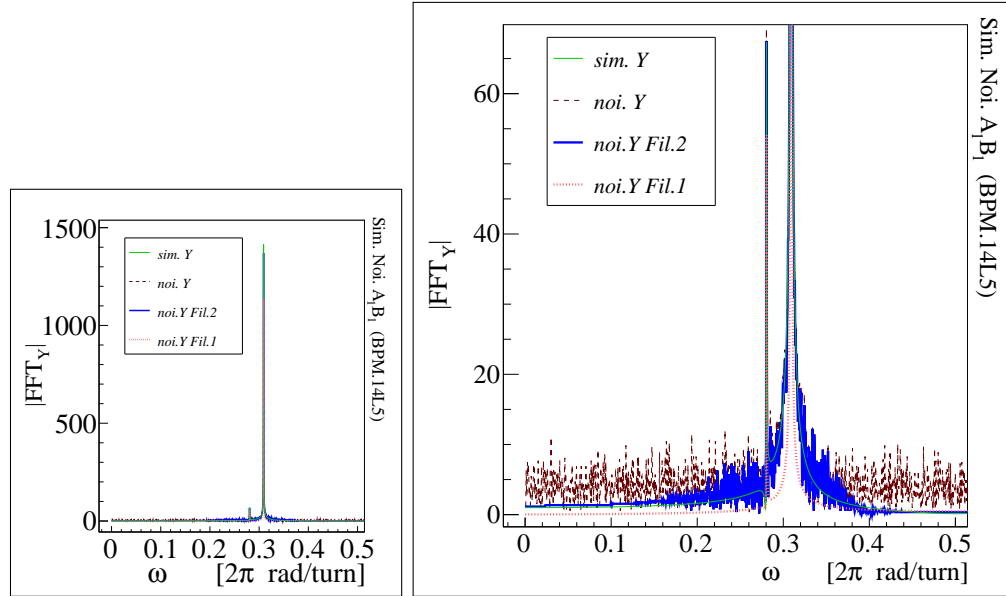


Figure 5-2.: FFT for the Vertical Positions at BPM.14L5.B1 after 2000 turns. Ideal orbits with noise from a Normal Distribution. The left plots are the complete spectrum while the right plots are a close-up for the bottom of the spectra. In both cases a superimpose of a simulated trajectory (*sim. Y*), a *sim.* with noise added (*noi. Y*), and two *noi.* filtered signals (*noi. Y Fil.2* and *noi. Y Fil.1*), is presented. The bandwidths used for the filtered signals *Fil.2* and *Fil.1* are 0.004 and 0.001, in 2π rad/turn units, respectively.

Figure 5-2 contains the beam y -trajectory in the frequency space for one BPM of the LHC. Four signals are plotted in the same axis, the FFT of: the simulated, with noise, and filtered, trajectories. This representation allows to observe how the amplitude of the noise signal is reduced in the filtered signals. Filter *Fil N.1* is the filter with a narrow central frequency band (Bandwidth of 0.001 tune units) while filter *Fil N.8* is the filter with a more broad central frequency band (Bandwidth of 0.004 tune units).

When noise is presented in the orbits, The Action (J) and Phase (δ) are modified in both planes X and Y. Figure 5-3.left contains J against s , while Figure 5-3.right contains δ against s . The plots are for the Y plane under these conditions: without noise, for Gaussian noise and filtered. The value of J is affected after the use of the filter *Fil N.1*. The dispersion of the action and phase variables is reduced using the filters (keeping the jump produce by the

magnetic errors).

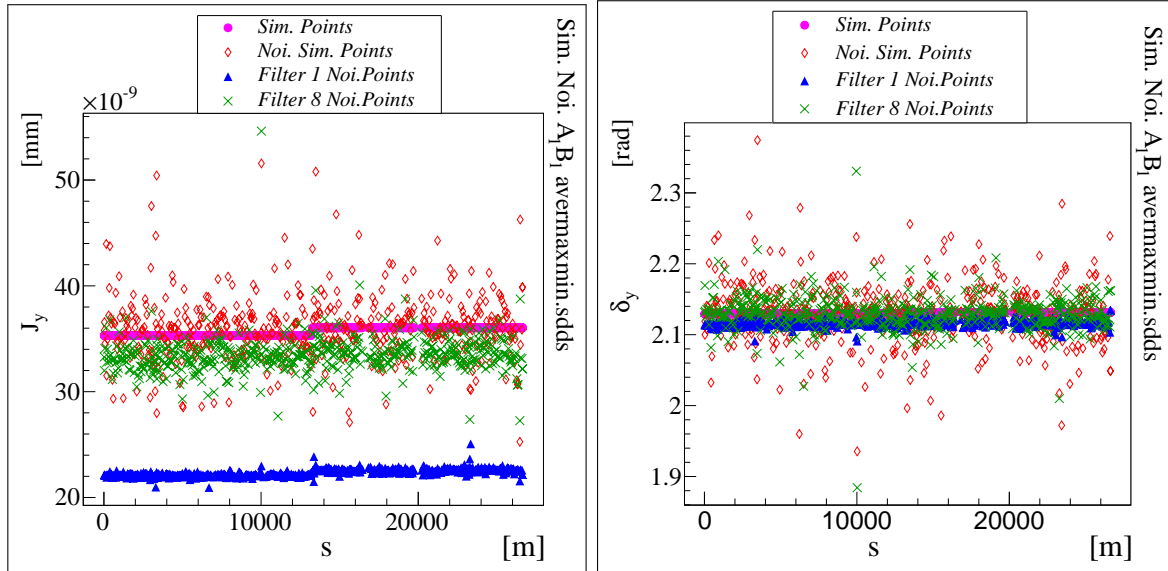


Figure 5-3.: Action (J) and Phase (δ) along the LHC ring for one orbit type. Obtained from the simulation, without noise (Sim.), with Gaussian Noise (Noi. Sim.), and using filters with a narrow and broad frequency band (Filter 1 with a bandwidth of 0.001 tune units and Filter 8 with a bandwidth of 0.004 tune units). Two thin magnetic errors are installed at 13271 m .

A report about this filter have been already presented at a Conference during the development of this dissertation, refer to [41], for the details of the filters. The machine tunes after added the magnetic errors are 0.309 in Y and 0.2805 in X.

Preliminary Results with Simulated Orbits

The Action and Phase obtained in the previous plots, Figure 5-3, are obtained from a simulation of Beam 1 in the LHC simulator in MAD-x. Two magnetic errors B_1 and A_1 were installed in the same longitudinal position of MQXA.3L5 at the accelerator.

Figure 5-4 shows the results for the uncertainty of the magnetic measurements when noisy orbits are filtered with the Dual Band-pass Filter. The Uncertainty (uncert. corresponds to relative error) is plotted against the bandwidth $\Delta\omega$, for the different studied cases.

According to S.Y. Lee in [6] the closed orbit can be extracted from the turn-by-turn orbits using a low-band pass filter. In Figure 5-4, results using a low-band pass filter ($\omega_{cut} = 0.075$)

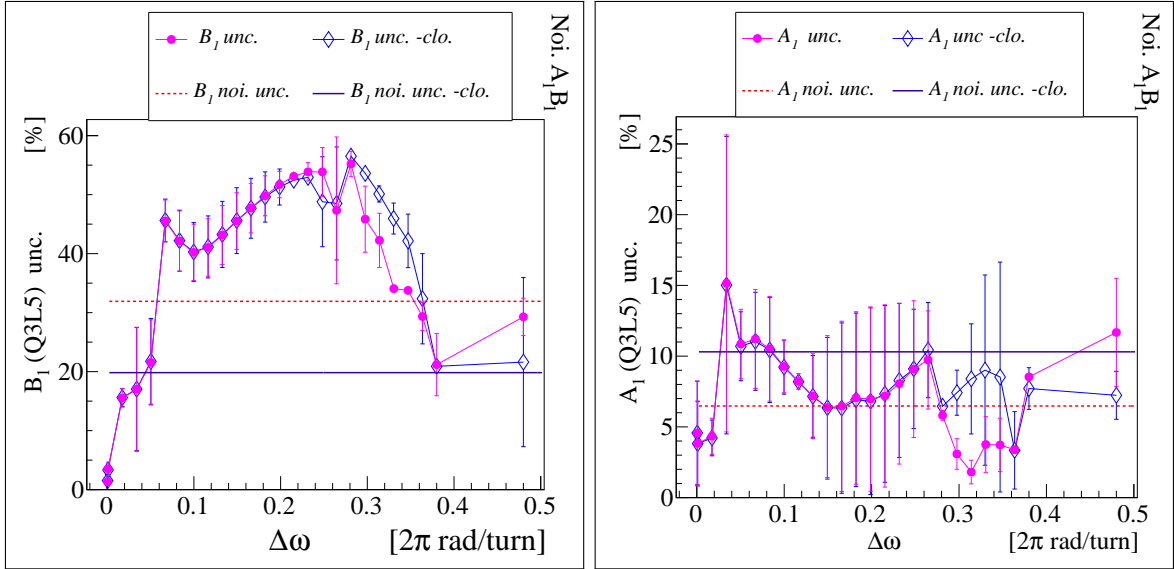


Figure 5-4.: Results for Dual Band-pass Filter in orbits with Gaussian Noise. The Uncertainty (unc.) for B_1 and A_1 are plotted against the bandwidth. The results without filter are included as a horizontal line. Also, the results when the closed-orbit is obtained from a Low-band pass filter is included as -clo.

for the closed-orbit calculation are reported with the line labelled as -clo. In the others, the closed-orbit is the average of the TBT trajectories. When there is noise at many frequencies a discrepancy on the results, in how the closed orbits is obtained, is observed.

Something similar occurs when noise from a uniform distribution is added to the orbits instead of the noise from a Gaussian or Normal distribution. Comparing the results from the two distributions, the noise from a uniform distribution implies a less dispersion in the magnetic errors measurements.

In conclusion, the dual band-pass filter with a bandwidth of 0.0174 around the transverse tunes can be used to highly decrease Gaussian and Uniform noise in LHC orbits, when measure A_1 and B_1 at the same quadrupole using the APJ method as presented.

The results reported in this section have modifications of the original method APJ, these are: To obtain A_1 and B_1 , the selection of the orbits in here implies that 8 points (two from each 4-type orbit, which are coming from the symmetry in the sinusoidal function, refer to [41] to know about this formable orbits) are available to solve:

$$\theta_x = -xB_1 + yA_1 \quad \text{and} \quad \theta_y = xA_1 + yB_1 \quad (5-2)$$

for a higher precise level, an implementation of a 2D independent fit is done. The orbits were selected in between a phase interval of 0.15 rad. Each orbit, called a formable orbit, is

the average of the TBT orbits that have the maximum. Also, an initial reformulation of the error position estimation is done in the PYTHON APJ code. The transverse error position is taken as:

$$z_{error} = \sqrt{2\bar{J}_0\beta_{z,error}} \sin(\psi_{z,error} - \bar{\delta}_0) \quad (5-3)$$

where \bar{J}_0 and $\bar{\delta}_0$ are the average of the Action and Phase in a region before the error (generally the arc before the IR), respectively, and $\beta_{z,error}$ and $\psi_{z,error}$ are the beam β -function and phase advance, at the longitudinal position of the magnetic error, respectively.

5.2. Signal to Noise Ratio for the Band-Pass Filter

With several values of tunes in the simulator of the LHC but keeping the same LHC optics, the collision sequence V.6.5 for the LHC accelerator, the Band-pass filter (as described above and reported in [41]) was evaluated. It was found necessary, along this process, to include some improvements in the filter. Mainly to take into account the case where the vertical transverse tune is larger than the horizontal transverse tune; also there was found a mistake in the writing code, that does not change the previous results, but that was corrected.

Therefore, the filter proven to be useful in all the ranges of frequencies. The simulations were made using two normal quadrupole errors at IR1 of 0.00001 and 0.000015 m^{-2} . The errors were installed in the quadrupoles MQXB.A2L1 and MQXA.1L1, and the tunes were modified to have close values of the LHC experiment of 2010.

For this dissertation it was studied as well, the efficiency of the band-pass filter to reduce the noise. This was done by obtaining the corresponding Signal to Noise Ratio. For this, to isolate the amount of noise was a concern. The different approaches end up in the problem that the filter reduces the amplitude of the final signal so the initial and final signals cannot be compare to get noise. Those strategies were to get the noise from the difference between an orbit without noise and an orbit (selected in the same way that the previous one) obtained from the treated orbits, where noise was added and had been filtered.

Therefore, to get the amount of noise property, the signal without noise was filtered and subtracted from the signal where noise was added and had been filtered. The measure of the noise is done for each transverse plane independently. The noise was taken to have a statistical dispersion along the ring given by:

$$\sigma = \sqrt{\frac{\sum_{i=1}^N (z_i)^2}{N-1}} \quad (5-4)$$

where z_i is the amplitude or transverse position, in units of length, at the position where the

measurement is made, in the BPM i th, and N is the amount of measurements or BPMs used.

This study includes the analysis of the difference in efficiency for the specific regions defined in the accelerator by the APJ method, in other words, to get to know if there is a dependency on the filter efficiency and the analyzed region, which is the region before or after the magnetic error. In Figure 5-5 there is the plots for the signal to noise Ratio for small band-widths $\Delta\omega$. In the Ratio, the Amplitude is taken as the amplitude of the analyzed orbit which is given by the maximum value of the orbit in the corresponding region. The graphs in the figure are for the *maxmax* orbit of the case.

From the plots it is observed that there is not a difference in how the filter is less or more effective with the APJ region, neither there is a difference with respect to the transverse plane involves. Additionally, for this particular case, two normal quadrupole magnetic errors (which imply narrow peaks in the frequency spectra), there is not a single optimum band-width, it is observed that as the bandwidth is getting shorter, the greater the amount of noise that is reduced.

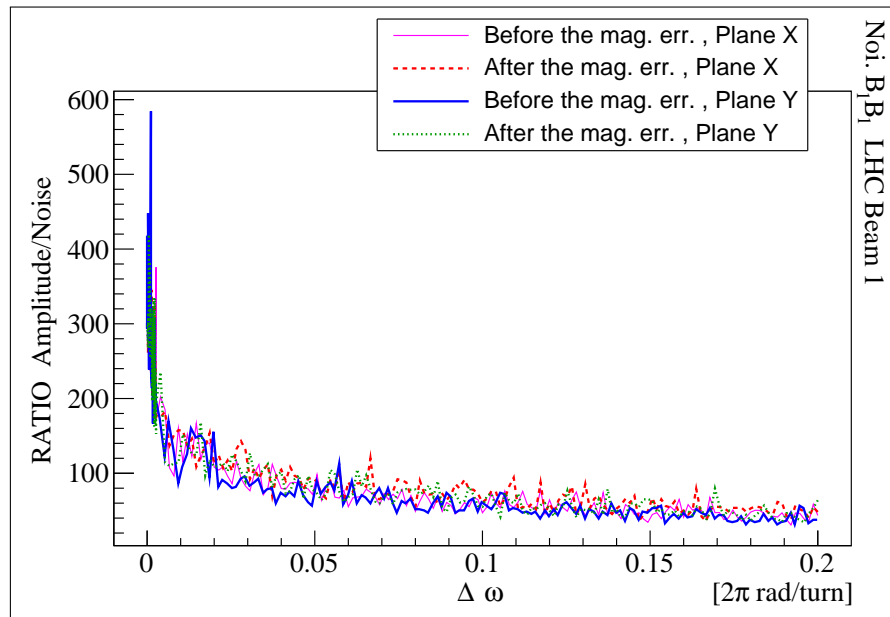


Figure 5-5.: Ratio Amplitude/Noise against the Band-Width for the *Band* Filter. Results for the regions before and after the location of the magnetic error in the transverse planes X and Y.

These studies for the Ratio allow to evaluate the quality of the filter, more than just to identify if the filter reduce the noise or not. This because it could be possible that the noise decreases with the amount of signal that the filter always takes, and at the end, the final

signal (after it had been filtered) obtained gives less information than the case of the signal with just noise added.

All the previously described studies are important because the efficiency of the filter is independent on the APJ, the technique used to measure the magnetic errors. And, it was obtained that the band-pass filter decreases the noise as its bandwidth becomes shorter, in this way the filter is getting more efficient as its bandwidth reduces in size.

Also it was studied the sensitivity of the filter with the frequency. This was done in two ways, the first one, by taking the signal as the obtained from the simulator orbits, and the second, by taking a fictitious sinusoidal signal. In the first case, the function MATCH of MAD-X is used to obtain fractions between 0.0 and 0.5 for the accelerator tune; the trajectories are obtained after 1000 turns, noise with a normal distribution is added, and then the orbits are selected. In the second case, the fictitious signal was created as a specific sinusoidal with a phase distribution closes to the obtained from the simulated orbit; noise is then added as other sinusoidal signals but with a lesser amplitude. In both cases it was found that the filter is effective.

5.3. Different Ways to Reduce Noise in the Orbits by applying Digital Filters.

The different ways explored to reduce noise during this dissertation, correspond to the several combinations of the digital filters which have been already tested to be effective in the reduction of noise in the LHC orbits.

These filters are:

- Filter obtained as the Average of many orbits, as reported in [3], in here denoted by **Prom**. The suitable final orbit is able to be obtained even for experimental orbits.
- Band-pass Filter, developed for this dissertation, described at the beginning of this chapter and reported in [41], where trials for orbits with noise from normal distribution and uniform distribution are introduced. In here this filter is denoted by **Band**.
- Filter from the Singular Values Decomposition, as reported in [43], in here denoted by **Svd**. Studies during this dissertation started with 100 singular values, and then with 10, 8, and 4 (best for two K_1 errors), agreed with what is reported in [43] and in all cases the results presented in this dissertation are obtained using 8 singular values. This is done in an effort to compare to the techniques developed and used in the LHC and the taken program is *svd_clean.py* (version at 2011).

Therefore the combinations of filters are seven. For this dissertation these different ways to reduce noise are denoted by:

1. **Prom**
2. **BandProm**
3. **BandSvdProm**
4. **Band**
5. **Svd**
6. **SvdProm**
7. **SvdBandProm**

Where each combination of names indicates the hierarchy or sequence that is followed to obtain the final filtered orbits, the first applied filter is the one with the name more at the left. For example the combination denoted by *BandProm* implies that the original orbits which includes noise are filtered first using the *Band* filter and immediately the resulted orbits are filtered using the filter *Prom*.

Nevertheless, before presenting the results for the different ways to reduce the noise, which are developed in the following chapters, some tools are implemented and presented below. This is because most of the filters have as an outcome a turn-by-turn orbit, generally with the same amount of orbits or turns that the one initially given as input, while the filter *Prom* gives as an output a single orbit.

When using the Action and Phase Jump method, as mentioned before, four types of orbits are obtained from the turn-by-turn orbit. Therefore after filtering the orbits, with filters different than *Prom*, the selection of the orbits have to be done. According to the theory, the orbits must be selected taking into account that the phase of the selected orbit ψ_0 is equal or relatively close to the phase ψ_d of the point in the accelerator where the magnetic error is measured.

Two approaches were developed to select the orbits without using *Prom*, these are called **Best** and **Sel1**. In Figure 5-5, presented above, the selection of the orbit *maxmax* is made using the *Sel1* option, although similar results were obtained from the orbits selected in other ways.

In all cases the selection of the single orbit is performed from a reference phase ψ_0 , given by the expected phase at the APJ region which contains the magnetic errors.

The selection of the orbits made by *Best* is based in the minimization of:

$$\sqrt{(\psi_{x,0} - \psi_{x,d})^2 + (\psi_{y,0} - \psi_{y,d})^2} \quad (5-5)$$

which is given as distance for the two transverse planes X and Y.

The selection of the orbits made by *Sell* is based on the idea that the planes has an opposite relation, if the difference in phase ($\psi_0 - \psi_d$) in X is maximum then the difference in Y must be a minimum. Therefore the quantity used to minimize is:

$$|\psi_{x,0} - \psi_{x,d}| - |\psi_{y,0} - \psi_{y,d}| \quad (5-6)$$

Both selections were tested during this dissertation and the values obtained for the magnetic errors were almost similar and close to the expected values installed in the LHC simulator for beam 1. Some differences are observed when noise is included but, unless specified, in the following chapters, the reported results are made with the selection *Best*. The selection of the orbits starts with orbits which have a phase as far as ± 0.5 rad from the expected phase.

On the other hand, there are some comments about the filter *Band*, to tell. A difficulty found when using *Band* is to obtain an optimal bandwidth, as it is observed in the following chapters.

Even more, from the trials changing the transverse tunes, in the range 0.0 to 0.5, it was found that the optimal bandwidth is different for each tune case, and later also with the formulation of APJ which is used to obtain the magnetic errors. However, for some of the combinations of filters, the optimal bandwidth is reduced to a smaller range.

Nevertheless, as expected, the trials showed that the filter *Band* has the advantage of reduce or eliminate orbits which have frequency values further from the central frequency of the filter. Even though, during the process, some Fourier frequencies values close to the central frequency change a little bit, so the filter selection is not perfect. This last does not seem to be a problem to obtain the magnetic errors using the APJ method.

In any case, it is expected to plot some calibration graphs before doing the analysis of experimental data. These plots are to obtain the most suitable bandwidth and are discussed and presented during this dissertation, in the following chapters.

An extension of what can be used to filter the orbits are the filters used in the LHC besides the Svd. One of them is the *window* type filter, although it is mainly development to take out the constant part of the signal, which is not necessary to reduce noise. This is left for further investigations.

6. Reformulation of the APJ, and Orbits Analysis

This chapter is one of the core chapters for this dissertation. It contains the main aspects developed for the reformulation of the Action and Phase Jump Method and its corresponding results on simulated orbits. It is divided in four main sections. The first two present the theoretical development of the new formulation, while the last two subsections present the results of the comparison using both formulations.

For the theoretical part, it is recommended to have done a previous review of the precedent chapter. The reformulation presented in here is based on the concepts already explained in this dissertation, which are taken as granted. First, the equations for the removal of the BPM dependency are introduced. Then the equations which include the quadrupole phase advances are introduced.

The comparison between the formulations is performed using simulated orbits, which are considered the ideal orbits to test the deduced theoretical equations. Because the method is developed for analysis on experimental orbits, trials using a normal distribution to add noise to the ideal orbit were performed. In the last part of this chapter, the results of the analysis are presented. First a direct comparison of the formulations is made and then the results for the different ways to reduce noise are presented. The simulated orbits are obtained using the MAD-x simulator of the LHC.

6.1. Theoretical Equations Removing the Central BPM Dependency

To measure the quadrupole magnetic errors in an IR, the APJ method uses the BPMs at the Arc previous to the error region, and the Arc after it. As mentioned before, the Action and Phase variables along the accelerator are obtained from these measurements.

Afterwards, from the Action (J) and Phase δ variables, before and after the magnetic error, the observed kick for the orbit, can be determined. The relation to obtain that quantity is

(equation (15) in [2]), which is:

$$\theta_z = \sqrt{\frac{2J_0 + 2J_1 - 4\sqrt{J_0J_1} \cos(\delta_1 - \delta_0)}{\beta_z(s_\theta)}} \longrightarrow \theta_z \sqrt{\beta_{s\theta}} = \sqrt{2J_0 + 2J_1 - 4\sqrt{J_0J_1} \cos(\delta_1 - \delta_0)} \quad (6-1)$$

where the values J_n , δ_n are the average of the measurements before and after the magnetic error region.

And at the same time for the X plane, for instance, $\theta_x = -B_1x + A_1y$, hence, the transverse positions x, y are needed to obtain the magnetic errors B_1 and A_1 . As described in the previous chapter, the transverse position at the error region is inferred from one BPM measurement at the IR [32]. In some cases, this BPM measurement can become the biggest source of uncertainty when the action and phase jump technique is used, because it is a single measurement and also because the high noise that LHC BPM system has for low bunch crossing measurements, which is the configuration for the magnetic error measurements.

The central BPM dependency is given by the measurement taken for the error positions x, y , given explicitly in equation (4-10). The reformulation consists in to change the total kick produced in the orbit by the magnetic error, equation (6-1) or (4-6), given by the dependency to the magnetic strength multipolar components, to end up obtaining an expression where the error position is not included.

The changes start by including more than one source of magnetic error. From the theoretical trajectory after the magnetic error (reported in Table 4-1):

$$\begin{aligned} z(s) &= \sqrt{2J_1\beta_{z(s)}} \sin(\psi_{z(s)} - \delta_1) \\ z(s) &= \sqrt{2J_0\beta_{z(s)}} \sin(\psi_{z(s)} - \delta_0) + \theta_z \sqrt{\beta_{z(s)}\beta_{s\theta}} \sin(\psi_{z(s)} - \psi_{s\theta}) \end{aligned} \quad (6-2)$$

but assuming that many magnetic errors are presented, so equation (11) in [] is obtained

$$\begin{aligned} z(s) &= \sqrt{2J_1\beta_{z(s)}} \sin(\psi_{z(s)} - \delta_1) \\ z(s) &= \sqrt{2J_0\beta_{z(s)}} \sin(\psi_{z(s)} - \delta_0) + \sum_i \theta_{z,i} \sqrt{\beta_{z(s)}\beta_{s\theta,i}} \sin(\psi_{z(s)} - \psi_{s\theta,i}) \end{aligned} \quad (6-3)$$

and the sum is over the number of magnets, each one denoted by i .

If, by first approximation it is considered that the phase advance does not change along the IR region, or that the change is almost null, the factor $\sin(\psi_{z(s)} - \psi_{s\theta,i})$ is $\sin(\psi_{z(s)} - \psi_{s\theta})$

and can be taken out of the sum, therefore

$$\begin{aligned} z(s) &= \sqrt{2J_1\beta_{z(s)}} \sin(\psi_{z(s)} - \delta_1) \\ z(s) &= \sqrt{2J_0\beta_{z(s)}} \sin(\psi_{z(s)} - \delta_0) + \sin(\psi_{z(s)} - \psi_{s\theta}) \sum_i \theta_{z,i} \sqrt{\beta_{z(s)}\beta_{s\theta,i}} \end{aligned} \quad (6-4)$$

Even more, the terms can be organized in a similar way performed in the original formulation described in section 4.1. The sinusoidals are expressed as the trigonometric sum of the product of sinusoidal functions:

$$\begin{aligned} z(s) &= \sqrt{2J_1\beta_{z(s)}} \sin(\psi_{z(s)} - \delta_1) = \sqrt{2J_1\beta_{z(s)}} [\sin(\psi_{z(s)}) \cos(\delta_1) - \cos(\psi_{z(s)}) \sin(\delta_1)] \\ z(s) &= \sqrt{2J_0\beta_{z(s)}} [\sin(\psi_{z(s)}) \cos(\delta_0) - \cos(\psi_{z(s)}) \sin(\delta_0)] + \\ &\quad + [\sin(\psi_{z(s)}) \cos(\psi_{s\theta}) - \cos(\psi_{z(s)}) \sin(\psi_{s\theta})] \sum_i \theta_{z,i} \sqrt{\beta_{z(s)}\beta_{s\theta,i}} \end{aligned} \quad (6-5)$$

therefore, taking the coefficients for $\sin(\psi_{z(s)})$ separately from the coefficients of $\cos(\psi_{z(s)})$, the final system of equations is:

$$\sqrt{2J_1\beta_{z(s)}} \cos(\delta_1) = \sqrt{2J_0\beta_{z(s)}} \cos(\delta_0) + \cos(\psi_{s\theta}) \sum_i \theta_{z,i} \sqrt{\beta_{z(s)}\beta_{s\theta,i}} \quad (6-6)$$

$$\sqrt{2J_1\beta_{z(s)}} \sin(\delta_1) = \sqrt{2J_0\beta_{z(s)}} \sin(\delta_0) + \sin(\psi_{s\theta}) \sum_i \theta_{z,i} \sqrt{\beta_{z(s)}\beta_{s\theta,i}} \quad (6-7)$$

Using the trigonometric identity for sinusoidals of δ_1 and taking $\sin(\delta_1)$ from equation (6-7) and $\cos(\delta_1)$ from equation (6-6), after simplifying it is obtained that

$$J_1 = J_0 + \sqrt{2J_0} \cos(\psi_{s\theta} - \delta_0) \sum_i [\theta_{z,i} \sqrt{\beta_{s\theta,i}}] + \frac{1}{2} \left[\sum_i \theta_{z,i} \sqrt{\beta_{s\theta,i}} \right]^2 \quad (6-8)$$

On the other hand, multiplying equation (6-6) by $\sin(\delta_0)$ and equation (6-7) by $\cos(\delta_0)$, some terms are simplified and the final expression is:

$$\sqrt{2J_1} \cos(\delta_1 - \delta_0) = \sqrt{2J_0} + \cos(\psi_{s\theta} - \delta_0) \sum_i [\theta_{z,i} \sqrt{\beta_{s\theta,i}}] \quad (6-9)$$

and in this last equation the term $\cos(\psi_{s\theta} - \delta_0) \sum_i [\theta_{z,i} \sqrt{\beta_{s\theta,i}}]$ is obtained from equation (6-8), so

$$\sqrt{2J_1} \cos(\delta_1 - \delta_0) = \sqrt{2J_0} + \frac{J_1}{\sqrt{2J_0}} - \frac{J_0}{\sqrt{2J_0}} - \frac{1}{2\sqrt{2J_0}} \left[\sum_i \theta_{z,i} \sqrt{\beta_{s\theta,i}} \right]^2 \quad (6-10)$$

therefore

$$2J_1 + 2J_0 - 4\sqrt{J_0J_1} \cos(\delta_1 - \delta_0) = \left[\sum_i \theta_{z,i} \sqrt{\beta_{s\theta,i}} \right]^2 \quad (6-11)$$

and a final result very close to equation (6-1) is obtained

$$\sqrt{2J_0 + 2J_1 - 4\sqrt{J_0 J_1} \cos(\delta_1 - \delta_0)} = \sum_i [\theta_{z,i} \sqrt{\beta_{z,i}(s_\theta)}] \quad (6-12)$$

A way to understand this last equation is to notice that the magnetic error strength is given by equation (6-1) but applied to every magnetic error i independently.

From the trajectory solution in the region of the magnetic error, given by the theoretical development of the APJ method,

$$z(s_j) = \sqrt{2J_{z,0} \beta_z(s_j)} \sin(\psi(s_j) - \delta_0) \quad (6-13)$$

the *kick* can be expressed as:

$$\begin{aligned} \theta_{x,i} &= B_{0,i} - B_{1,i} m_{s_i^\varepsilon, x} \sqrt{\beta_{x, s_i^\varepsilon}} + A_{1,i} m_{s_i^\varepsilon, y} \sqrt{\beta_{y, s_i^\varepsilon}} + 2A_{2,i} m_{s_i^\varepsilon, x} \sqrt{\beta_{x, s_i^\varepsilon}} m_{s_i^\varepsilon, y} \sqrt{\beta_{y, s_i^\varepsilon}} + \dots \\ \theta_{y,i} &= A_{0,i} + A_{1,i} m_{s_i^\varepsilon, x} \sqrt{\beta_{x, s_i^\varepsilon}} + B_{1,i} m_{s_i^\varepsilon, y} \sqrt{\beta_{y, s_i^\varepsilon}} + 2B_{2,i} m_{s_i^\varepsilon, x} \sqrt{\beta_{x, s_i^\varepsilon}} m_{s_i^\varepsilon, y} \sqrt{\beta_{y, s_i^\varepsilon}} + \dots \end{aligned} \quad (6-14)$$

where a new variable is defined as:

$$m_{j,z} = \sqrt{2J_{z,0}} \sin(\psi_{z(s_j)} - \delta_{z,0}) \quad \text{therefore} \quad z(s_j) = m_{j,z} \sqrt{\beta_{z,j}} \quad (6-15)$$

Taking the equal side of the previous equations, the reformulation presented as a system of equations is:

$$\begin{aligned} &\sqrt{2J_{x,0} + 2J_{x,1} - 4\sqrt{J_{x,0} J_{x,1}} \cos(\delta_{x,1} - \delta_{x,0})} = \\ &\sum_i \left[B_{0,i} \sqrt{\beta_{x, s_i^\varepsilon}} - B_{1,i} m_{s_i^\varepsilon, x} \beta_{x, s_i^\varepsilon} + A_{1,i} m_{s_i^\varepsilon, y} \sqrt{\beta_{y, s_i^\varepsilon}} \beta_{x, s_i^\varepsilon} + 2A_{2,i} m_{s_i^\varepsilon, x} \beta_{x, s_i^\varepsilon} m_{s_i^\varepsilon, y} \sqrt{\beta_{y, s_i^\varepsilon}} + \dots \right] \\ &\sqrt{2J_{y,0} + 2J_{y,1} - 4\sqrt{J_{y,0} J_{y,1}} \cos(\delta_{y,1} - \delta_{y,0})} = \\ &\sum_i \left[A_{0,i} \sqrt{\beta_{y, s_i^\varepsilon}} + A_{1,i} m_{s_i^\varepsilon, x} \sqrt{\beta_{y, s_i^\varepsilon}} \beta_{x, s_i^\varepsilon} + B_{1,i} m_{s_i^\varepsilon, y} \beta_{y, s_i^\varepsilon} + 2B_{2,i} m_{s_i^\varepsilon, x} \sqrt{\beta_{x, s_i^\varepsilon}} m_{s_i^\varepsilon, y} \beta_{y, s_i^\varepsilon} + \dots \right] \end{aligned} \quad (6-16)$$

In this system, the left hand side in the equations depends only on measured quantities, while at the right hand side the values taken from the model of the accelerator are presented, the unknowns of the system and the phases δ_0 . In this way, if all the variables on the left hand side are obtained from more than one measurement, there is an intrinsic improvement of the reformulation compared to the old one.

Taking the most general case, to obtain the magnetic errors for a triplet, in the LHC, the composed by two normal quadrupole magnetic errors and one skew quadrupole error ([34]),

the reformulated equations imply that:

$$\begin{aligned}
& \sqrt{2J_{x,0} + 2J_{x,1} - 4\sqrt{J_{x,0}J_{x,1}} \cos(\delta_{x,1} - \delta_{x,0})} = \\
& \quad \hat{\beta}_{K_{1s}} m_{s,y} \mathbf{K}_{1s} - \hat{\beta}_{x,K_{1,I}} m_{K_{1I},x} \mathbf{K}_{1,I} - \hat{\beta}_{x,K_{1,II}} m_{K_{1II},x} \mathbf{K}_{1,II} \\
& \sqrt{2J_{y,0} + 2J_{y,1} - 4\sqrt{J_{y,0}J_{y,1}} \cos(\delta_{y,1} - \delta_{y,0})} = \\
& \quad \hat{\beta}_{K_{1s}} m_{s,x} \mathbf{K}_{1s} + \hat{\beta}_{y,K_{1,I}} m_{K_{1I},y} \mathbf{K}_{1,I} + \hat{\beta}_{y,K_{1,II}} m_{K_{1II},y} \mathbf{K}_{1,II}
\end{aligned} \tag{6-17}$$

where

$$\hat{\beta}_{z,t} = \int \beta_z ds \quad \text{for} \quad t = \mathbf{K}_{1,I}, \mathbf{K}_{1,II} \tag{6-18}$$

$$m_{s,z} = m_{K_{1s},z} \quad \text{and} \quad \hat{\beta}_{K_{1s}} = \int \sqrt{\beta_x \beta_y} ds / L_s \tag{6-19}$$

where L_s is the length for the skew quadrupole.

In equation (6-17), the notation and units correspond to the nomenclature in MAD-X [5]. These are: K_1 , for *The normal quadrupole coefficient* and K_{1s} for *The skew quadrupole coefficient*), respectively.

To obtain the magnetic errors an additional step have to be done. The system of equations are composed by only two equations while the unknowns are $\mathbf{K}_{1,I}$, $\mathbf{K}_{1,II}$, \mathbf{K}_{1s} . To overcome this issue, a couple of orbits are used to obtain the magnetic errors. These orbits are taking from the 4 type selected orbits, mentioned earlier.

For this dissertation, the final system of equations was solved numerically, and the final magnetic error for each TBT orbit was taken as the average of the four combinations of a couple of orbits that are available. The numerical function used is *linalg.solve* implemented in the PYTHON library [42].

Alternatively, there is a possibility of solving the system in an explicit way. In that case the system of equations obtained is:

$$\begin{aligned}
\mathbf{K}_{1,I} &= \frac{k_x \hat{\beta}_{y,II} - k_y \hat{\beta}_{x,II}}{\hat{\beta}_{x,I} \hat{\beta}_{y,II} - \hat{\beta}_{x,II} \hat{\beta}_{y,I}} \\
\mathbf{K}_{1,II} &= \frac{k_x \hat{\beta}_{y,I} - k_y \hat{\beta}_{x,I}}{\hat{\beta}_{x,II} \hat{\beta}_{y,I} - \hat{\beta}_{x,I} \hat{\beta}_{y,II}} \\
\mathbf{K}_{1s} &= \frac{-T_{y,d} M_{y,f} + T_{y,f} M_{y,d}}{\hat{\beta}_{K_{1s}} (M_{x,f} M_{y,d} - M_{x,d} M_{y,f})}
\end{aligned} \tag{6-20}$$

where

$$k_x = \frac{T_{x,d}M_{y,f} - T_{x,f}M_{y,d}}{-M_{x,d}M_{y,f} + M_{x,f}M_{y,d}} \quad (6-21)$$

$$k_y = \frac{T_{y,d}M_{x,f} - T_{y,f}M_{x,d}}{M_{y,d}M_{x,f} - M_{y,f}M_{x,d}} \quad (6-22)$$

$$\text{where } M_{z,t} = \sqrt{2J_{z,0}^t \sin(\psi(s_{z,E}) - \delta_{z,0}^t)} \quad (6-23)$$

$$T_{z,t} = \sqrt{2J_{z,0}^t + 2J_{z,1}^t - 4\sqrt{J_{z,0}^t J_{z,1}^t} \cos(\delta_{z,1}^t - \delta_{z,0}^t)} \quad (6-24)$$

for the pair of chosen orbits $t = \{d, f\}$, in each of the transverse planes $z \in \{x, y\}$ and the Courant-Snyder parameters in the triplet according to the label in subscript E .

The magnetic errors measured using APJ are obtained for the IR triplets, and the above relations are valid for any triplet, independently.

In particular for the LHC, there is a change in phase advance of almost π rad, between the triplets at the left and right of the IP. The reformulation presented was obtained taking into account that the selected orbits are in certain phase with all the quadrupoles at the same time. If quadrupoles at the right triplet are chosen as a corrector but the orbit is selected for a magnetic error at the left triplet, a change in of $-\pi$ rad in the quadrupole phase advance must be included, inversely, an orbit selected for a magnetic error at the right triplet implies that the phase advance of a quadrupole at the left triplet must be corrected to have π rad more.

Therefore, for the LHC lattice the above equations can be used with quadrupoles at the left triplet and at the right triplet, at the same time.

On the other hand, the system can be solved explicitly when the analyzed case is of only two normal quadrupole errors K_1 . Even more, the calculation can be made from just one orbit. The magnetic errors are obtained from the following relations:

$$\begin{aligned} K_{1,I} &= \frac{k_x \hat{\beta}_{y,II} + k_y \hat{\beta}_{x,II}}{\hat{\beta}_{x,II} \hat{\beta}_{y,I} - \hat{\beta}_{y,II} \hat{\beta}_{x,I}} \\ K_{1,II} &= \frac{k_x \hat{\beta}_{y,I} + k_y \hat{\beta}_{x,I}}{-\hat{\beta}_{x,II} \hat{\beta}_{y,I} + \hat{\beta}_{y,II} \hat{\beta}_{x,I}} \end{aligned} \quad (6-25)$$

where $k_z = \frac{\sqrt{2J_{z,0} + 2J_{z,1} - 4\sqrt{J_{z,0} J_{z,1}} \cos(\delta_{z,1} - \delta_{z,0})}}{\sqrt{2J_{z,0} \sin(\psi_{z,E} - \delta_{z,0})}}$ and the sub-index E corresponds to the longitudinal position of the triple that contains the quadrupoles or magnetic errors.

The results using this reformulation of the Action and Phase method are presented below with simulated orbits and in the next chapter for the experimental orbits.

6.2. Theoretical Equations Including Different Phase Advances at the Quadrupoles Triplets

Two different approximations are established to take into account the case where the phase advances of the quadrupoles at the triplets of the LHC IRs are not equal.

The first option is considering the total *kick* as the directly sum of the oscillations produced for each magnetic error individually.

This development is done for the case of the betatron oscillations induced by two quadrupole magnetic errors from the same LHC triplet. The theoretical approach is to follow what it is stated in [14].

Starting with the position after the error given by the APJ method (Table 4-1)

$$z(s) = \sqrt{2J_0\beta_{z(s)}} \sin(\psi_{z(s)} - \delta_0) + \theta_z \sqrt{\beta_s\beta_{s\theta}} \sin(\psi_s - \psi_{s\theta}) \quad (6-26)$$

the individual contribution of the magnetic errors is therefore given by $\theta_z \sqrt{\beta_s\beta_{s\theta}} \sin(\psi_s - \psi_{s\theta})$.

For the two magnetic errors a and b , if only the linear quadrupole error component is taking into account, the change in the orbit in the horizontal plane is given by

$$x(s) = -B_1^a \sqrt{\beta_x\beta_{xa}} x_a \sin(\psi_x - \psi_{xa}) - B_1^b \sqrt{\beta_x\beta_{xb}} x_b \sin(\psi_x - \psi_{xb}) \quad (6-27)$$

these contributions can be added as they were phasors, therefore the total change in the orbit due to the presence of the linear quadrupole magnetic errors is:

$$x(s) = -\sqrt{B_1^a B_1^b} \sqrt{\beta_x(s)} \sqrt{\beta_{xa}\beta_{xb}} x_{eqv} \sin(\psi_{eqvi}) \quad (6-28)$$

where

$$x_{eqv}^2 = x_a^2 \sqrt{\frac{\beta_{xa} B_1^a}{\beta_{xb} B_1^b}} + x_b^2 \sqrt{\frac{\beta_{xb} B_1^b}{\beta_{xa} B_1^a}} + 2x_a x_b \cos(\psi_{xa} - \psi_{xb})$$

$$\text{and } \psi_{eqvi} = \tan^{-1} \left(\frac{B_1^a \sqrt{\beta_{xa}} x_a \sin(\psi_{xa}) + B_1^b \sqrt{\beta_{xb}} x_b \sin(\psi_{xb})}{B_1^a \sqrt{\beta_{xa}} x_a \cos(\psi_{xa}) + B_1^b \sqrt{\beta_{xb}} x_b \cos(\psi_{xb})} \right)$$

The distortion of the orbit in the phase-space can also be obtained. This is done as a first approximation of the derivative of the transverse position: $x' = \frac{x(s)}{\Delta s} = \frac{\partial x}{\partial s}$, and at the same time $\Delta s = \beta \Delta \phi$ provided that the β -function inside the quadrupole is almost constant.

After the mathematical procedure, the total magnetic error can be expressed in terms of the total orbit distortion $\theta = -B_1 x$, and the corresponding magnetic error is given by

$$B_1 = \frac{1}{\beta_x(s)} \left[\frac{\Delta \beta(s)}{4\beta_x(s)\Delta \psi(s)} \right] \quad (6-29)$$

from the theoretical relations in accelerator physics expected for the RMS β -beating, the corrector strength is given by:

$$B_1 \approx \frac{1}{\beta_x(s)} \left[\frac{\sqrt{(B_1^a)^2 \beta_{xa}^2 + (B_1^b)^2 \beta_{xb}^2}}{4(2\sqrt{2}|\sin(2\pi\nu_x)|)\Delta \psi_x(s)} \right] \quad (6-30)$$

where ν_x is the decimal part of the horizontal transverse tune.

This same procedure can be followed for the vertical plane and the results is the similar when the vertical plane is evaluated in the variables. In both cases, with only one corrector the two magnetic errors are taking into account.

Analogously, the procedure can be followed to obtain a single skew quadrupole error from two skew quadrupole errors. The result is the same as given by equation (6-30).

Sometimes the measurement of $\Delta \psi_x(s)$ and $\beta_x(s)$ at the equivalent error position can be a difficult task or with a large inaccuracy during the experiment. Also, ideally the formulation will be inversible for instance to get magnetic strength corrections at some quadrupoles from an equivalent point in the accelerator, but in the equations are not. Therefore this approach is impracticable.

Even more, when taking directly the result for the orbit given by (6-28), the equivalent phase not necessary implies an available measurement position in the accelerator, therefore a procedure as described above is also a non-practical way to measure magnetic errors, although it is a base to calculate the errors.

Secondly, an alternative way to include the case that the phases advances at the triplet quadrupoles are different is to express the correction of the magnetic errors as the values to cancel the magnetic errors measured inside a LHC triplet, inside the theoretical expressions.

Starting, again, from the position after the magnetic error, equation (6-26), for single turn analysis:

$$z(s) = \sqrt{2J_0\beta_{z(s)}} \sin(\psi_{z(s)} - \delta_0) + \sum_i \theta_{z,i} \sqrt{\beta_s\beta_{s\theta,i}} \sin(\psi_s - \psi_{s\theta,i}) \quad (6-31)$$

the distortion of the orbit is taken as the sum of distortions produced by many quadrupoles that after the correction are canceled, therefore:

$$\sum_i \theta_{z,i} \sqrt{\beta_s\beta_{s\theta,i}} \sin(\psi_s - \psi_{s\theta,i}) = 0 \quad (6-32)$$

if two correctors are chosen to overcome the magnetic error at a certain position close to those quadrupoles, only three contributions to the distortion are obtained:

$$\theta_{z,a} \sqrt{\beta_s\beta_{s\theta,a}} \sin(\psi_s - \psi_{s\theta,a}) + \theta_{z,b} \sqrt{\beta_s\beta_{s\theta,b}} \sin(\psi_s - \psi_{s\theta,b}) + \Theta_z \sqrt{\beta_s\beta_{s\theta}} \sin(\psi_s - \psi_{s\theta}) = 0 \quad (6-33)$$

and if the *kick* produced for the quadrupoles are replaced, the equations for each are summarized in:

$$\begin{aligned} sgn_z z_a B_{1,a} \sqrt{\beta_s\beta_{s\theta,a}} \sin(\psi_s - \psi_{s\theta,a}) + sgn_z z_b B_{1,b} \sqrt{\beta_s\beta_{s\theta,b}} \sin(\psi_s - \psi_{s\theta,b}) + \\ + \Theta_z \sqrt{\beta_s\beta_{s\theta}} \sin(\psi_s - \psi_{s\theta}) = 0 \end{aligned} \quad (6-34)$$

where sgn_z is +1 if the equation is written for the plane $z=Y$ and -1 if the equation is written for the plane $z=X$, according to the multipolar expansion of the magnetic field and their kick produced, as mentioned earlier (equation 4-7).

Expanding each sinusoidal function as product of sinusoids

$$\begin{aligned} sgn_z z_a B_{1,a} \sqrt{\beta_s\beta_{s\theta,a}} [\sin(\psi_s) \cos(\psi_{s\theta,a}) - \cos(\psi_s) \sin(\psi_{s\theta,a})] + sgn_z z_b B_{1,b} \sqrt{\beta_s\beta_{s\theta,b}} [\sin(\psi_s) \times \\ \times \cos(\psi_{s\theta,b}) - \cos(\psi_s) \sin(\psi_{s\theta,b})] + \Theta_z \sqrt{\beta_s\beta_{s\theta}} [\sin(\psi_s) \cos(\psi_{s\theta}) - \cos(\psi_s) \sin(\psi_{s\theta})] = 0 \end{aligned}$$

Taking the coefficients for the sinusoidals of ψ_s given by the orthogonal properties, a couple of equations are obtained, where a division by β_s is done previously

$$\begin{aligned} sgn_z z_a B_{1,a} \sqrt{\beta_{s\theta,a}} \cos(\psi_{s\theta,a}) + sgn_z z_b B_{1,b} \sqrt{\beta_{s\theta,b}} \cos(\psi_{s\theta,b}) + \Theta_z \sqrt{\beta_{s\theta}} \cos(\psi_{s\theta}) = 0 \\ sgn_z z_a B_{1,a} \sqrt{\beta_{s\theta,a}} [-\sin(\psi_{s\theta,a})] + sgn_z z_b B_{1,b} \sqrt{\beta_{s\theta,b}} [-\sin(\psi_{s\theta,b})] + \Theta_z \sqrt{\beta_{s\theta}} [-\sin(\psi_{s\theta})] = 0 \end{aligned} \quad (6-35)$$

And as before, each position z_i at the quadrupoles can be obtained from the Action and Phase method, equation (6-13), and using the notation given by equation (6-15), which is $z(s_j) = m_{j,z} \sqrt{\beta_{z,j}}$, all the positions z_i in each corresponding plane are determinated. Also,

the *kick* produced by the magnetic errors in the orbits, Θ_z can be obtained from the APJ method using equation (6-1). Therefore the system of equations to solve is:

$$\begin{aligned}
& -m_{a,x}\beta_{x,a}B_{1,a}\cos(\psi_{x,a}) - m_{b,x}\beta_{x,b}B_{1,b}\cos(\psi_{x,b}) + \frac{\sqrt{2J_0^x + 2J_1^x - 4\sqrt{J_0^x J_1^x}\cos(\delta_1^x - \delta_0^x)}}{\cos(\psi_{\theta,x})^{-1}} = 0 \\
& -m_{a,x}\beta_{x,a}B_{1,a}\sin(\psi_{x,a}) - m_{b,x}\beta_{x,b}B_{1,b}\sin(\psi_{x,b}) + \frac{\sqrt{2J_0^x + 2J_1^x - 4\sqrt{J_0^x J_1^x}\cos(\delta_1^x - \delta_0^x)}}{\sin(\psi_{\theta,x})^{-1}} = 0 \\
& m_{a,y}\beta_{y,a}B_{1,a}\cos(\psi_{y,a}) + m_{b,y}\beta_{y,b}B_{1,b}\cos(\psi_{y,b}) + \frac{\sqrt{2J_0^y + 2J_1^y - 4\sqrt{J_0^y J_1^y}\cos(\delta_1^y - \delta_0^y)}}{\cos(\psi_{\theta,y})^{-1}} = 0 \\
& m_{a,y}\beta_{y,a}B_{1,a}\sin(\psi_{y,a}) + m_{b,y}\beta_{y,b}B_{1,b}\sin(\psi_{y,b}) + \frac{\sqrt{2J_0^y + 2J_1^y - 4\sqrt{J_0^y J_1^y}\cos(\delta_1^y - \delta_0^y)}}{\sin(\psi_{\theta,y})^{-1}} = 0
\end{aligned} \tag{6-36}$$

The orbits selected using APJ, the 4-type orbits, can be used in the above equations, with the values of $\beta_{x,a}$, $\psi_{x,a}$, $\beta_{x,b}$ and $\psi_{x,b}$ given by the model of the accelerator. In this way for each orbit, four equations are written with $B_{1,a}$ and $B_{1,b}$ as the unknowns, taking into account the values of $\psi_{\theta,x}$, $\psi_{\theta,y}$ as the selected phases for each orbit.

From the results obtained with ideal orbits it is found that the best combinations of equations to obtain the magnetic errors are:

$$\begin{aligned}
& -m_{a,x}\beta_{x,a}B_{1,a}\sin(\psi_{x,a}) - m_{b,x}\beta_{x,b}B_{1,b}\sin(\psi_{x,b}) + \frac{\sqrt{2J_0^x + 2J_1^x - 4\sqrt{J_0^x J_1^x}\cos(\delta_1^x - \delta_0^x)}}{\sin(\psi_{\theta,x})^{-1}} = 0 \\
& m_{a,y}\beta_{y,a}B_{1,a}\cos(\psi_{y,a}) + m_{b,y}\beta_{y,b}B_{1,b}\cos(\psi_{y,b}) + \frac{\sqrt{2J_0^y + 2J_1^y - 4\sqrt{J_0^y J_1^y}\cos(\delta_1^y - \delta_0^y)}}{\cos(\psi_{\theta,y})^{-1}} = 0
\end{aligned} \tag{6-37}$$

For each quadrupole $\psi = \int_0^s [1/\beta(s)]ds$ is a calculated integral (the *Simpson's Rule* were used during this dissertation), and ψ_{θ} is given by the point error in the orbit selections. As mentioned above, when using magnets at the right triplet but with the orbit selected to be a maximum at the left triplet, it is necessary to take the phase advance of the right quadrupole as its corresponding value plus $-\pi$. Also, the magnetic errors recovery using MAD-x simulations are made with βB_1 equal to $\hat{\beta}K_1$ as given in the previous equations, see equation (6-18).

6.3. Comparison Reformulation and Old Formulation using Ideal Orbits

In this section the results for the analysis of simulated orbits when using the new formulation removing the central BPM measurement and the new formulation including the quadrupoles phase advances are presented. The orbits are obtained from the LHC simulator in MAD-x [5].

The results when using the new formulation of APJ, discussed previously in this chapter, are obtained from the numerical solution of the equations (6-17) and (6-37), and in this section the same orbits are used with the old formulation (equations (4-11) and (6-18)). The orbits are considering *ideal* because they are obtained from the same simulator used as the corresponding model and there is not included noise or different errors from the ones measured.

Initially, from simulations developed during this investigation, where three magnetic errors are included, (the same three used in most of the demonstrations in $K_1(Q2L5)$, $K_1(Q2R5)$, $K_{1s}(MQSL5)$), it have been checked up that the new formulation of the Action and Phase preserved the fact that the magnetic errors recovery is independently of the initial amplitude of the turn-by-turn orbits.

Table 6-1 shows the results for the relative errors to obtain the three magnetic errors at the LHC region IR5. The measurements are made for Beam 1 and Beam 2. For both formulations the integrals of the β -functions were used, for each corrector quadrupole.

Table 6-1.: Comparison of the Relative Errors when using the reformulation of the APJ (**New**) and the previous formulation (**Old**) to recover the Magnetic Errors.

sim. $\beta^* = 2.0 m$	$\Delta K_1(Q2L5)$ [%]	$\Delta K_1(Q2R5)$ [%]	$\Delta K_{1s}(MQSL5)$ [%]
Beam 1			
Old Formulation	0.163	0.663	0.524
New Formulation	0.484	0.209	0.323
Beam 2			
Old Formulation	0.248	0.619	0.323
New Formulation	0.682	0.418	0.282

Therefore, it was obtained that both formulations have accuracies, in general, similar and in

all the cases the recovery of the errors are within a 1 % range. However, taking a detailed look it is noticed that the new formulation improves mainly the recovery of the skew quadrupole error, and in general, taking into account the three quadrupoles at the same time, the new formulation is more accurate than the previous formulation, because its worst calculation compared to the older formulation is compensated by the better calculations of the other two magnetic errors.

Even more, when measured a single quadrupole magnetic error the direct advantage for the new formulation is evident, this is that the new formulation does not depend on the measurements of the BPMs at the IR; in fact a reduction in the relative error of the magnetic error measurement is also obtained. Simulations performing for Beam 1, with a magnetic error of 0.0001 m^2 at the LHC magnet MQXA.1L1 (using $\beta^* = 2.0 \text{ m}$), shows a change in the relative error from 0.2035 % (std 0.03407, taking as the statistical deviation of the measurement with 8 values) when all the BPMs measurements are presented, to 3.896 % (std 0.3607) when the BPMs measurements at the left triplet of IR1 had been removed. In both cases, the new formulation implies a relative error of 0.1734 % (std 0.009543). The difference in the old formulation results comes from the fact that in the first case the measurement taken as the central BPM is the measurement from BPMSW.1L1.B1, while in the second case the measurement is taken from BPMSW.1R1.B1. In the simulation, the results are obtained using the average of 8 orbits resulting from the 4-type orbits in each transverse plane, and the magnetic error calculation is made using the information from just one transverse plane each time, following the procedure mentioned earlier in equation (4-12).

On the other hand, a simulation of the LHC using the injection optics V6.5 ($\beta^* = 11.0 \text{ m}$), where the phase advances in the quadrupole triplets differ from one another is performed to recover two normal quadrupole magnetic errors at IR5. Using the reformulation which takes into account that the quadrupoles have a different phase advance and following the traditional formulation of the APJ, the recovery of the magnetic errors are done.

Table **6-2** presents the results for the relative errors in the recovery of the magnetic errors using ideal orbits obtained from the LHC simulator. In the first row, there are the results when the analysis of the orbits is done using the reformulation including the quadrupole phases (New-Ph) while in the second row the results obtained using the previous APJ formulation (Old) are presented.

From the results it is clear that the reformulation including the phase advances reduce the relative error in the recovery of the magnetic errors. The presented reduction is more than 50 % for each magnetic error, hence it is significant. Nevertheless, relative errors close to 4 % are obtained for a different example, therefore this approach is not suitable for the experimental analysis because the expected relative errors are below 1 % using ideal orbits.

Table 6-2.: Comparison of the reformulation including the quadrupole phases (New-Ph) and Old formulation, for the Recovery of Magnetic Errors.

sim. $\beta^* = 11.0 m$	$\Delta K_1(Q2L5)$ [%]	$\Delta K_1(Q2R5)$ [%]
Beam 1		
New-Ph	0.868	1.06
Old	4.10	10.7

From here and to the end of this paper, the reformulation is taken as the reformulation obtained from the removing of the central BPM dependency, mainly because the data and simulations developed for this dissertation are corresponding to the LHC with the configuration of low- β , when the phase advances of the quadrupoles at the LHC triplet are almost the same.

However, the phase of the quadrupoles is also taken into account in the systems of equations in the reformulation of APJ (equation (6-17)), but it is pointing out as well that there is the assumption that the single point of error is extended over the quadrupoles with the same phase advance.

Several simulations were performed using the APJ methods, especially for Beam 1. And although in the simulation not all what is happening in the experiment can be included, due to the complexity of the accelerator, the simulation reported above is closer to the experimental data taken on April 13th, 2010, at 12:54:09, 12:56:24 and 12:59:18 CEST. In the simulator the tunes were adjusted (after adding the magnetic errors) to the experimental tunes, using the function MATCH of MAD-x. The observed frequency spectra is closer to the experimental case, see appendix in [44].

Figure 6-1 shows the scheme followed to obtain the magnetic error at LHC using the Action and Phase method. The numbers are just a reference to the drawn scheme. The general description of the steps is below.

Module 1 is to create the multiple turns of 1000 or 2000 turns, this is done with the package MAD-x, and the output is converted to a file generally called *orbit.sdds.new*. Optionally, noise is added to each position using the Module 5 which takes the output from Mad-x and returns a file called *orbit.sdds.new* as before. In case of experimental orbits, Modules 1 and 5 are replaced for the experiment and it is expected to obtain an *orbit.sdds.new* file.

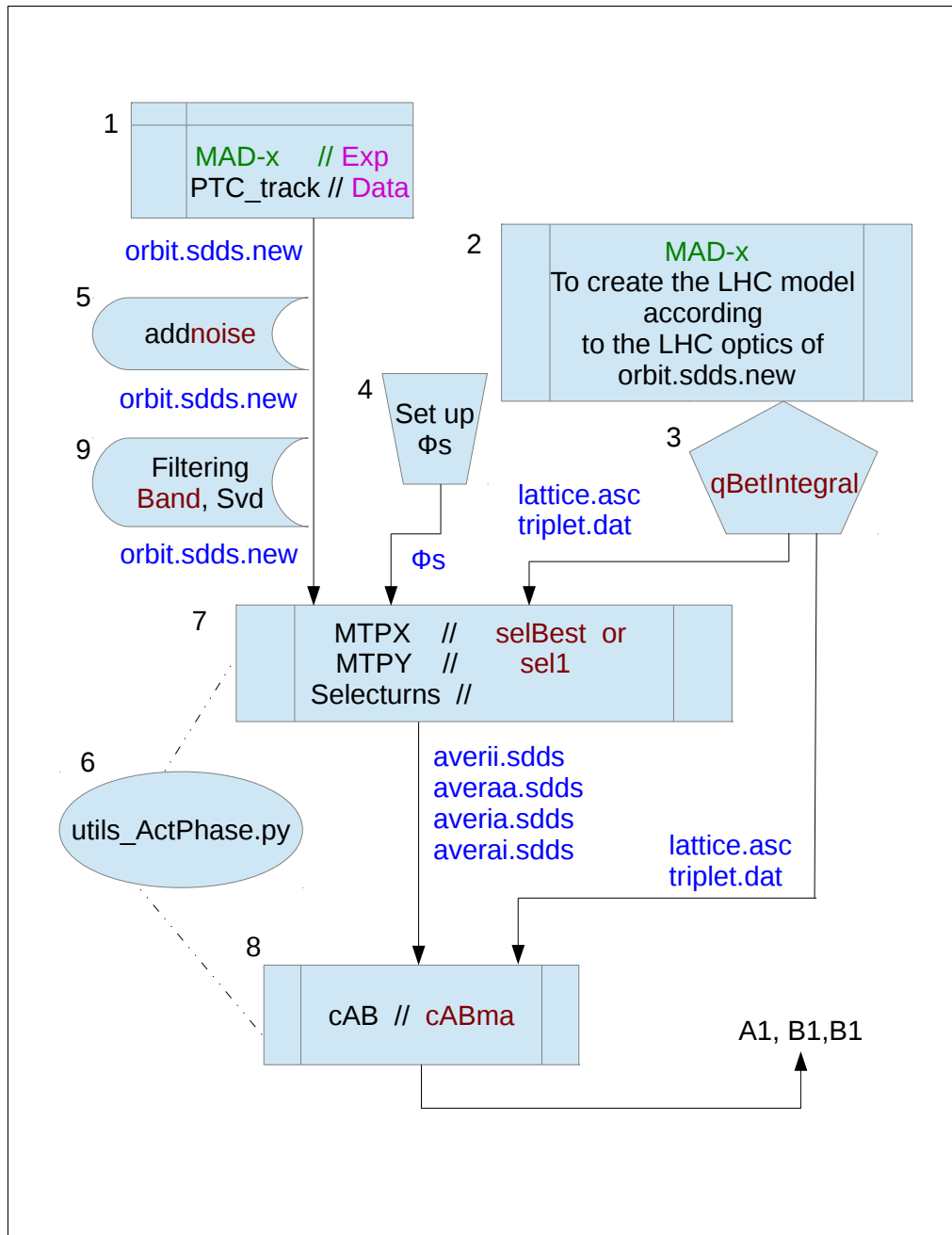


Figure 6-1.: Modules Scheme for the APJ Method. During this dissertation modules 3, 7, 8 and 9 were created from scratch and as an alternative. Modules 1 and 2 are written in MAD-x while the others are in PYTHON.

To the multiple orbits some digital filters are applied to reduce noise, before the APJ calculations. This is done in Module 9, with the filters and their combinations.

Module 2 is the step to create the LHC model. This is done using MAD-X with parameters very close to the experimental conditions. Additionally the integrals of the β -function along the quadrupoles are calculated in Module 3 (and the calculation of $\hat{\phi}$ if the case of the reformulation including different phase advances). The outputs are files *lattice.asc* and *triplet.dat*. From the model, in a manually way, after have decided the equivalent error position, the phase advances for the selected orbits are identified, this is Module 4.

In Module 7, the orbit TBT, the phase advances at some point closer to the magnetic errors, and the model are used to select the 4-Type orbits, using the average described previously as *Prom*. The four type of chosen orbits, have been already mentioned: "maxmax", "minmax", "maxmin" and "minmin", in the scheme they are renamed as **averaa.sdds**, **averia.sdds**, **averai.sdds** and **averii.sdds**, those are the output of the programs MTP and selecturns, which initially make the calculations for each plane separately. Alternatively, the selection of a single orbit is done using the algorithms introduced in this dissertation, equations (5-5) and (5-6), *Best* and *Sel1* (in Chapter 5).

The calculation of the magnetic errors is done in Module 8, according to the models and for the orbits previously selected.

Module 6, the *utils*, contains the basic equations which are discussed in Chapter 4 and presented in the 2009 paper [2], plus some generic functions used for the other steps or Modules.

During this dissertation, Module 3 was created from scratch based on the given instructions for previous calculations that were not automatic, Module 8 is replaced by the alternative equations given by the reformulation of the APJ and Module 9 is introduced to perform the reduction of noise using digital filters. Also, during the time of this dissertation small updates were incorporated in some modules.

When analyzing the experimental data from this year 2015, several configurations for the LHC-II were studied, for the stages where the beam reaches lowest sizes. These optics are $\beta^* = 1.0, 0.8, 0.65,$ and $0.40\ m$ at the LHC regions IR5 and IR1.

Tables **6-3** and **6-4** are obtained for the recovery of the magnetic errors installed in three magnets at IR5 and three magnets at IR1, in the LHC simulator of the 2015's data. In the tables, the strength of the magnetic errors installed are reported in the rows labeled *Sim.*, the APJ new formulation results are labeled *New*, while the previous formulation results are labeled *Old*.

These results were obtained as the average of APJ results in Beam 1 and Beam 2.

Table 6-3.: Magnetic Errors Recovery in IR5 using APJ with Ideal Orbits

Case	β^* [m]	$K_1(\text{Q2L5})$ $10^{-5} [m^{-2}]$	$K_1(\text{Q2R5})$ $10^{-5} [m^{-2}]$	$K_{1s}(\text{MQSL5})$ $10^{-4} [m^{-2}]$
Sim.	1.0	-1.00	-1.30	3.00
Old	1.0	-0.9993	-1.295	3.019
New	1.0	-0.9955	-1.299	3.008
Sim.	0.80	-1.00	-1.30	3.00
Old	0.80	-0.9996	-1.294	3.019
New	0.80	-0.9953	-1.299	3.008
Sim.	0.65	-1.00	-1.30	3.00
Old	0.65	-1.000	-1.294	3.030
New	0.65	-0.9965	-1.298	3.009
Sim.	0.40	-1.00	-1.30	3.00
Old	0.40	-0.9996	-1.295	3.019
New	0.40	-0.9952	-1.301	3.011

The reported results are consistent to what is expected, and for both formulations, the recovery values are very closer to the simulated ones. This holds for all the studied LHC configurations and regions IR5 and IR1.

The orbits used in this analysis can be considered to the ones created by the AC Dipole because their amplitude does not decrease with the number of turns, as mentioned earlier.

Table 6-4.: Magnetic Errors Recovery in IR1 using APJ with Ideal Orbits

Case	β^* [m]	$K_1(\text{Q2L1})$ 10^{-6} [m^{-2}]	$K_1(\text{Q2R1})$ 10^{-5} [m^{-2}]	$K_{1s}(\text{MQSL1})$ 10^{-5} [m^{-2}]
Sim.	1.0	5.00	-1.00	1.00
Old	1.0	4.987	-0.9974	1.034
New	1.0	4.972	-0.9947	0.9965
Sim.	0.80	5.00	-1.00	1.00
Old	0.80	4.983	-0.9983	1.004
New	0.80	4.968	-0.9945	0.9952
Sim.	0.65	5.00	-1.00	1.00
Old	0.65	4.988	-0.9994	1.121
New	0.65	4.972	-0.9961	1.003
Sim.	0.40	5.00	-1.00	1.00
Old	0.40	5.010	-1.007	1.002
New	0.40	4.968	-0.9959	0.999

6.4. Comparison Reformulation and Old Formulation using Noised Orbits

When noise is added to the positions in the trajectories of the simulated orbits, diverse effects are observed, which will be discussed in this section. First a direct comparison of the formulations is made and then the results for the different ways to reduce noise are presented.

In the simulations reported along this dissertation, the noise was added directly in the trajectory as a random number, obtained from a normal (also called Gaussian) distribution. The range for the random number as explained earlier is 0.3 mm according to the discussions studied and reported in [41]. However, in the appendix B interesting results were also observed when the distribution used for the noise is uniform.

Tables **6-5** and **6-6** present the results for the simulation including noise using orbits where three magnetic errors had been installed. In the tables, the results for the two formulations are reported. To obtain the magnetic errors, the noise was reduced using the filter *Prom*, and the generation of the orbits is done using the LHC simulator with the configuration for the experiment in 2010, discussed above in this dissertation.

The statistical average for the obtained three magnetic errors is presented in Table **6-5**. Each average is from 20 values obtained from an equal number of orbits turn-by-turn. In the table, the rows labeled by *w/o Filter* correspond to the result obtained for a single orbit selected using *Best* and no further filter is applied.

Table 6-5.: Comparison for the Magnetic Errors, obtained using the Old and New Formulation with Simulated Orbits. ($\beta^* = 2.0 \text{ m}$)

Sim LHC_B1 noi.	$K_1(\mathbf{Q2L5})$ $10^{-6} [\text{m}^{-2}]$	$K_1(\mathbf{Q2R5})$ $10^{-6} [\text{m}^{-2}]$	$K_{1s}(\mathbf{MQSL5})$ $10^{-5} [\text{m}^{-2}]$
w/o Filter-New	-10.5	-12.7	31.4
Prom-New	-9.93	-13.1	29.8
w/o Filter-Old	-46.1	-5.31	-36.1
Prom-Old	-10.1	-12.9	30.0

The results for the corresponding statistical uncertainty are presented in Table **6-6**. A similar notation as the previous table was used.

Table 6-6.: Comparison for the Uncertainty of the Magnetic Errors, obtained using the Old and New Formulation with Simulated Orbits. ($\beta^* = 2.0 m$)

Sim. LHC_B1 noi.	$\sigma K_1(\mathbf{Q2L5})$ $10^{-7} [m^{-2}]$	$\sigma K_1(\mathbf{Q2R5})$ $10^{-7} [m^{-2}]$	$\sigma K_{1s}(\mathbf{MQSL5})$ $10^{-7} [m^{-2}]$
w/o Filter-New	20.9	17.5	691
Prom-New	1.55	1.14	59.6
w/o Filter-Old	10718	3569	34817
Prom-Old	2.48	1.58	132

It is observed that the new formulation reduces the uncertainty to almost half of the obtained value using the previous formulation. This observation is stronger for the magnetic error given by $K_1(\mathbf{Q2R5})$. Also, all the average values obtained using both formulations are like each other, and at the same time, they are closer to the expected values given by the installed errors. These values are the ones installed in the simulator: $K_1(\mathbf{Q2L5})=1.0 \times 10^{-5} m^{-2}$, $K_1(\mathbf{Q2R5})=1.3 \times 10^{-5} m^{-2}$ and $K_{1s}(\mathbf{MQSL5})=3 \times 10^{-4} m^{-1}$.

Recently, the results for the comparison between the formulations were presented in a conference, refer to [45] for more details. The noise reduction observed is notorious for some cases when using the experimental data, as it is presented in further chapters, and it constitutes one of the advantages for the new formulation. These results, in some way, deal with the accuracy to obtain the magnetic errors in the experiments.

The results from all the seven combinations of filters, are summarized to the best combinations observed, as below. The procedure to obtain the best combination is explained and described in appendix B, for uniform noise. The complete sequence of plots for all the different ways to reduce noise (from normal distribution) is presented in the appendix of [44].

Tables **6-7** and **6-8** presents the results for the different measurements of the magnetic errors, when using the new formulation of APJ. To a manner of comparison, the results from the individual filters are included. The best three filters are reported for the measurement of each magnetic error. A best combination of filters is understood to be the combination which implies the lesser value of uncertainty, at a particular bandwidth of the filter *Band*. In the tables, two bandwidths are reported for the measurements with a same filter, the first bandwidth implies the lesser value of uncertainty, while the second is the most common bandwidth from 10 values, the best 5 bandwidths using the new formulation and the other 5 best bandwidths using the APJ old formulation.

In Table 6-7 the results for the normal quadrupole errors are reported. The first column corresponds to the analyzed case, the 2nd and 5th correspond to the bandwidth for $Band$, $\Delta\omega$, and it has tune units, while columns 3th and 6th are the statistical average, and, 4th and 7th are their corresponding statistical uncertainty σ .

Table 6-7.: Results for the Normal Quadrupole Magnetic Errors. Simulated Orbits using the New Formulation. ($\beta^* = 2.0 m$)

noi.	$\Delta\omega$	$K_1(\mathbf{Q2L5})$	$\sigma K_1(\mathbf{Q2L5})$	$\Delta\omega$	$K_1(\mathbf{Q2R5})$	$\sigma K_1(\mathbf{Q2R5})$
Normal Dist.	$2\pi[\text{rad}]$	$10^{-6} [m^{-2}]$	$10^{-7} [m^{-2}]$	$2\pi[\text{rad}]$	$10^{-5} [m^{-2}]$	$10^{-7} [m^{-2}]$
w/o Filter	—	-10.2	20.6	—	-1.28	15.8
Prom	—	-9.93	1.54	—	-1.30	1.90
SvdProm	—	-9.95	1.28	—	-1.30	1.00
	0.0850	-9.91	1.15	0.0130	-1.30	0.587
BandSvdProm	0.0850	”	”	0.0050	-1.31	0.764
	0.0100	-9.94	1.08	0.0130	-1.30	0.695
SvdBandProm	0.0050	-9.93	1.21	0.0130	”	”

Table 6-8.: Results for the Skew Quadrupole Magnetic Errors. Simulated Orbits using the New Formulation. ($\beta^* = 2.0 m$)

noi.	$\Delta\omega$	$K_{1s}(\mathbf{MQSL5})$	$\sigma K_{1s}(\mathbf{MQSL5})$
Normal Dist.	$2\pi[\text{rad}]$	$10^{-4} [m^{-2}]$	$10^{-6} [m^{-2}]$
w/o Filter	—	2.90	78.2
Prom	—	3.01	7.42
SvdProm	—	3.01	4.23
	0.0550	3.02	3.34
BandSvdProm	0.0003	3.02	3.43
	0.0550	3.02	3.47
SvdBandProm	0.0004	3.04	3.85

The corresponding results for the skew quadrupole error K_{1s} (MQSL5) are presented in the Table **6-8**. The same scheme and notation as in the previous tables is followed, so the best bandwidths are selected as if these measurements were independent from the others magnetic errors.

Taking the results of the normal quadrupole magnetic error uncertainties (σB_1) as the addition of the uncertainties for K_1 (Q2L5) and K_1 (Q2R5), the results for the cases *w/o Filter*, *SvdProm* and *SvdBandProm* are summarized in a total uncertainty of 36.4, 2.28, and $1.84 \cdot 10^{-7} m^{-2}$, respectively (the average of the two bands is taken as the final result before taking the sum). While the same uncertainties for skew quadrupole error are 78.2, 4.23, and $3.66 \cdot 10^{-6} m^{-2}$, respectively.

In a similar way, the results using the old formulation are reported in Tables **6-9** and **6-10**, for the normal quadrupole errors and the skew quadrupole error, respectively. The orbits used during the analysis for both formulations are the same.

Using the previous formulation, the total uncertainty for the normal quadrupole errors (σB_1) is 43.1, 2.36, and $1.77 \cdot 10^{-7} m^{-2}$, for the cases *w/o Filter*, *SvdProm* and *SvdBandProm*, respectively. The uncertainties for the skew quadrupole error are 96.1, 4.8, and $6.18 \cdot 10^{-6} m^{-2}$, respectively.

Table 6-9.: Results for the Normal Quadrupole Magnetic Errors. Simulated Orbits using the Old Formulation. ($\beta^* = 2.0 m$)

noi.	$\Delta\omega$	$K_1(\mathbf{Q2L5})$	$\sigma K_1(\mathbf{Q2L5})$	$\Delta\omega$	$K_1(\mathbf{Q2R5})$	$\sigma K_1(\mathbf{Q2R5})$
Normal Dist.	$2\pi[\text{rad}]$	$10^{-6} [m^{-2}]$	$10^{-7} [m^{-2}]$	$2\pi[\text{rad}]$	$10^{-5} [m^{-2}]$	$10^{-7} [m^{-2}]$
w/o Filter	—	-99.6	22.9	—	-1.35	20.2
Prom	—	-1.01	1.39	—	-1.27	1.35
SvdProm	—	-1.02	1.22	—	-1.28	1.14
	0.0850	-1.02	1.06	0.0450	-1.28	0.568
BandSvdProm	0.0850	”	”	0.0050	-1.28	0.852
	0.0500	-1.02	1.09	0.0130	-1.28	0.681
SvdBandProm	0.0500	”	”	0.0130	”	”

One of the facts observed when the results from both formulations are taking into account,

Table 6-10.: Results for the Skew Quadrupole Magnetic Errors. Simulated Orbits using the Old Formulation. ($\beta^* = 2.0 m$)

noi.	$\Delta\omega$	$K_{1s}(\text{MQSL5})$	$\sigma K_{1s}(\text{MQSL5})$
Normal Dist.	$2\pi[\text{rad}]$	$10^{-3} [m^{-2}]$	$10^{-6} [m^{-2}]$
w/o filter	—	3.44	96.1
Prom	—	3.03	5.31
SvdProm	—	3.07	4.80
	0.0003	3.14	3.53
BandSvdProm	0.0003	"	"
	0.0004	3.16	6.18
SvdBandProm	0.0004	"	"

and also all the seven combinations are studied, is that the worst filters are always *BandBest* and *BandSell* when $\Delta\omega > 0.03$, for every type of magnetic error.

From the reported results in the tables, it is observed that the optimal bandwidth is not always the same for both formulations, as mentioned above, and neither the same for all the magnetic errors measurements.

The graphs presented in the following part of this section are the suggested plots to obtain the optimal bandwidth $\Delta\omega$ for the best combinations of filters for all the magnetic errors, *BandSvdProm* and *SvdBandProm*. The idea, before analyzing the experimental data, is to follow two steps. First, to perform a simulation closer to the configuration used in the experiment, and then identify the bandwidth, which imply the lower uncertainty and at the same time an average close to the expected values. The results for the individual filters are taking into account, in case the combination gives a worst result than the individual cases.

The plots are for the magnetic error measurement against the bandwidth, and its corresponding uncertainty. In the following plots, Figure 6-2 to Figure 6-5, 20 orbits TBT were used from where 20 values were averaged, to obtain each point in the plots. The orbits include noise.

Error bars were added in the plots for the average of the magnetic errors. For each point, a single value of uncertainty is obtained. While, for the cases of the individual filters that are

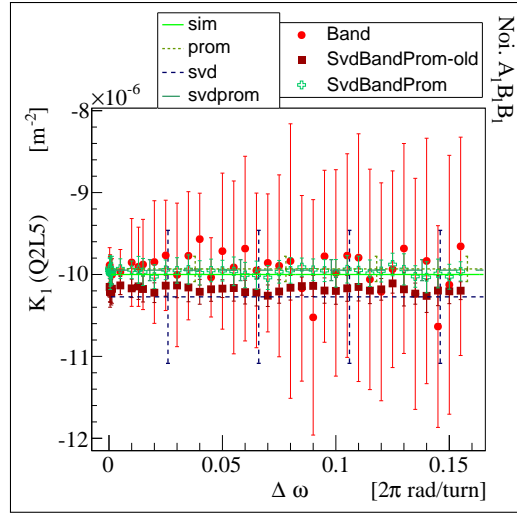


Figure 6-2: Comparison including *Band*, for K_1 (Q2L5), between individual filters (orbits selected using *Best*) and the best combinations of Filters, using the New and Old (-old) formulations of APJ. Orbits from the simulation of 3 magnetic errors and noise from normal distribution.

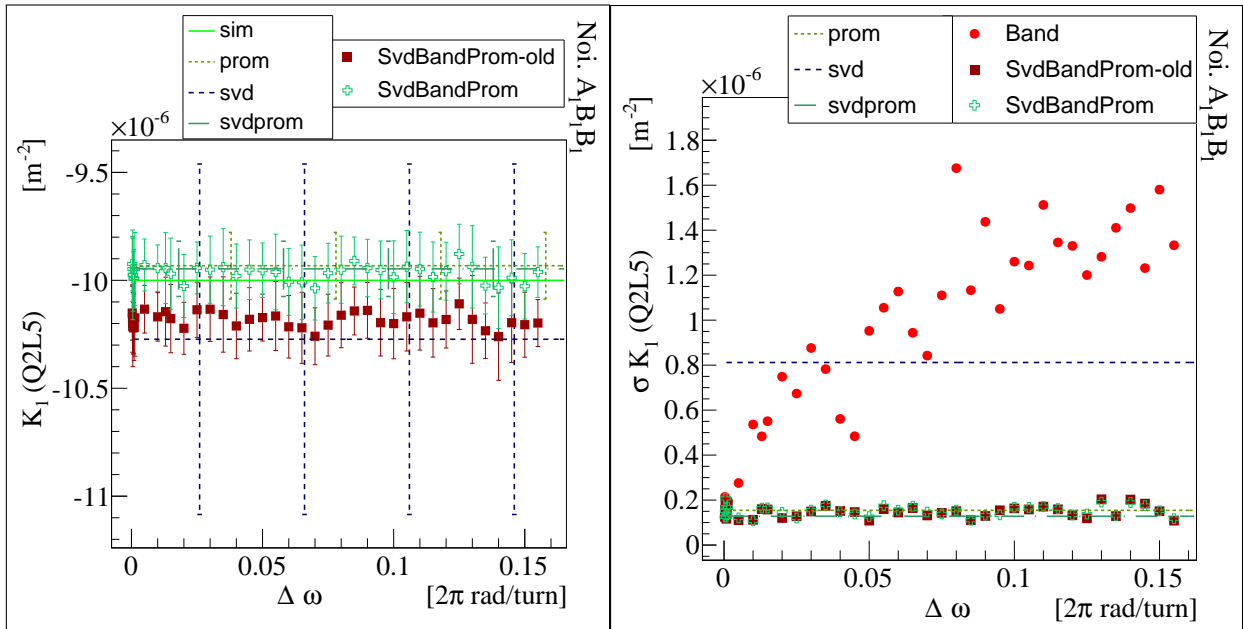


Figure 6-3: Comparison between the formulations when the filters and their combinations are applied, for K_1 (Q2L5) (left) and its uncertainty (right) calculation. Results for simulation including three magnetic errors and noise, using the New Formulation and the best case using the **Old** Formulation.

independent from $\Delta\omega$, four error bars with the same width are located at four equidistant points along the bandwidth range.

In Figure 6-2 the results for the statistical average at the magnetic error K_1 (Q2L5) against the bandwidth are presented. It is observe that the error bars for *Band* are the largest compared to other filter or combinations.

To have a better view of the plots, the results for the statistical average at the magnetic error K_1 (Q2L5) against the bandwidth are plotted without the filter *Band*. This is presented at the left in Figure 6-3.

The corresponding uncertainties, which have the half size of the error bars, are plotted at right in Figure 6-3. In this plots it is noticed that the errors bars using *Band* decrease almost linearly with the bandwidth, but the best filters have a lesser value of uncertainty.

For the other measurements of the magnetic errors the behavior is almost similar, the differences are which filter is the best. Results for K_1 (Q2R5) are in Figure 6-4, while the results for K_{1s} (MQSL5) are in Figure 6-5.

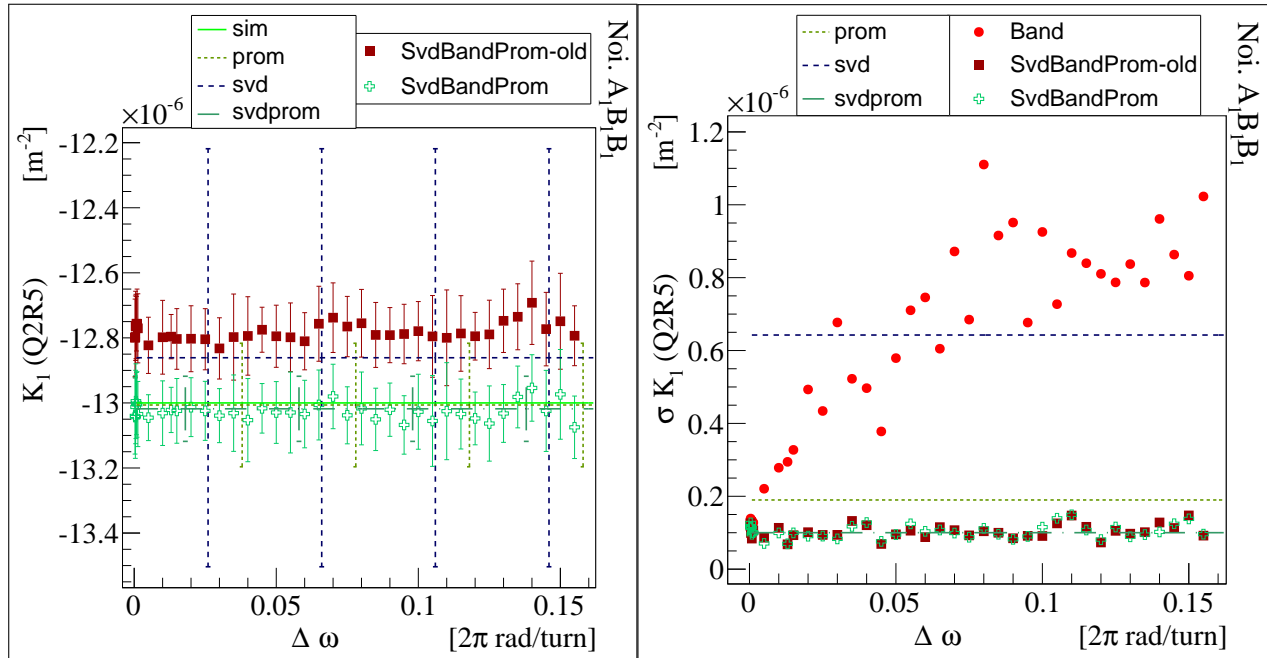


Figure 6-4.: Comparison between the formulations when the filters and their combinations are applied, for K_1 (Q2R5) (left) and its uncertainty (right) calculation. Results for simulation including three magnetic errors and noise, using the New Formulation and the best case using the **Old** Formulation.

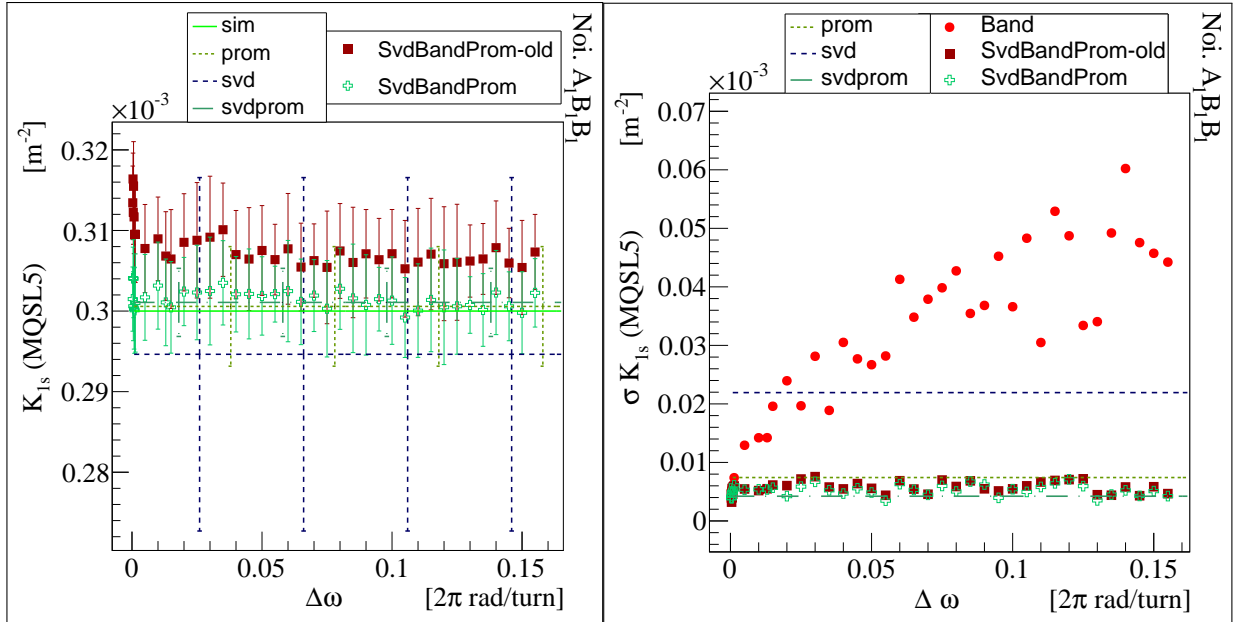


Figure 6-5.: Comparison between the formulations when the filters and their combinations are applied, for K_{1s} (MQSL5) (left) and its uncertainty (right) calculation. Results for simulation including three magnetic errors and noise, using the New Formulation and the best case using the **Old** Formulation.

In Figure 6-5, with exception of the results for the filter *Svd*, the average of the values recovery for the magnetic errors are closer to the simulated value. This last is presented as the green straight line, labeled by *sim*. Even more, including the results when using *Svd*, the obtained results are inside the expected range, due to the fact that the error bars crosses the expected value line.

From all the results, the best combinations found are *BandSvdProm* and *SvdBandProm*, and have similar error bars for any of the APJ formulations used. Also, the results for the best combinations of filters when the bandwidth is $\Delta\omega > 0.02$, is closer to the results given by *Prom*, in the case of the dispersion or uncertainty σ . When $\Delta\omega < 0.002$ all the best combinations are seen as effective to reduce the uncertainty in the measurement of the magnetic errors.

Also, for this simulation it is observed that the dispersion for the combination *BandSvdProm* is greater than the dispersion for *SvdBandProm*, and this is valid for both the new and previous formulation. On the other hand the variations for the uncertainty using the new formulation is lesser than the variations in the uncertainty given by the old formulation.

Results for the comparison between filters, especially for filter *Svd* are reported in a recent conference, refer to [46].

Finally, just to leave no space for doubts the details for the simulations are given. The magnetic errors were installed in the injection lattice of the LHC, with the modifiers for $\beta^* = 2.0$ m at IP5 and IP1. Also, the accelerator is arranged to have the transverse tunes obtained by LHC, during the experiment of April 13th, 2010 with the orbits generated by the AC Dipole. The number of turns used is 2000. And the magnetic errors were installed in the LHC simulator optics at the magnets (MQXB.A2.L5, MQXB.B2L5), (MQXB.A2R5, MQXB.B2R5) and MQSX.3L5, as errors of type K1. These magnets belong to the IR5, and along this dissertation the notation used is their corresponding quadrupole not-integrated components, these are: $K_1(Q2L5)$, $K_1(Q2R5)$ and $K_{1s}(MQSL5)$, respectively.

7. Methods used for Linear Corrections of Magnetic Errors in the LHC

In the LHC several investigations to obtain magnetic errors have been done, as well as investigations of methods to guarantee that the beams collide under the expected characteristics. In this dissertation, the results obtained with the main methods used to obtain the linear magnetic errors in the LHC triplets are presented. The main method is the so called Segment-by-Segment (SBS), which at the same time incorporated principles from the Resonance Driving Terms method (RDT).

For a comparison with the APJ method, the SBS method without the RDT is used to obtain the normal quadrupole magnetic errors B_1^I and B_1^{II} , while the RDT alone or with the SBS are used to obtain the skew magnetic error A_1 . The results of the comparison using experimental data is presented in the next chapter.

Other techniques have been also implemented in the LHC, this is the case of the **Model Iterative Correction** in the LHC lattice, refer to [13]. It is based in the Inverse Model Response Matrix (IMRM) which has a mathematical description as presented in the following equation (7-21), but in the general case when the \mathbf{R} matrix is not diagonal. The iterative approach consist in calculate the model phase advance, using the corrections of the previous iteration and then it is subtracted from the measured phase advance for the next iteration.

7.1. Resonance Driving Terms Method

The trajectory along a storage ring for a non-synchronous particle, after multiple turns of betatron oscillations, has a rich frequency spectra, if magnetic errors from several types are presented. In that case, the amplitude of the spectra bands is related with the strength of the magnetic errors presented. To generate the trajectories for the non-synchronous particle, a dipole kick can be used.

The Resonance Driving Terms (RDT) Method consists in the measurement of the magnetic strength from the Fast Fourier Transformation (FFT) of the beam position. The theoretical part of the Method is based on the Lie Algebra to obtain the generating function of the

transformation for the trajectory along the elements of the accelerator. With the Generating Function different observables can be constructed, and the magnetic strengths can be derive from the amplitude of the spectral FFT lines.

The above is possible because the magnetic strength of the magnets can be related with the Hamiltonian coefficients and those at the same time are related with the coefficients of the generating function. In a storage ring the Hamiltonian is mainly given by the magnetic components, if there is only one magnet presented, the Hamiltonian can be writing as:

$$\mathcal{H}^n = -\Re \left(\frac{1}{n!} (K_{n-1} + \mathbf{i}J_{n-1})(x + \mathbf{i}y)^n \right) \quad (7-1)$$

where n represents the order of magnet ($n=1$ for a dipole, $n=2$ a quadrupole, $n=3$ a sextupole, $n=4$ an octupole,...), K_{n-1} is the normal component of the magnet, J_{n-1} is called the skew component and corresponds to a rotation of the normal component of the magnet by an angle of $\pi/(2n)$, and both are evaluated for a certain position (x, y) in the transverse plane of the motion direction.

As pointing out in [47] the Hamiltonian can be expressed in a different way, by using the binomial expansion on the $(x + \mathbf{i}y)^n$ term. The binomial coefficients can be split using a new index set, the expression looks like:

$$\mathcal{H}^n = -\Re \left(\sum_{j+k=0}^n \sum_{l+m=0}^{j+k} \frac{x^{j+k}(\mathbf{i}y)^{l+m}}{(l+m)!(j+k)!} (K_{n-1} + \mathbf{i}J_{n-1}) \right) \quad (7-2)$$

It is convenient also to change the coordinates to the Courant-Snyder parameters (β, ϕ) , for a storage ring the transformation looks like:

$$q = \frac{\sqrt{\beta_q}}{2} (h_{q-} + h_{q+}) = \frac{\sqrt{\beta_q}}{2} \sqrt{2J_q} (e^{-i(\phi_q + \phi_{q,0})} + e^{i(\phi_q + \phi_{q,0})}) \quad (7-3)$$

where q represents the Cartesian coordinates x or y , β_q is the beta (betatron) function in the axis q , h_{q-} , h_{q+} are the observables that can be related with: J_q which is the action for each plane of the phase space q , ϕ_q is the phase; and $\phi_{q,0}$ is the initial phase of the motion.

The initial change of coordinates to facilitate the above derivation is given by the resonance basis, this is:

$$h_x^\pm = \hat{x} \pm \mathbf{i}\hat{p}_x = \sqrt{2J_x} e^{\mp \mathbf{i}(\phi_x + \phi_{x,0})} \quad (7-4)$$

$$h_y^\pm = \hat{y} \pm \mathbf{i}\hat{p}_y = \sqrt{2J_y} e^{\mp \mathbf{i}(\phi_y + \phi_{y,0})} \quad (7-5)$$

where \hat{x} , \hat{y} , \hat{p}_x and \hat{p}_y are the normalized coordinates.

As explained in [47], the Hamiltonian contribution for a magnet can be derived to be:

$$\mathcal{H}^n = - \left(\sum_{j,k,l,m}^n h_{jklm} (2J_x)^{(j+k)/2} (2J_y)^{(l+m)/2} e^{i[(\phi_x+\phi_{x_0})(j-k)+(\phi_y+\phi_{y_0})(l-m)]} \right) \quad (7-6)$$

where h_{jklm} is the Hamiltonian coefficient, and it relates the magnet strengths K_{n-1} and J_{n-1} by:

$$h_{jklm} = \frac{\beta_x^{(j+k)/2} \beta_y^{(l+m)/2} \mathbf{i}^{l+m} (K_{n-1} \Omega[l+m+1] + \mathbf{i} J_{n-1} \Omega[l+m])}{2^{(j+k+l+m)} k! j! m! l!} \quad (7-7)$$

where Ω takes the values of 1 or 0 according to:

$$\Omega[w] = 1 \text{ if } w \text{ is even, and } \Omega[w] = 0 \text{ if } w \text{ is odd} \quad (7-8)$$

The above relation is the same as the equation (3.51) in [17]:

$$h_{jklm} = Re \left\{ \sum_w \frac{-qL_w}{p} \frac{(j+k+l+m-1)!}{2^n j! k! l! m!} (b_{n,w} + \mathbf{i} a_{n,w}) \mathbf{i}^{(l+m)} \beta_w e^{-\mathbf{i}[(j-k)\phi_{x,w} + (l-m)\phi_{y,w}]} \right\} \quad (7-9)$$

where $\beta_w = (\beta_{x,w})^{\frac{j+k}{2}} (\beta_{y,w})^{\frac{l+m}{2}}$ is the β -function product in the magnet, according to the index used for the coefficients, L_w is the magnetic length of the magnet w , and multipolar components of the magnetic field associated to the magnet are a_n or b_n , which are given as discussed in Chapter 2 by $A_n = qBLa_n/p$ and $B_n = qBLb_n/p$, where q is beam charge with generalized momentum p , and total magnetic field magnitude B .

The Hamiltonian coefficients and RDTs

In an accelerator, it is usual to have more than one magnet and more than one type of error is expected to obtain, therefore the preceding results have to be generalized to many magnets. This is done by setting a fixed position, b , in the accelerator where the measurements are going to take place. The total Hamiltonian is just the summation over all magnets of the same order presented around the ring, this is

$$\mathcal{H}_{(b)}^n = - \left(\sum_{j,k,l,m}^n h_{(b)}^{jklm} (2J_x)^{(j+k)/2} (2J_y)^{(l+m)/2} e^{i[(\phi_x+\phi_{x_0})(j-k)+(\phi_y+\phi_{y_0})(l-m)]} \right) \quad (7-10)$$

more or less like equation (7-6) but now there is a new coefficient that depends on the observation point, given by:

$$h_{(b)}^{jklm} = \sum_g h_{g,jklm} e^{i[\Delta\phi_{g,x}^b(j-k) + \Delta\phi_{g,x}^b(l-m)]} \quad (7-11)$$

where the sum is over all the multipoles presented and each contribution is weighted according its position in the ring, hence the relation involves $\Delta\phi_{g,x}^b$ and $\Delta\phi_{g,xy}^b$, which are the phase advances for each magnet g with respect to the point of observation b .

The term $h_{g,jklm}$, is the called *hamiltonian coefficient*, and is given as equation (7-7) but evaluate in each magnet g

$$h_{g,jklm} = \frac{\beta_{x,g}^{(j+k)/2} \beta_{y,g}^{(l+m)/2} \mathbf{i}^{l+m} (K_{g,n-1}\Omega[l+m+1] + \mathbf{i}J_{g,n-1}\Omega[l+m])}{2^{(j+k+l+m)} k!j!m!!} \quad (7-12)$$

This coefficient can be related with the coefficients of the generating function for the transformation that describes the trajectory turn by turn in the storage ring. This is done used the Lie Algebra, as presented in [17] and [23]. The bottom line is that the lattice of the accelerator form a Taylor Map, which is characterized for been symplectic. A map is the function that transforms the coordinates from the initial phase space to the final phase space, and the fact that is symplectic allow to write the transformations as Lie operators.

Using the Drag Fit theorem, the map that represents the total accelerator can be expressed as the multiplication of the maps or transformations of the individual elements that composed the accelerator. These properties allow to express the generating function as:

$$F(b) = \sum_{jklm} f_{jklm}^{(b)} (2I_x)^{(j+k)/2} (2I_y)^{(l+m)/2} e^{\mathbf{i}[(\Phi_x+\Phi_{x_0})(j-k)+(\Phi_y+\Phi_{y_0})(l-m)]} \quad (7-13)$$

where I_x , I_y , Φ_x , Φ_y are the Action and Phases variables for the coordinates (x,y) on the accelerator, while Φ_{x_0} and Φ_{y_0} are the initial arbitrary phases of the motion. The coefficient f_{jklm} , to first order, is related with the Hamiltonian coefficient by (equation (3.74) in [17]):

$$f_{jklm}^{(b)} = \frac{h_{jklm}^{(b)}}{1 - e^{2\pi\mathbf{i}[Q_x(j-k)+Q_y(l-m)]}} \quad (7-14)$$

where Q_x and Q_y are the horizontals and verticals tune of the accelerator. The denominator of this expression diverges when $Q_x(j-k) + Q_y(l-m)$ is an integer. This discontinuity is known as the resonance and because of that, the factor $f_{jklm}^{(b)}$ is called *Resonance Driving Terms* (RDT). In the FFT of the beam position this resonance numbers produce the spectral lines from where the magnetic strength can be obtain.

It was shown in [48] (see also a more detailed proof in [17]) that the resonance basis can be decompose as a sum of frequency terms given by

$$h_x^-(N) = \sqrt{2I_x} e^{\mathbf{i}(2\pi Q_x N + \phi_{x_0})} + \quad (7-15)$$

$$-2\mathbf{i} \sum_{jklm} j f_{jklm} (2I_x)^{\frac{(j+k-1)}{2}} (2I_y)^{\frac{(l+m)}{2}} e^{\mathbf{i}[(1-j+k)(2\pi Q_x N + \phi_{x_0}) + (m-l)(2\pi Q_y N + \phi_{y_0})]}$$

where N is the number of turns, I_z are the amplitude invariants of the orbits (as the Action J), Q_x and Q_y are the decimal part of the accelerator tunes in the corresponding planes X and Y, and f_{jklm} are the so called resonance driving terms or (RDT).

RDTs for Linear Quadrupole Errors

During this dissertation the RDTs are used to measure the skew quadrupole component. In general, the quadrupole magnetic errors implies the multipolar component $n = 2$ and, from them the coefficients f_{1001} and f_{1010} are the RDTs affected by the skew quadrupole error.

Rewriting the equations (7-12) and (7-14) explicitly for f_{1001} , it is obtained [49]:

$$f_{1001}(s) = \frac{1}{1 - e^{-2\pi i(Q_x - Q_y)}} \sum_w \frac{1}{4} \sqrt{\beta_x^w \beta_y^w} K_w(s) e^{i(\Delta\phi_x^{s,w} - \Delta\phi_y^{s,w})} \quad (7-16)$$

where the sum is over all the w skew quadrupole magnets with strength $K_w(s)$; β_x^w , β_y^w are the β -function evaluated in the w -th magnet; $\Delta\phi_x^{s,w}$ and $\Delta\phi_y^{s,w}$ are the phase advance difference between the magnet w and the BPM from where the observable had been obtained, in the longitudinal position given by s in the accelerator.

It is possible to infer that f_{1001} is keeping a constant value along the accelerator and only change it when skew quadrupole components are presented.

An example is shown in Figure 7-1. In this, the plots for the RDTs with $jklm = 1010$ and 1001 along the LHC are shown. There are jumps in an abrupt way at the locations close to IP1 and IP5, these are the closest regions to where magnetic errors were installed in the LHC simulator.

The orbits used to generate the plots are obtained from the LHC simulator in MAD-x when three magnetic errors are installed along the regions IR1 and IR5, simultaneously. The three magnetic errors are the same selection of three correctors discussed in most of this dissertation.

In addition, in Figure 7-1, the plots show that the contribution given by f_{1001} is the greatest contribution far from the contribution given by the other term, f_{1010} . This is not only the case for the example, most of the times in the LHC the term f_{1001} is the dominant, see also Figure 5.21 and Figure 5.22 in [50]. These plots are part of the output obtained from the package for the SBS analysis [51], the figure is the screen from the corresponding GUI.

To obtain the RDTs along the accelerator, from simulated or experimental orbits, as many as possible BPMs are used and from each one the quantities h_z^\pm are obtained, according to

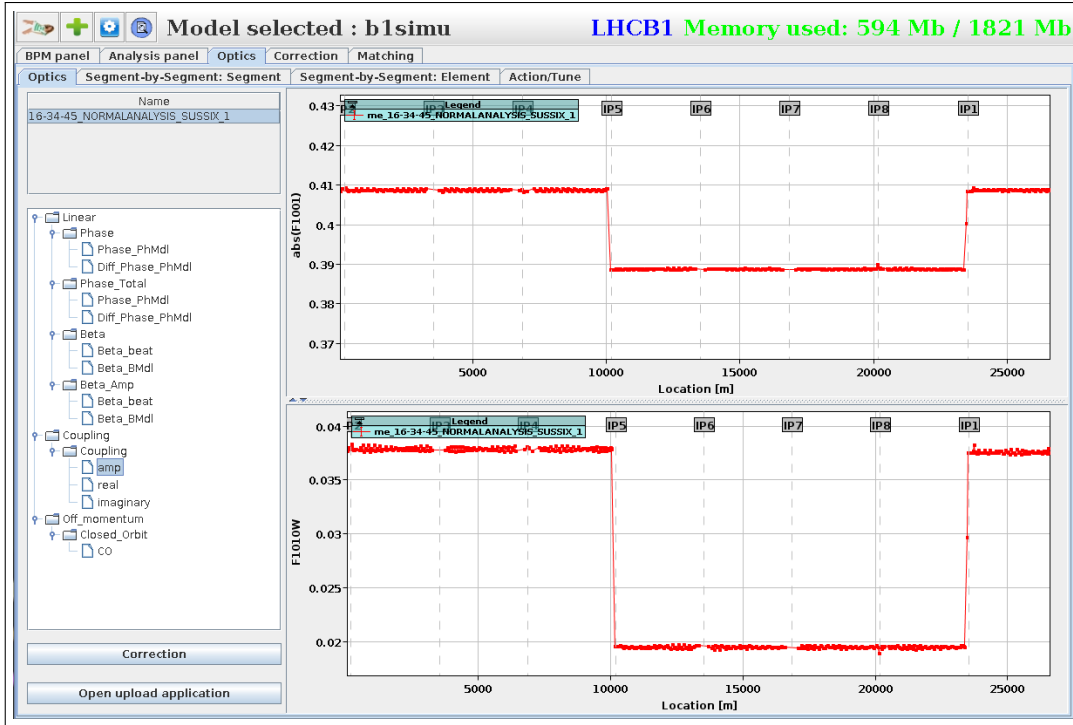


Figure 7-1.: RDT for $n = 2$ along LHC as obtained in the GUI version of SbS. Simulated orbits including magnetic errors at IR1 and IR5, and the expected noise in the BPMs.

equations (7-4) and (7-5).

Once the quantities h_z^\pm are obtained, they are analyzed to obtain their corresponding spectral distribution (in the frequency space). The band from the spectra can be related with the resonance driving terms, through simple expressions.

The bands lines of the h_z^\pm spectrum are named according to a nomenclature which counts the resonance conditions. In the spectra, the bands are denoted by:

$$\text{Horizontal Bands} \rightarrow H(1 - j + k, m - l) \quad (7-17)$$

$$\text{Vertical Bands} \rightarrow V(-j + k, 1 - l + m) \quad (7-18)$$

In particular, the allowed combinations for the resonance with $n = 2$, corresponding to the normal and skew quadrupole components, are presented in Table 7-1 as given by the tables in [47].

For the case of the resonance driving terms f_{1010} and f_{1001} , the simple expressions for the

j	k	l	m	Resonance	Bands Name
0	0	0	2	(0,-2)	—
0	0	1	1	(0,0)	V(0,1)
0	0	2	0	(0,2)	V(0,-1)
0	2	0	0	(-2,0)	—
1	1	0	0	(0,0)	H(1,0)
2	0	0	0	(2,0)	H(-1,0)
0	1	1	0	(1,-1)	V(1,0)
1	0	0	1	(1,-1)	H(0,1)
1	0	1	0	(1,1)	H(0,-1), V(-1,0)

Table 7-1.: Combinations $ijklm$ for $n = 2$. The observed spectral lines must hold $j \neq 0$ in the horizontal plane and $l \neq 0$ in the vertical plane.

spectra lines given by h_z^\pm are:

$$f_{1010}^{HO} = \frac{H(0, -1)}{2V(0, 1)} ; f_{1010}^{VE} = \frac{V(-1, 0)}{2H(1, 0)}$$

$$f_{0110}^{VE} = \frac{V(1, 0)}{2H(1, 0)} ; f_{1001}^{HO} = \frac{H(0, 1)}{2V(0, 1)}$$

Alternatively, the spectra can be calculated with a different observable and although the mathematical expressions differ from the f_{ijklm} terms, the relation between the spectral lines is preserved. This new observable, although more complex is more precise than the previous one, refer to [52]. It is given by:

$$\begin{aligned} \chi_q &= \sum_{j>k, l>m} 4(j\delta_{qx} + l\delta_{qy})|\chi_{q,ijklm}|(2I_x)^{(j+k-2\delta_{qx})/2}(2I_y)^{(l+m-2\delta_{qy})/2} \cos(\rho) & (7-19) \\ \text{with } \rho &= 2\pi N(\tau_{1q}Q_x + \tau_{2q}Q_y) + \phi_{q,ijklm} \\ \text{and } \tau_{1q} &= \delta_{qx} - j + k , \quad \tau_{2q} = \delta_{qy} - l + m \end{aligned}$$

where δ_{qw} is the Kronecker function, Q_q is the accelerator tune in plane q , N is the number of turns, $\phi_{q,ijklm}$ is the phase, while the coefficient $\chi_{q,ijklm}$ related the magnetic strengths for magnets w located between the three BPMs as follows:

$$\chi_{q,ijklm} = \sum_g e^{i[\tau_{1q}\phi_{xg} + \tau_{2q}\phi_{yg}]} h_{g,ijklm} SEN \phi_{qg} \quad (7-20)$$

where ϕ_{qg} is the phase advance of the magnet with respect to the BPM and $SEN\phi_{qg}$, equation 19 in [47], is $\sin \phi_{qg} \sqrt{1 + \tan^2 \delta_1}$ if $\phi_{qg} < \phi_{q2} - \phi_{q1}$ and $\sin(\phi_{qg} - \delta_1 - \delta_2) \sqrt{1 + \tan^2 \delta_2}$ in the opposite way.

When the Fourier series are obtained for χ_q in the equation (7-19), the resonance driving terms $\chi_{q,jklm}$ are corresponding to the amplitude of the spectra lines.

An example of the use of this observable to obtain sextupole magnetic errors were also studied and implemented during this dissertation, refer to [53] for the results and details.

Plenty of references are available for the development and specialties of the Resonance Driving Terms Method, some of these are [47, 52, 54, 23, 48, 50] and also [17, 53].

7.2. Segment-by-Segment Method

As its name implies, the Segment-By-Segment Method (SBS or SBST) is a technique which consists in the splitting of the entire ring into several segments. Consequently, each segment is treated as an independent transfer line [13]. In the case of the LHC the partition corresponds with the splitting of the machine in the arcs and insertion regions (as discussed in section 3.3).

SBS is based on the theoretical principle that the physical quantities measured at any point along the accelerator must be equal to the expected quantities values given by the theoretical propagation of the initial conditions up to the particular point. In the basic formulation, it is considered that the measured α and β functions at the entrance of each segment are the initial conditions for the optical parameters propagate along the respective segment. The Transfer Matrix is the usual tool for the propagation of the optical parameters.

The advantage of this method and its procedure described above, is that in this way there is a reduction of the dimensionality of the problem, because only the variables of each sector are included in the calculation. This is a valuable advantage, compared to other methods.

The phases advance on the each BPM ($\Delta\phi_1$) are propagated as:

$$\begin{pmatrix} \Delta\phi_1 \\ \Delta\phi_2 \\ \vdots \\ \Delta\phi_N \end{pmatrix} = \mathbf{R} \begin{pmatrix} \Delta K_1 \\ \Delta K_2 \\ \vdots \\ \Delta K_N \end{pmatrix} = \begin{pmatrix} R_1 & 0 & \dots & 0 \\ 0 & R_2 & \dots & 0 \\ \vdots & \ddots & \ddots & \vdots \\ 0 & 0 & \dots & R_N \end{pmatrix} \begin{pmatrix} \Delta K_1 \\ \Delta K_2 \\ \vdots \\ \Delta K_M \end{pmatrix} \quad (7-21)$$

where the \mathbf{R} matrix is a diagonal matrix, with N independent blocks each one represented as an independent response matrix R_i . The \mathbf{R} is multiply by the vector that contains the M

gradient variables K_i to obtain the phases advances.

The magnetic gradient error is detected (or localized) by direct comparison of the ideal optical parameters and the propagation of the measured parameters; any deviation of the parameters is considered a gradient error. In the words of the authors *The amplitude of the errors within the segment can be determined by matching the propagated optics to the measured one via the preferred matching algorithm* Page 0810002-4, this includes any perturbation order for the equation of motion. In this way this theory can be considered a local approximation.

In the publication of December 2010 [13], this method was successfully used in the LHC, where a cable swap between the two-beam apertures of a trim quadrupole was identified as the source of an unexpected large β beating.

To obtain the linear skew magnetic errors and other magnetic errors the SBS uses the Resonance Driving Terms Methods. This is done by obtaining the magnetic strengths that match the measured RDTs. So in practice, when using the experimental orbits, the function MATCH in the LHC simulator is used to obtain the parameters instead of inverting the matrix directly.

The function MATCH is also used in the LHC simulator to obtain the normal quadrupole magnetic errors, in this case the phase advances are the variables which are mainly involved.

7.2.1. Results using SBS and RDT with Simulated Orbits

To reinforce the acquired knowledge in the main methods used for Linear Corrections in the LHC, simulations were performed. Those simulations are similar to what is done for the previous analysis using the APJ method. Magnetic errors are installed in the LHC simulator to obtain its values back. In particular below are reported the results for the configurations closer to the Experiments on May 11th, 2015.

The package for the SBS analysis was used to obtain the results, this was done from the terminal directly without using the GUI interface. A small change in the procedure is done for Beam 2, due to the fact that the simulation does not give the results in the same way that the experiments. Therefore, when executing Beam 2 the configuration to use is LHCB4 instead of LHCB2, according to the indications given by the OMC team at CERN, when the phase advances and other variables are calculated.

The scheme to obtain the magnetic errors is, first to obtain the physical variables at each longitudinal position of the accelerator from the information measured at the BPMs, then the spectrum at each transverse plane is obtained and the main orbits are selected, from

this last the optical measurements like the phases, the beta-functions, and more, are obtained. The programs that perform these task are *Drive_God.lin* and *GetLLM*. Then the SBS technique is used and the magnetic errors are determined when using the *matching* function. More information for sequence of programs that composed the SbS analysis, in the recent versions or in detail, is available in [51] or [55].

Table 7-2 presents the results for the recovery of three magnetic errors in the LHC regions IR5 and IR1, simultaneously. In the simulator, the tunes are set up to be the experimental tunes given by the AC Dipole. The rows with the label *Sim.* are the values of the installed errors in the simulator, while the other rows correspond to the results for the several studied configurations.

Table 7-2.: Magnetic Errors Recovery using SBS (function *SegmentBySegmentMatch.py*). Simulated Orbits without noise.

Opt.	IR5		
	$K_1(\mathbf{Q2L5})$	$K_1(\mathbf{Q2R5})$	$K_{1s}(\mathbf{MQSL5})$
$\beta^* [m]$	$10^{-7}[m^{-2}]$	$10^{-5}[m^{-2}]$	$10^{-4} [m^{-2}]$
Sim.	3.20	-1.87	3.00
0.40	4.146	-1.866	3.0048
0.65	3.341	-1.8673	2.9936
0.80	3.309	-1.8667	2.9937
1.0	3.349	-1.861	3.1068
Opt.	IR1		
	$K_1(\mathbf{Q2L1})$	$K_1(\mathbf{Q2R1})$	$K_{1s}(\mathbf{MQSL1})$
$\beta^* [m]$	$10^{-6}[m^{-2}]$	$10^{-6}[m^{-2}]$	$10^{-4}[m^{-2}]$
Sim.	-3.10	7.40	1.00
0.40	-2.6922	7.1237	0.99991
0.65	-2.9282	7.3630	0.98706
0.80	-2.9773	7.3859	0.98791
1.0	-2.9509	7.3716	1.0249

According to the results, the differences between the recovered values and the expected ones are larger than the differences obtained using the APJ method (Table 6-1). In fact, the

results obtained with SBS imply a recovery relative error as higher as 10 %, while the results using APJ imply just 1 % as the highest recovery relative error. During this investigation the simulations and configurations were reviewed to establish a reason for the differences but no further improvements were obtained.

Another difference between the results from the APJ and SBS, is that the analysis using SBS takes into account the two beams at the same time, therefore only one result is obtained from each LHC configuration studied.

Nevertheless, the SBS technique also imply a fit to a modified model. The modification in the model is that the magnetic errors corrections obtained from the experimental data are added. The fit process is the step forward from what we call in here *the first iteration* with the software, and it is done generally by hand and view.

Even more, although the differences in the tables are larger, when doing the fits, all the curves obtained are closer to each other. This is something unexpected though it is an explanation of the higher relative errors encounter when using the simulated orbits.

It is noteworthy that in the simulator the errors are installed in the skew quadrupoles MQSX.3L5 and MQSX.3L1, and in the normal quadrupoles MQXB.A2L5, MQXB.B2L5, MQXB.B2R5, MQXB.A2R5, MQXB.A2L1, MQXB.B2L1, MQXB.B2R1 and MQXB.A2R1, while the corresponding variables in SbS are kqsx3.l5, kqsx3.l1, ktqx2.l5, ktqx2.r5, ktqx2.l1, ktqx2.r1, respectively. These variables for the quadrupoles are the same used in previous analysis with APJ method, and in the table the results are reported with the notation used along this dissertation.

Also, the sequence of programs and commands used to obtain the local magnetic errors after the execution of *Drive_God_lin* and *GetLLM*, for instance at IR5, are:

- `/usr/bin/python2.6 /afs/cern.ch/eng/sl/lintrack/Beta-Beat.src/SegmentBySegmentMatch/ SegmentBySegmentMatch.py variables -beam1=NORMALANALISIS_SUSSIX_B1/ -beam2=NORMALANALISIS_SUSSIX_B2/ -ip=5 -temp=.`
- *To change the variables according to the expected measurements*
- `/usr/bin/python2.6 /afs/cern.ch/eng/sl/lintrack/Beta-Beat.src/SegmentBySegmentMatch/ SegmentBySegmentMatch.py constraints -beam1=NORMALANALISIS_SUSSIX_B1/ -beam2=NORMALANALISIS_SUSSIX_B2/ -ip=5 -temp=.`
- `/usr/bin/python2.6 /afs/cern.ch/eng/sl/lintrack/Beta-Beat.src/SegmentBySegmentMatch/ SegmentBySegmentMatch.py -beam1=NORMALANALISIS_SUSSIX_B1/ -beam2 =NORMALANALISIS_SUSSIX_B2/ -ip=5 -temp=.`
- `/usr/bin/python2.6 /afs/cern.ch/eng/sl/lintrack/Beta-Beat.src/SegmentBySegmentMatch/ SegmentBySegmentMatch.py variables -mode=coupling -beam1=NORMALANALISIS_SUSSIX_B1/ -beam2=NORMALANALISIS_SUSSIX_B2/ -ip=5 -temp=.`
- *To change the variables according to the expected measurements*
- `/usr/bin/python2.6 /afs/cern.ch/eng/sl/lintrack/Beta-Beat.src/SegmentBySegmentMatch/ SegmentBySegmentMatch.py constraints -mode=coupling -beam1=NORMALANALISIS_SUSSIX_B1/ -beam2=NORMALANALISIS_SUSSIX_B2/ -ip=5 -temp=.`
- `/usr/bin/python2.6 /afs/cern.ch/eng/sl/lintrack/Beta-Beat.src/SegmentBySegmentMatch/ SegmentBySegmentMatch.py -mode=coupling -beam1=NORMALANALISIS_SUSSIX_B1/ -beam2 =NORMALANALISIS_SUSSIX_B2/ -ip=5 -temp=.`

The steps *To change the variables according to the expected measurements* are performed to guarantee that the only the expected variables, the ones used in the APJ analysis, are taking into account. And, the option *coupling* was obtained by taking a look of the written code because it was not found in the references, although this configuration for SbS was suggested (by me) during my stay at CERN. The values reported in Table 7-2 are obtained using the above list of steps.

There are bigger differences in the recovery of the magnetic errors using the SBS technique rather than the expected differences, for instance like the differences given by the Action and Phase Method. These results change if the SUSSIX method used is replaced for instance by SVD, a different option for the SBS method.

Another way to measure the Skew Quadrupole Errors

During this dissertation the RDT method was studied to obtain the skew quadrupole error in a direct way. This could be done by evaluating the output of the SbS without start the *matching* calculations, in this way a value for each beam is obtained separately. Nevertheless, the results obtained does not improved what is obtained above.

Also, to obtain the coupling in the LHC, the SBS software have different configurations. One of these includes the fact to make global or local corrections by using *knobs* or the *Skew* quadrupoles at the IRs.

For the configuration for a local measurement of the coupling, the SbS uses all the magnets MQSX. These last variables are only for the skew magnets at the triplets. As mentioned earlier, each IR have two skew quadrupoles at each IR.

Table 7-3 reports what it is obtained in IR5, for three simulations with a different strength of the magnetic error each time. The installed magnetic error is reported in the first column, while obtained values at the skew quadrupoles are in the second and third column. In the last column the corresponding total error is reported.

The last column is obtained as the addition of the two previous columns and corresponds to the total skew quadrupole error for the two triplets. This is possible because the symmetry of the triplets. Even more, the length of the skew quadrupole is also taking into account in the total error calculation.

To obtain these results, the subroutine *correct_coupleDy.py* is used, and the LHC configuration in the simulator is $\beta^* = 0.40$ m, with magnetic errors at IR1, IR5 and IR8. The results

Sim. $\beta^* = 0.40 \text{ m}$	kqsx3.l5 [m ⁻¹]	kqsx3.r5 [m ⁻¹]	$K_{1s}(\text{MQSL5})$ [m ⁻²]
0.0004	-0.0002717	0.00018019	0.0004106
0.0003	-0.0002009	0.0001317	0.0003102
0.0002	-0.00013346	0.000085907	0.0002128

Table 7-3.: Recovery values for the Skew Quadrupole Error in IR5 using *correct_coupleDy.py*.

corresponds to what it is obtained with beam 1 and a single magnet is not possible to select for each IR.

The reported values in the Table **7-3** have relative errors from 3% to 6%. With this alternative way to obtain the skew quadrupole errors, it is not enough to decrease the relative errors to the levels observed when using APJ.

The observed differences between the results when using APJ and SBS could be explained by the fact that SbS analyzes the all ring at the same time and do not only locally at each region. In fact, the magnetic errors are obtained for kqsx3.l2, kqsx3.r2, kqsx3.l5, kqsx3.r5, kqsx3.l8, kqsx3.r8, kqsx3.l1 kqsx3.r1 at the same time.

8. Analysis of Experimental LHC Orbits

With the update made on the LHC in the year of 2014, new experiments related with the measurement of magnetic errors have been made. In this dissertation the squeeze configuration of the LHC are analyzed. The results obtained are from the experiments made on April 13th, 2010 and May 11th, 2015. The analysis is made mainly using both formulations of the APJ method, though a comparison using SBS and RDT is presented for the 2015's orbits.

All the data presented in this chapter was obtained under the guidelines of the OMC Team at CERN, to whom a special acknowledgement are given.

8.1. Comparison New and Old APJ Formulation with 2010's Orbits

To the experimental data from the April 13th, 2010 experiment, the different ways to decrease the noise in the orbits, described in chapter 6, were applied. In this section the corresponding results are presented. First, a comparison between the formulations, using the filter *Prom* is introduced. And then, results for the best combinations of filters are introduced, using the same methodology as presented for the analysis with simulated orbits.

Previous analysis on the same experimental orbits were performed before the development of this dissertation [3]. It was found that the reported magnetic errors given by SBS on the LHC orbits, for MQXB2.R5 and MQXB2.L5, cannot be adjusted each one individually as it was wrong assumed [56]. In fact the change in those quadrupoles MQXB2.R5 and MQXB2.L5 implies as well a change in the quadrupoles MQXA2.R5 and MQXA2.L5, because they share the same power supply. This issue is counted in the analysis presented during this dissertation, so the final magnetic measurements differ from what is reported for Action and Phase Analysis in the previous comparison presented in [3].

Table 8-1 shows a comparison between the APJ formulations using the experimental orbits from April 13th, 2010 at 12:54:09, 12:56:24 and 12:59:18 CEST. In this case, the new formulation does not give a bigger change in the uncertainty and its value could sometimes be worst, compared to what is observed using the simulated data. One of the reason could be that there are few experimental orbits available comparing to the simulated case (in here

there are only 3 orbits corresponding to 6 values, while in the simulation there were 20 orbits from where 20 values were obtain). For each orbit, three combinations of the 4-type orbits are selected, from where the measurements are obtained.

Table 8-1.: Results using Old and New Formulations of APJ. LHC-2010's Experimental Orbits ($\beta^* = 2.00 m$)

Exp. Data					K_{1s}	σK_{1s}
Beam 1	$K_1(\mathbf{Q2L5})$	$\sigma K_1(\mathbf{Q2L5})$	$K_1(\mathbf{Q2R5})$	$\sigma K_1(\mathbf{Q2R5})$	(MQSL5)	(MQSL5)
Apr13/10	$10^{-6} [\text{m}^{-2}]$	$10^{-7} [\text{m}^{-2}]$	$10^{-6} [\text{m}^{-2}]$	$10^{-7} [\text{m}^{-2}]$	$10^{-4} [\text{m}^{-2}]$	$10^{-5} [\text{m}^{-2}]$
New - APJ						
w/o Filter	-21.0	133	-0.59	1050	6.03	63.00
Prom-New	-8.28	6.98	-1.54	92.2	3.06	3.76
Old - APJ						
w/o Filter	-25.1	140	-0.47	1060	8.64	108
Prom-Old	-9.15	3.36	-1.39	78.0	3.19	3.08

When analyzing these experimental data an additional filter was implemented, and it was used as well in most of the simulations already reported. The filter is applied directly to the Actions and Phases obtained at the Arcs, before getting their average. It is expected that the filter removes changes in the variables, for instance produced by collective effects at the Arcs or experimental issues at the BPMs that prevents to recover a constant value of them. This filter effect is like a *smooth* filter for the variables Action and Phase in each region.

On the other hand, the analysis to determine the optimal bandwidth for the best combinations of filters is presented below. This is done as described previously in section 6.4 for the simulated orbits, by choosing the most common bandwidth and the others aspects.

In Tables **8-2** and **8-3** it is reported the magnetic errors measurements and its uncertainty, for the LHC region IR5, using the new and previous formulation, respectively.

The first rows of the tables shows the results *w/o Filter*, this means the noise level or just the measurements obtained when the selection of the orbits is made using *Best* and no filter is applied.

In summary for the new formulation it is found that, taking the total value for the nor-

Table 8-2.: Results using the New Formulation of APJ. LHC-2010's Experimental Orbits.
($\beta^* = 2.00 m$)

Data LHC.B1	$\Delta\omega$	$K_1(\mathbf{Q2L5})$	$\sigma K_1(\mathbf{Q2L5})$	$\Delta\omega$	$K_1(\mathbf{Q2R5})$	$\sigma K_1(\mathbf{Q2R5})$
Apr13/10	$2\pi[\text{rad}]$	$10^{-6} [m^{-2}]$	$10^{-7} [m^{-2}]$	$2\pi[\text{rad}]$	$10^{-5} [m^{-2}]$	$10^{-8} [m^{-2}]$
w/o Filter	—	-21.0	133	—	-0.59	1050
Prom	—	-8.28	6.98	—	-1.54	92.2
SvdProm	—	-8.05	4.34	—	-1.54	38.4
	0.0013	-8.11	2.49	0.02	-1.54	4.86
BandProm	0.0003	-8.49	2.63	0.02	"	"
	0.1050	-8.33	1.24	0.03	-1.54	5.97
BandSvdProm	0.095	-8.33	1.37	0.015	-1.53	11.1
	0.145	-8.03	2.96	0.015	-1.56	32.6
SvdBandProm	0.09	-8.03	2.97	0.125	-1.57	33.3

mal quadrupole magnetic error uncertainties (σK_1) as the addition of the uncertainties for $K_1(\mathbf{Q2L5})$ and $K_1(\mathbf{Q2R5})$, a total uncertainty of $1183 \cdot 10^{-7} m^{-2}$ is observed for the case *w/o Filter* and it is reduced to $99.18 \cdot 10^{-7} m^{-2}$ when using the filter *SvdProm*. On the other hand, for skew quadrupole error the reduction is from $63 \cdot 10^{-5} m^{-2}$ to $3.76 \cdot 10^{-5} m^{-2}$, respectively.

It is observed from the results that using the new formulation the reduction of the uncertainty is not as large as observed from the simulated case. Nevertheless, when using a combination of filters, the results show a considerable reduction of uncertainty of about 50% when compared to just the *Prom* case.

Using the previous (Old) formulation, the total uncertainty for the normal quadrupole errors (σK_1) is 1200 and $81.36 \cdot 10^{-7} m^{-2}$, for the cases *w/o Filter* and *SvdProm*, respectively. While the uncertainty for the skew quadrupole error is 108 and $3.08 \cdot 10^{-5} m^{-2}$, for the same cases, respectively.

With the experimental data, the plots for the three magnetic errors against the bandwidth are presented in Figure 8-1, Figure 8-2, Figure 8-3, and Figure 8-4, when analyzing IR5. These graphs are similar to the plots obtained for the simulated orbits showed in section 6.4, however, the best combination of filters is different from what is obtained for the simulated orbits.

Table 8-3.: Results using the previous formulation of APJ and Digital Filters. LHC-2010's Experimental Orbits. ($\beta^* = 2.00 m$)

Data LHC_B1	$\Delta\omega$	$K_1(\mathbf{Q2L5})$	$\sigma K_1(\mathbf{Q2L5})$	$\Delta\omega$	$K_1(\mathbf{Q2R5})$	$\sigma K_1(\mathbf{Q2R5})$
Apr13/10	$2\pi[\text{rad}]$	$10^{-6} [m^{-2}]$	$10^{-7} [m^{-2}]$	$2\pi[\text{rad}]$	$10^{-5} [m^{-2}]$	$10^{-8} [m^{-2}]$
w/o Filter	—	-25.1	140	—	-0.47	1060
Prom	—	-9.15	3.36	—	-1.39	78.0
SvdProm	—	-8.85	4.37	—	-1.40	37.5
	0.0013	-8.93	3.01	0.02	-1.40	10.5
BandProm	0.0003	-9.30	3.12	0.02	"	"
	0.1050	-9.14	1.39	0.02	-1.40	6.18
BandSvdProm	0.095	-9.14	1.54	0.015	-1.39	13.3
	0.16	-8.84	2.59	0.125	-1.42	32.8
SvdBandProm	0.09	-8.84	2.59	0.125	"	"

Once again it is observed that the error bars for *Band* are quite large compared to the others. This is what it is presented in **8-1** compared to **8-2**.left.

A straight green line labeled by *SbS* is the expected magnetic error measurement. This line is given by the measurement obtained using the Segment-by-Segment method and reported in [3] for the analysis performed for the same orbits. The measurements were done for the normal quadrupole errors only, therefore the plots for the skew quadrupole error are without this line.

From the normal quadrupole errors plots it is easy to observe that the old formulation is much closer to the expected values, though the new formulation has almost all its corresponding lines close to each other.

Therefore, for this experimental data the difference between reformulations is more notorious, if the results for the skew quadrupole error are ignored.

Also, it is inferred from the plots that, one of the largest reported uncertainties is the obtained when only the *Svd* filter is applied to the orbits, the selection of the orbit in this case is made with *Best*.

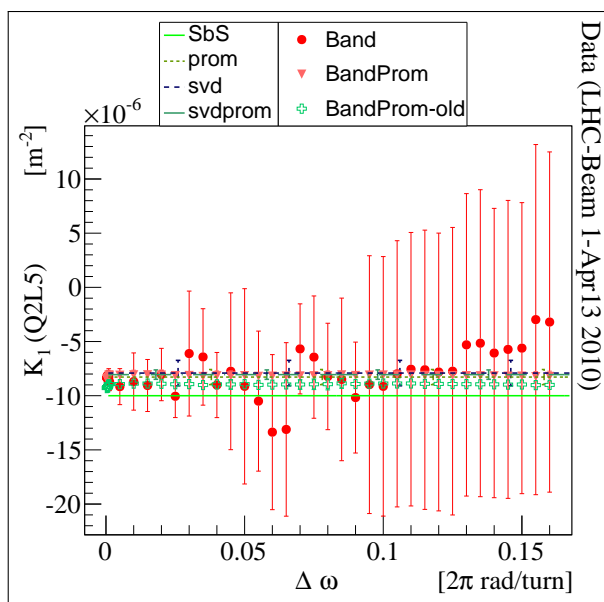


Figure 8-1.: Comparison including *Band*, for K_1 (Q2L5), between individual filters (orbits selected using *Best*) and the best combinations of Filters, using the New and Old (-old) formulations of APJ. 2010's Experimental Orbits.

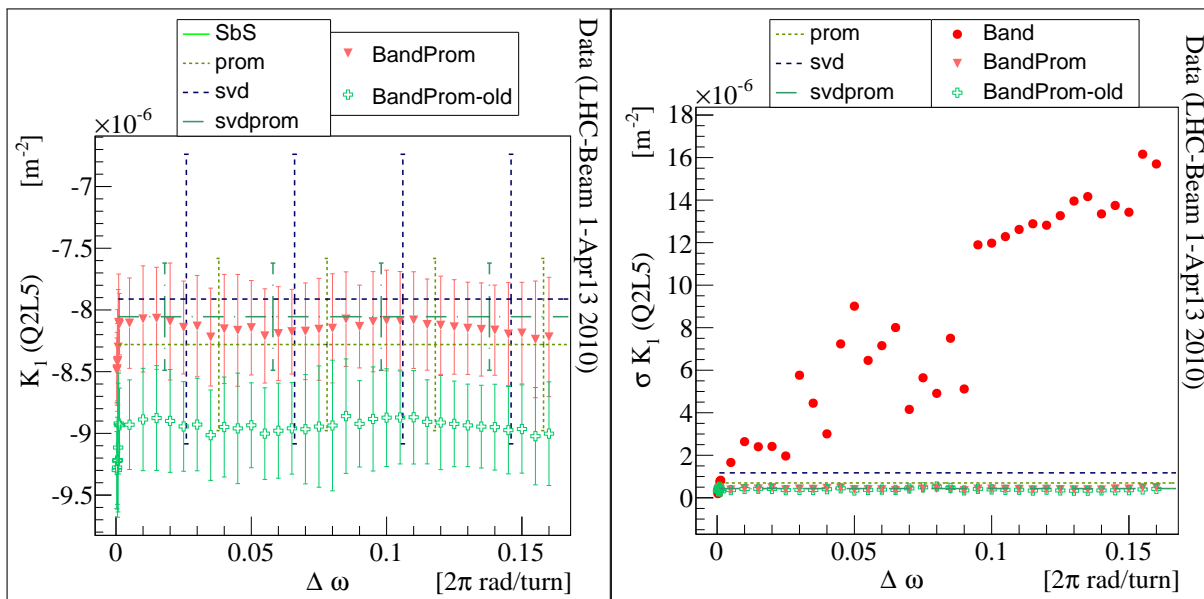


Figure 8-2.: Comparison between the formulations when the filters and their combinations are applied, for K_1 (Q2L5) (left) and its uncertainty (right) calculation. Results for 2010's Experimental Orbits (obtained three magnetic errors), using the New Formulation and the best case using the **Old** Formulation.

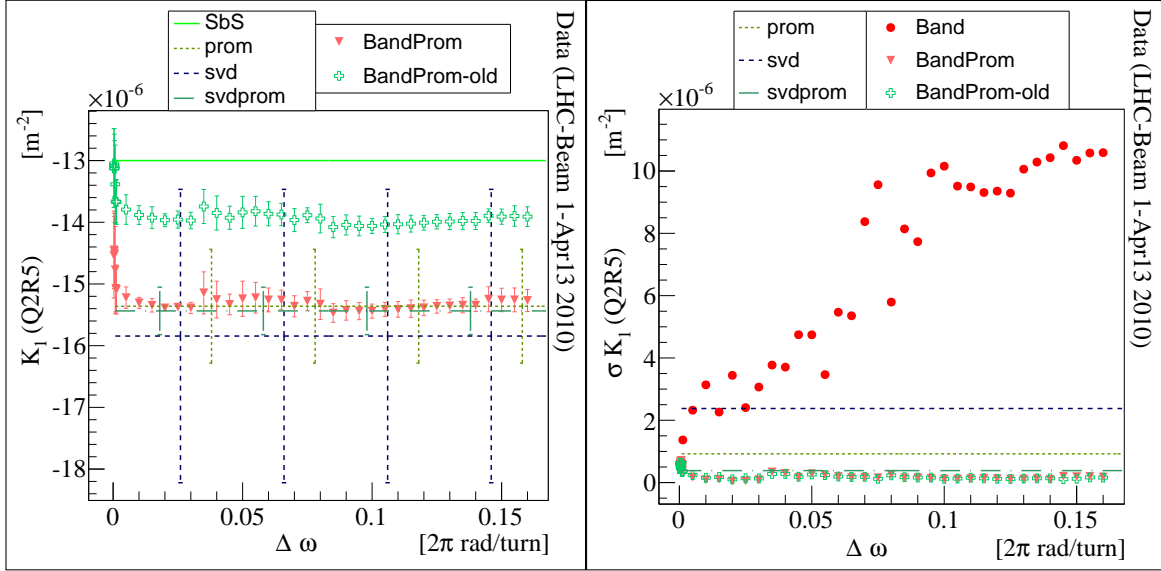


Figure 8-3.: Comparison between the formulations when the filters and their combinations are applied, for K_1 (Q2R5) (left) and its uncertainty (right) calculation. Results for 2010's Experimental Orbits (obtained three magnetic errors), using the New Formulation and the best case using the **Old** Formulation.

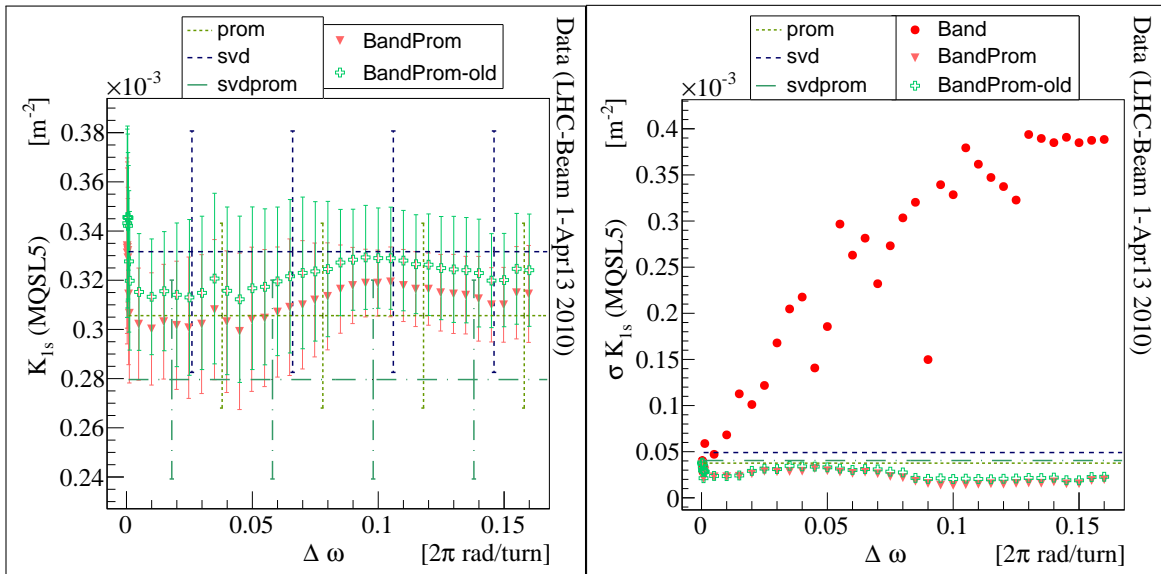


Figure 8-4.: Comparison between the formulations when the filters and their combinations are applied, for K_{1s} (MQSL5) (left) and its uncertainty (right) calculation. Results for 2010's Experimental Orbits (obtained three magnetic errors), using the New Formulation and the best case using the **Old** Formulation.

8.2. Magnetic Error Measurements using APJ with 2015's Orbits

In the middle of April/2015, arrangements were made to go along with the experimental measurements as part of this investigation. It was an opportunity to travel to CERN and observe how the experiments are made and to share the analysis of the recent orbits.

As mentioned earlier several configurations were taken during the experiments. In particular for this dissertation the magnetic errors were obtained from four different optics or conditions: $\beta^* = 1, 0.8, 0.65$ and 0.40 m. The analysis are done for the LHC regions IR1 and IR5. The data are the orbits obtained on May 11th, 2015 when the corrections were removed.

In Tables 8-4 and 8-5 the results obtained for the three magnetic errors measurements using the previous and new APJ formulations are presented, for the LHC regions IR5 and IR1, respectively. It is observe that in most cases the new formulation reduce the uncertainty of the magnetic errors measurements.

Taking the results for any optics and beam, from Table 8-4, the total average uncertainty for the normal quadrupole errors ($\langle \sigma K_1 \rangle$) is $2.48 \times 10^{-7} m^{-2}$ for the reformulation and $7.41 \times 10^{-7} m^{-2}$ for the previous formulation (labeled Old). While the uncertainty for the skew quadrupole error is in average $3.74 \times 10^{-6} m^{-2}$ and $10.7 \times 10^{-6} m^{-2}$, for the new and old formulations, respectively.

For both LHC regions IR5 and IR1, it is obtained that the measurements with $\beta^* = 1.0$ m show a higher reduction of noise when using the new formulation compared to the previous one. This reduction of noise is about 50% for the magnetic error at the quadrupole $K_1(Q2R5)$.

Table 8-4.: Results for the Magnetic Errors Measurements in IR5. LHC-2015's Experimental Orbits using the New and Old Formulations of APJ for different LHC Configurations

LHC Data	$K_1(\mathbf{Q2L5})$	$\sigma K_1(\mathbf{Q2L5})$	$K_1(\mathbf{Q2R5})$	$\sigma K_1(\mathbf{Q2R5})$	K_{1s}	σK_{1s}
May11/15	$10^{-7}[\text{m}^{-2}]$	$10^{-7}[\text{m}^{-2}]$	$10^{-5}[\text{m}^{-2}]$	$10^{-7}[\text{m}^{-2}]$	$10^{-5}[\text{m}^{-2}]$	$10^{-6}[\text{m}^{-2}]$
$\beta^*[\text{m}]$ /Beam	SvdProm-New					
0.40/B1	3.01	2.77	-1.81	1.02	-2.24	3.05
0.40/B2	-0.461	0.329	-1.79	0.472	-7.66	1.53
0.65/B1	3.41	2.37	-1.84	1.42	-2.43	4.95
0.65/B2	-5.50	0.824	-1.86	1.08	-8.18	1.72
0.80/B1	0.352	0.826	-1.84	0.879	-2.40	3.56
0.80/B2	-5.19	1.79	-1.90	1.81	-6.61	6.64
1.0/B1	-0.745	1.04	-1.84	0.664	-2.06	4.28
1.0/B2	-8.34	1.40	-1.93	1.16	-6.02	4.23
$\beta^*[\text{m}]$ /Beam	SvdProm-Old					
0.40/B1	2.12	2.93	-1.87	1.30	-2.03	4.84
0.40/B2	-1.86	0.238	-1.86	0.290	-8.82	1.09
0.65/B1	3.03	2.25	-1.89	1.23	-2.69	5.83
0.65/B2	-6.82	0.747	-1.92	1.10	-6.98	3.81
0.80/B1	-0.0336	0.859	-1.89	1.17	-2.66	4.47
0.80/B2	-6.13	2.17	-1.95	1.76	-5.00	6.88
1.0/B1	-18.5	30.7	-1.84	9.75	54.7	53.8
1.0/B2	-10.4	1.41	-1.97	1.40	-4.02	4.81

Table 8-5.: Results for the Magnetic Errors Measurements in IR1. LHC-2015's Experimental Orbits using the New and Old Formulations of APJ for different LHC Configurations.

LHC Data	$K_1(\mathbf{Q2L1})$	$\sigma K_1(\mathbf{Q2L1})$	$K_1(\mathbf{Q2R1})$	$\sigma K_1(\mathbf{Q2R1})$	K_{1s}	σK_{1s}
May11/15	$10^{-6} [\text{m}^{-2}]$	$10^{-7} [\text{m}^{-2}]$	$10^{-6} [\text{m}^{-2}]$	$10^{-8} [\text{m}^{-2}]$	$10^{-4} [\text{m}^{-2}]$	$10^{-6} [\text{m}^{-2}]$
$\beta^*[\text{m}]$ /Beam	SvdProm-New					
0.40/B1	-2.69	0.489	7.33	7.10	1.80	5.51
0.40/B2	-2.65	1.09	7.05	5.05	1.54	2.52
0.65/B1	-2.87	1.05	7.25	7.50	2.28	4.33
0.65/B2	-2.94	1.04	6.90	6.19	1.82	3.32
0.80/B1	-2.83	0.763	7.09	9.28	2.38	2.30
0.80/B2	-3.16	1.30	6.99	5.92	2.12	2.01
1.0/B1	-2.93	1.33	7.05	7.45	2.44	6.18
1.0/B2	-3.10	1.40	7.04	11.3	2.29	3.72
$\beta^*[\text{m}]$ /Beam	SvdProm-Old					
0.40/B1	-2.85	0.528	7.72	9.53	1.90	5.47
0.40/B2	-2.79	1.19	7.44	5.43	1.60	3.02
0.65/B1	-3.03	0.953	7.63	5.19	2.39	4.91
0.65/B2	-3.04	1.13	7.33	6.88	1.86	3.52
0.80/B1	-2.98	0.804	7.48	9.01	2.49	2.82
0.80/B2	-3.21	1.59	7.39	8.46	2.16	2.02
1.0/B1	-3.07	1.48	7.44	11.8	2.54	8.10
1.0/B2	-3.17	1.17	7.47	11.2	2.33	4.63

Although there is a different number of orbits available for each case, the Action J and Phase δ values are consistent for every set of orbits. Even more, the experimental plots have a very small jump or step between the region before and after the magnetic error. For instance, Figure 8-5 and Figure 8-6 show the case with the strongest jump observed, this is the measurements for Beam 1 in the LHC region IR5. The variables J and δ are obtained for the 4-type orbit *maxmax* as the average for many turns under the same condition.

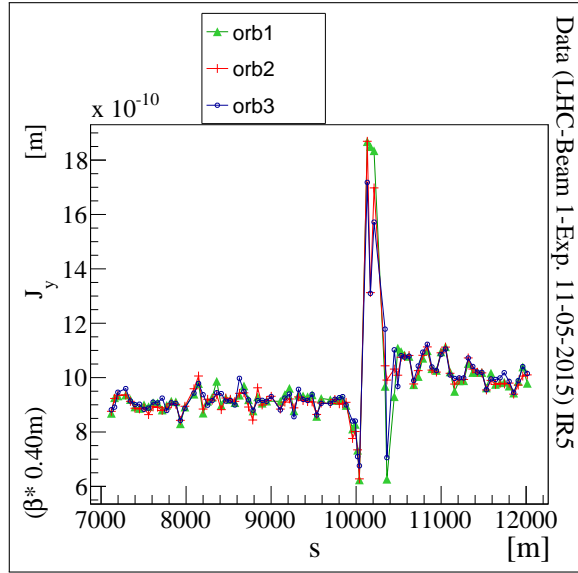


Figure 8-5.: Action in Y-axis (J_y) along the LHC. Results for Beam 1, $\beta^* = 0.40$ m, with 2015's Experimental Orbits.

The same behavior was observed for Beam 2. There are few jumps between the regions before and after the magnetic error, especially for the Action plots. Figure 8-7 shows the case for the stronger jump observed corresponding to the analysis in IR5. In the plots there are five orbits plotted, instead of three, the number of orbits in the plots for Beam 1. And the phase δ is obtained for the same 4-type orbit *maxmax*.

The experimental conditions for each set of orbits are the same, and the fact that the selected orbit is an average of many orbits, are the reasons of why, for all the orbits, the plots for each variable of Action or Phase are almost identical.

The observed differences in the variables for all the LHC configurations or optics are summarized in the plots for IR1 presented in Figure 8-8. The plots are for an individual orbit in each case and they are obtained for the 4-type orbit *maxmax*. For other cases it is observed a larger separations of the lines, as the effect observed for the region after the magnetic error

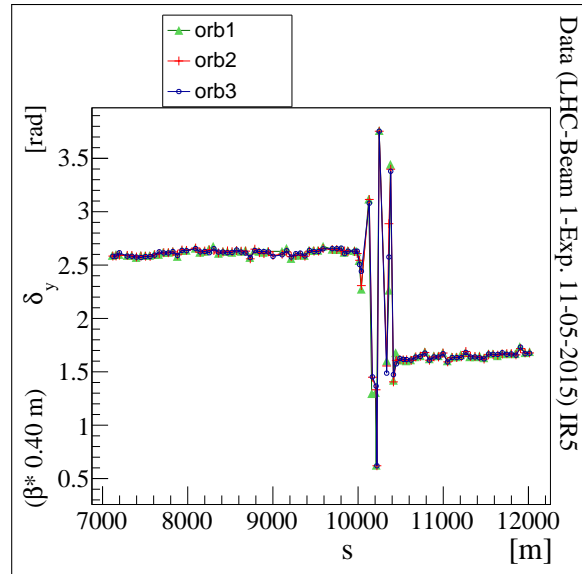


Figure 8-6.: Phase in Y-axis (δ_y) along the LHC. Results for Beam 1, $\beta^* = 0.40$ m, with 2015's Experimental Orbits.

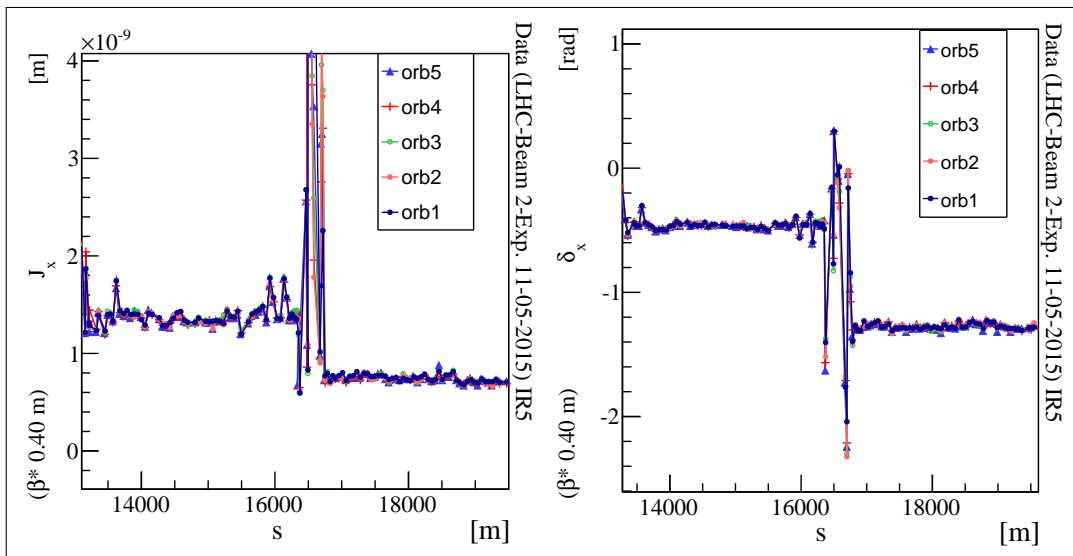


Figure 8-7.: Action and Phase in X-axis (J_x and δ_x) along the LHC. Results for Beam 2, $\beta^* = 0.40$ m, with 2015's Experimental Orbits.

for $\beta^* = 0.40$ m in Figure 8-8.

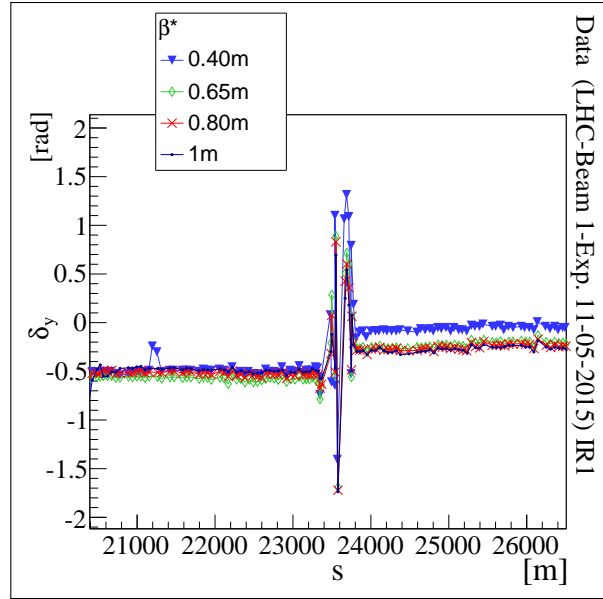


Figure 8-8.: Phase in Y-axis (δ_y) along the LHC for several LHC configurations. Results for Beam 1 from 2015's Experimental Orbits.

Filters Contributions to the Analysis of Experimental Orbits

According to the presented results, there is a small difference between the formulations which is evident for the average values and the corresponding statistical uncertainty. In general, there is a lesser value of the uncertainty when using the new formulation when the reduction is taken for the three magnetic errors at the same time.

The results for the experimental data of May 11th, 2015, using the filter *Band* combined with *Prom* and *Svd*, are in Tables 8-6 and 8-7, for the LHC regions IR5 and IR1, respectively.

In each table it is reported the average of the measured magnetic errors and their statistical uncertainty. For this analysis, the filter *SvdBandProm* is used, this is according to the simulated data results for the best filter to reduce noise (the one with least dispersion in the measurements) from the several filters studied.

As presented previously for the simulations, the results in the tables are obtained for each beam, in an independent way, and also for each turn-by-turn orbit from the experiment. Additionally, the results from both APJ formulations are reported, independently also. The results from the APJ formulations are obtained from the exactly the same selected orbit. In the tables, the new formulation results are with the header *-New* and corresponds to the first rows, while the previous formulation results are with the header *-Old*.

Table 8-6.: Results for the Magnetic Errors Measurements in IR5. LHC-2015's Experimental Orbits using the New and Old Formulations of APJ for different LHC Configurations.

LHC Data	$K_1(\mathbf{Q2L5})$	$\sigma K_1(\mathbf{Q2L5})$	$K_1(\mathbf{Q2R5})$	$\sigma K_1(\mathbf{Q2R5})$	K_{1s}	σK_{1s}
May11/15	$10^{-7}[\text{m}^{-2}]$	$10^{-7}[\text{m}^{-2}]$	$10^{-5}[\text{m}^{-2}]$	$10^{-8}[\text{m}^{-2}]$	$10^{-5}[\text{m}^{-2}]$	$10^{-6}[\text{m}^{-2}]$
$\beta^*[\text{m}]$ /Beam	SvdBandProm-New					
0.40 /B1	4.16	1.19	-1.78	1.05	3.11	3.61
0.40 /B2	1.96	0.327	-1.77	6.21	6.79	1.15
0.65 /B1	12.0	1.07	-1.84	7.50	6.15	0.968
0.65 /B2	-3.53	0.638	-1.84	6.38	6.78	1.84
0.80 /B1	10.4	0.716	-1.85	10.8	5.73	2.90
0.80 /B2	-4.82	0.842	-1.88	11.8	4.28	2.74
1.0 /B1	11.9	1.50	-1.87	8.01	7.88	7.10
1.0 /B2	-7.14	0.517	-1.92	11.3	2.98	4.03
$\beta^*[\text{m}]$ /Beam	SvdBandProm-Old					
0.40 /B1	3.41	1.20	-1.85	0.652	3.74	5.01
0.40 /B2	1.70	0.320	-1.85	7.14	8.11	0.394
0.65 /B1	11.8	0.774	-1.89	3.32	6.32	3.03
0.65 /B2	-5.32	0.562	-1.90	6.75	5.58	3.25
0.8 /B1	10.4	0.612	-1.90	13.8	5.79	2.13
0.8 /B2	-6.32	1.03	-1.93	6.02	2.58	3.73
1.0 /B1	-2.93	27.1	-1.86	116	11.4	59.0
1.0 /B2	-9.93	1.01	-1.96	13.1	0.855	5.08

When it is included the filter *Band*, its effect changes from one LHC region to another (IR5 or IR1), although generally it is observed a reduction in the uncertainty. Similarly, it is observed that the average values from each beam are now closer to each other than before.

The greatest evidence of the improvement in the measurement of the magnetic errors is observed in the $K_1(\mathbf{Q2L})$ and $K_1(\mathbf{Q2R})$ in the LHC regions IR5 and IR1, respectively. These cases are reported in Table 8-8 and Table 8-9 for IR5 and IR1, respectively. In the tables every row is for the cases without and with the filter *Band* under the same conditions. For this comparison the tables are constructed from the results reported previously in Table 8-6

Table 8-7.: Results for the Magnetic Errors Measurements in IR1. LHC-2015's Experimental Orbits using the New and Old Formulations of APJ for different LHC Configurations.

Data LHC	$K_1(\mathbf{Q2L1})$	$\sigma K_1(\mathbf{Q2L1})$	$K_1(\mathbf{Q2R1})$	$\sigma K_1(\mathbf{Q2R1})$	K_{1s}	σK_{1s}
May11/15	$10^{-6}[\text{m}^{-2}]$	$10^{-8}[\text{m}^{-2}]$	$10^{-6}[\text{m}^{-2}]$	$10^{-8}[\text{m}^{-2}]$	$10^{-4}[\text{m}^{-2}]$	$10^{-6}[\text{m}^{-2}]$
$\beta^*[\text{m}]$ /Beam	SvdBandProm-New					
0.40 /B1	-3.20	3.29	7.66	6.96	1.89	4.11
0.40 /B2	-2.60	3.41	7.29	4.10	1.40	0.874
0.65 /B1	-3.37	5.30	7.48	5.18	2.32	5.92
0.65 /B2	-2.86	7.88	7.04	5.78	1.75	2.99
0.80 /B1	-3.55	5.42	7.42	4.77	2.32	4.99
0.80 /B2	-3.00	6.12	6.94	2.96	2.25	5.72
1.0 /B1	-3.60	7.30	7.35	7.45	2.41	4.64
1.0 /B2	-3.10	9.32	7.02	8.36	2.43	4.15
$\beta^*[\text{m}]$ /Beam	SvdBandProm-Old					
0.40 /B1	-3.32	3.12	7.88	7.26	1.96	3.71
0.40 /B2	-2.75	3.49	7.66	3.87	1.47	0.760
0.65 /B1	-3.52	5.24	7.75	5.53	2.42	6.36
0.65 /B2	-2.97	8.42	7.44	5.58	1.78	2.76
0.80 /B1	-3.68	4.79	7.67	3.56	2.42	4.39
0.80 /B2	-3.12	7.96	7.39	5.52	2.30	5.97
1.0 /B1	-3.72	7.61	7.59	7.25	2.50	4.93
1.0 /B2	-3.22	8.27	7.48	7.29	2.48	5.10

and Table 8-7.

To obtain the results including *Band*, two trials were made to get the optimal bandwidth, letting for later studies a more precise and deep investigation the complete procedure as it is described in previous chapters, and as it will show in the next section this bandwidth selection favors the use of the SBS method.

Taking the results of the optics and beams using the filter *SvdBandProm*, from Table 8-6 , the total uncertainty for the normal quadrupole errors (σK_1) is 8.73 for the reformulation

Table 8-8.: Comparison between Filters for one of the Magnetic Errors at IR5. LHC-2015's Experimental Orbits using the New and Old Formulations of APJ for different LHC Configurations.

Data LHC	SvdProm		SvdBandProm	
	$K_1(\mathbf{Q2R5})$	$\sigma K_1(\mathbf{Q2R5})$	$K1(\mathbf{Q2R5})$	$\sigma K_1(\mathbf{Q2R5})$
May11/15	$10^{-5} [\text{m}^{-2}]$	$10^{-7} [\text{m}^{-2}]$	$10^{-5} [\text{m}^{-2}]$	$10^{-7} [\text{m}^{-2}]$
$\beta^*[\text{m}]$ /Beam	APJ-New			
0.40 /B1	-1.81	1.02	-1.78	0.105
0.40 /B2	-1.79	0.472	-1.77	0.621
0.65 /B1	-1.84	1.42	-1.84	0.750
0.65 /B2	-1.86	1.08	-1.84	0.638
0.80 /B1	-1.84	0.879	-1.85	1.08
0.80 /B2	-1.90	1.81	-1.88	1.18
1.0 /B1	-1.84	0.664	-1.87	0.801
1.0 /B2	-1.93	1.16	-1.92	1.13
$\beta^*[\text{m}]$ /Beam	APJ-Old			
0.40 /B1	-1.87	1.30	-1.85	0.00652
0.40 /B2	-1.86	0.290	-1.85	0.714
0.65 /B1	-1.89	1.23	-1.89	0.332
0.65 /B2	-1.92	1.10	-1.90	0.675
0.80 /B1	-1.89	1.17	-1.90	1.38
0.80 /B2	-1.95	1.76	-1.93	0.602
1.0 /B1	-1.84	9.75	-1.86	11.6
1.0 /B2	-1.97	1.40	-1.96	1.31

and $14.11 \cdot 10^{-7} \text{ m}^{-2}$ for previous (old) formulation. While the total uncertainty for the skew quadrupole error is 3.04 and $10.2 \cdot 10^{-6} \text{ m}^{-2}$, for the new and old formulations, respectively.

The difference in the average of the uncertainties does not come from a remarkable difference in the uncertainties founded for each optics independently from the formulations used; it is obtained from one or two values of some particular optics and the filter *Band* is not able to suppress that difference. Such case is for instance $\beta^* = 1.0 \text{ m}$ as it is clearly shown in Table 8-8. These results are closer to the predicted results from the simulations.

Table 8-9.: Comparison between Filters for one of the Magnetic Errors at IR1. LHC-2015's Experimental Orbits using the New and Old Formulations of APJ for different LHC Configurations.

Data LHC May11/15	SvdProm		SvdBandProm	
	$K_1(\mathbf{Q2L1})$ $10^{-6}[\text{m}^{-2}]$	$\sigma K_1(\mathbf{Q2L1})$ $10^{-7}[\text{m}^{-2}]$	$K_1(\mathbf{Q2L1})$ $10^{-6}[\text{m}^{-2}]$	$\sigma K_1(\mathbf{Q2L1})$ $10^{-7}[\text{m}^{-2}]$
$\beta^*[\text{m}]$ /Beam	APJ-New			
0.40 /B1	-2.69	0.489	-3.20	0.329
0.40 /B2	-2.65	1.09	-2.60	0.341
0.65 /B1	-2.87	1.05	-3.37	0.530
0.65 /B2	-2.94	1.04	-2.86	0.788
0.80 /B1	-2.83	0.763	-3.55	0.542
0.80 /B2	-3.16	1.30	-3.00	0.612
1.0 /B1	-2.93	1.33	-3.60	0.730
1.0 /B2	-3.10	1.40	-3.10	0.932
$\beta^*[\text{m}]$ /Beam	APJ-Old			
0.40 /B1	-2.85	0.528	-3.32	0.312
0.40 /B2	-2.79	1.19	-2.75	0.349
0.65 /B1	-3.03	0.953	-3.52	0.524
0.65 /B2	-3.04	1.13	-2.97	0.842
0.80 /B1	-2.98	0.804	-3.68	0.479
0.80 /B2	-3.21	1.59	-3.12	0.796
1.0 /B1	-3.07	1.48	-3.72	0.761
1.0 /B2	-3.17	1.17	-3.22	0.827

In the case of the region IR1, the use of the filter *Band* reduce the uncertainty in all cases for the quadrupole $K_1(\mathbf{Q2L1})$, regarding the optics or the formulation of the APJ used, as presented in Table 8-9. Also the obtained uncertainties are in general slightly lower using the reformulation of the APJ method.

8.3. Magnetic Error Measurements using SbS with 2015's Orbits

In the following, the results for the analysis using the Orbits of May 11th, 2015 are presented. The results might differ from an analysis on the same orbits in CERN, initially because of the configuration used for the filter *Svd*. For this dissertation the raw data are filtered using *Svd* to have the exact same initial orbits as the analysis performed using the Action and Phase Method. Recent changes in the format of the *Svd* software have been made, and mostly a different number of singular values was found as the default in the package of the SBS method, SbS, so the older version of the filter *Svd* is kept for the analysis. Nevertheless, the results obtained in here are quite similar and consistent to the ones obtained at CERN, as it is presented in the next section.

From the established configurations for the SBS when doing experimental analysis, as described previously, the magnetic errors are measured in the exact same magnets used in the previous APJ analysis, for the same experimental data. Therefore the measurements are performed in the LHC regions IR5 and IR1.

In Table **8-10** the results for the normal quadrupole magnetic error at the LHC region IR5 are presented. The results are from the available configuration at the experiments. The corresponding nomenclature in SbS for the negative value of the magnetic errors at the quadrupoles K_1 (Q2L5) IR5 and K_1 (Q2R5) are *dktqx2.l5* and *dktqx2.r5*, respectively.

Table 8-10.: SBS Results for the Measurement of the Normal Quadrupole Errors at IR5. LHC-2015's Experimental Orbits with filter *Svd*.

Optics	<i>dktqx2.l5</i>	K_1 (Q2L5)	<i>dktqx2.r5</i>	K_1 (Q2R5)
β^* [m]	10^{-7} [m ⁻²]	10^{-7} [m ⁻²]	10^{-5} [m ⁻²]	10^{-5} [m ⁻²]
0.40	7.03	-7.03	1.75	-1.75
0.65	31.0	-31.0	1.74	-1.74
0.80	35.0	-35.0	1.72	-1.72
1.0	-7.31	7.31	1.92	-1.92

The results are obtained using the same segment length for all the optics. Also, the results are from the first iteration of the program, this means that the obtained values are directly given by the computer.

Likewise as presented for the LHC region IR5, the results for IR1 using the same experimental turn-by-turn orbits are obtained. Now, the corresponding variables in SbS are *dktqx2.l1* and *dktqx2.r1*. The results for the normal quadrupole magnetic errors are shown in Table 8-11.

Table 8-11.: SBS Results for the Measurement of the Normal Quadrupole Errors at IR1. LHC-2015's Experimental Orbits with filter *Svd*.

Optics	dktqx2.l1	$K_1(Q2L1)$	dktqx2.r1	$K_1(Q2R1)$
β^* [m]	10^{-6} [m^{-1}]	10^{-6} [m^{-2}]	10^{-6} [m^{-1}]	10^{-6} [m^{-2}]
1.0	3.88	-3.88	-7.62	7.62
0.40	3.44	-3.44	-7.68	7.68
0.65	12.1	-12.1	-18.6	18.6
0.80	3.17	-3.17	-16.0	16.0

The number of rows in Tables 8-11 and 8-10 are lesser than the previous results on the same data, using the APJ method. This is because the SBS results are obtained using the information from the two beams at the same time. This last leads to decrease the possibility that the corrections obtained from one beam destabilize the other beam.

Before reporting the results for the skew quadrupole magnetic errors, the FFT spectra from the transverse position are presented. These plots are very close to the spectra used in the Resonance Driving Terms method to obtain the skew magnetic errors. For each beam and for each transverse plane, the FFT of the transverse position at the BPM 21L5 is obtained, and it is expected to get similar spectra with the same bands, for the other positions along the accelerator. Results for Beam 1 are shown in Figure 8-9, while results for Beam 2 are shown in Figure 8-10.

In each figure there is an overlap of the results obtained for the FFT from: the experimental Turn-by-Turn orbit without filtering (labeled **Exp.Dat.**), the experimental Turn-by-Turn orbit with the filter *Svd* (as the configuration established in this investigation), the experimental Turn-by-Turn orbit with the filter *SvdBand*. For Beam 1, the experimental orbit is the so called 2015_05_11@12_12.36 corresponding to $\beta^* = 0.80$ m in the LHC Experiment of May 11th, 2015 ($Q_x=0.265$, $Q_y=0.325$). For Beam 2, the experimental orbit is the so called 2015_05_11@12_11.57 corresponding to the same characteristics of beam 1.

Using the RDT method the main bands in the FFT were named, and it is observed that the expected bands from the normal quadrupole and skew quadrupole magnetic errors are

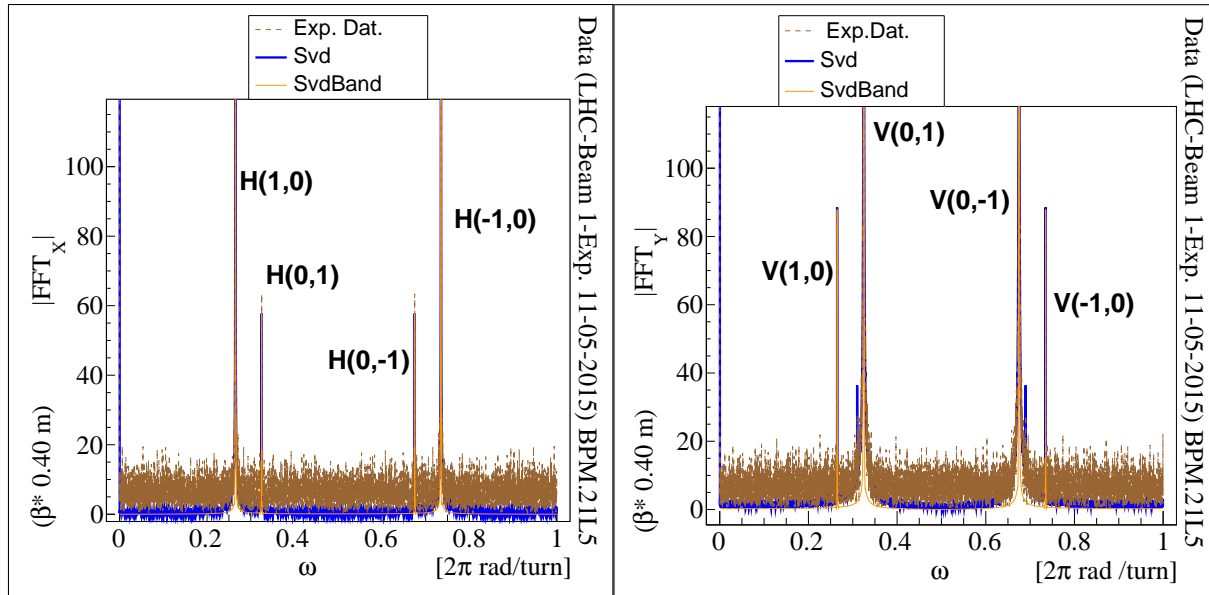


Figure 8-9.: FFT of the position with and without filters, for plane X (left) and plane Y (right). Results for Beam 1 and spectral bands identified using the RDT Method. 11-05-2015's Experimental Orbits.

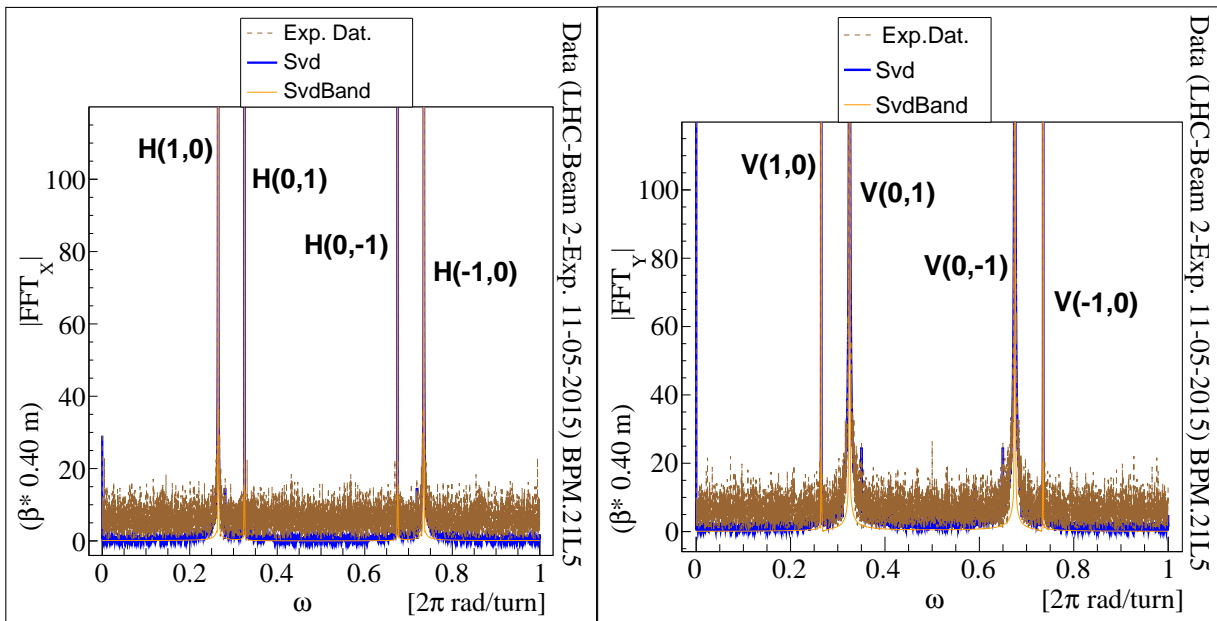


Figure 8-10.: FFT of the position with and without filters, for plane X (left) and plane Y (right). Results for Beam 2 and spectral bands identified using the RDT Method. 11-05-2015's Experimental Orbits.

very clear. In these plots (Figure 8-9 and Figure 8-10) the bottom part of the spectra is presented, this is done also to have an idea of the noise presented and subtracted. For beam

1, the bands reach intensities up to 2400 and 2000 for the two main bands, while for beam 2 the band reach intensities up to 900 and 2500.

Therefore, the plots shown that the noise is reduced in larger amount when just the *Svd* filter is applied, but then it is reduced further when *SvdBand* is used. These plots are the similar presented in other parts of this dissertation and in [35] and [41], for different magnetic error simulations where the filter *Band* was used.

In Table **8-13**, results for the magnetic skew quadrupole errors are presented. These are obtained using SbS for the LHC Regions IR5 and IR1 independently. From the table it is inferred that there is not a dependency between the results and the analyzed optics. In this calculations, compared to the previous ones for the normal quadrupole errors, is necessary to change the segment length for each LHC configuration or optics. This last because there are BPMs at the IRs which do not reported any measurement, and in particular those measurements are very relevant to obtain the magnetic errors.

According to the results, it is observed that there are variations in the magnetic errors measurements which are very big notorious for each configuration studied. This same behavior, as mentioned previously, is observed in the analysis using APJ with the same orbits, especially for the skew quadrupole magnetic errors.

Going a step forward, the results for the filter *SvdBand* are presented. When the SBS method is used on experimental data after filtering with *SvdBand*, it is observed that the results are even much closer to each other than with the filter *Svd*. Even more, these results are closer to what is obtained using APJ, as presented in the next chapter .

Table **8-12** presents results when the measurement of the magnetic errors are obtained using the SBS method. The results are for the Experimental orbits from May 11th, 2015 (same Turn-by-turn orbits using the previous analysis using the APJ method).

The most notorious case of improvement in the results, when adding the filter *Band*, could be $K_1(Q2R5)$: according to results on Table **8-11** the initial range in the results for the different LHC configurations is from -1.86×10^{-5} to -7.62×10^{-6} , while now the range in the magnetic error is only from 1.82×10^{-5} a $1.84 \times 10^{-5} m^{-2}$.

The results for the skew quadrupole magnetic error are in Table **8-13** for both LHC regions IR5 and IR1, and for the filters *Svd* and *SvdBand*, at the top and at the bottom of the table, respectively. Similarly to what is observed for the normal quadrupole errors, the uncertainty in the magnetic error measurement for the magnet $K_{1s}(MQSL5)$ is reduced with the additional use of *Band*, and this holds for all the LHC configurations studied. However, the average

Table 8-12.: Magnetic Errors Corrections using SBS. LHC-2015's Experimental Orbits applying the *SvdBand* Filter.

IR5				
Optics	dktqx2.l5	$K_1(Q2L5)$	dktqx2.r5	$K_1(Q2R5)$
β^* [m]	10^{-7} [m ⁻²]	10^{-7} [m ⁻²]	10^{-5} [m ⁻²]	10^{-5} [m ⁻²]
0.40	2.05	-2.05	-1.82	1.82
0.65	3.60	-3.60	-1.84	1.84
0.80	1.95	-1.95	-1.82	1.82
1.0	8.45	-8.45	-1.83	1.83
IR1				
Optics	dktqx2.l1	$K_1(Q2L1)$	dktqx2.r1	$K_1(Q2R1)$
β^* [m]	10^{-6} [m ⁻²]	10^{-6} [m ⁻²]	10^{-6} [m ⁻²]	10^{-6} [m ⁻²]
0.40	-3.92	3.92	7.23	-7.23
0.65	-2.85	2.85	6.99	-6.99
0.80	-1.85	1.85	6.94	-6.94
1.0	-4.02	4.02	7.52	-7.52

of the magnetic errors decreases in amount compared to the normal quadrupole error case.

8.4. Summary of Results from the Different Methods with 2015's Orbits

The APJ and SBS method share the fact that a theoretical division in the Accelerator is done, and for each region separately the measurements are made from the BPM's measurements.

Also, all methods implicate an expected model for the accelerator to obtain the magnetic errors, despite the fact, that they deal with different physical quantities.

In addition, APJ and RDT methods start with the normalized positions obtained from the β function of the accelerator model.

Nevertheless, each method uses the measurements in a different way. The SBS uses the information from three consecutive BPMs while the other takes the information from two or

Table 8-13.: Magnetic Errors Corrections for Local Coupling using SBS. LHC-2015's Experimental Orbits.

β^*	$K_{1s}(\mathbf{MQSL5})$	$K_{1s}(\mathbf{MQSL1})$
[m]	$10^{-5} [m^{-2}]$	$10^{-4} [m^{-2}]$
Svd Filter		
0.40	-11.5	4.84
0.65	-7.24	3.11
0.80	-5.18	3.67
1.00	-6.46	2.15
SvdBand Filter		
0.40	-8.83	5.30
0.65	-5.30	3.00
0.80	-5.38	2.93
1.00	-6.08	1.11

one BPM.

Even more, the theoretical divisions in the accelerators differ from one method to the other. For instance, the reformulated APJ introduced in this dissertation uses the information from the BPMs at the LHC Arcs, while the SBS uses the BPMs at the IRs, including the BPMs at the triplets. The previous formulation of the APJ uses only one measurement from the LHC IR.

As a comparative analysis of the methods studied, Table 8-14 shows a summary of the quadrupole linear corrections obtained from the measurement of the magnetic errors at IR1 and IR5 for the LHC-2015's Experimental Orbits. The magnetic error measurements for the quadrupole $K_1(\mathbf{Q2L5})$ is omitted in the table because its average value is as close as its uncertainty, and also its average value is much lesser compared to the results for the magnet $K_1(\mathbf{Q2R5})$.

Two main observations can be obtained from the general results for the studied IRs. The first observation is that the calculated magnetic errors for IR5 have a different strength (or magnitude) in comparison with the obtained values for IR1. The second observation is that all the magnetic corrections for the IR1 normal quadrupoles are within the same range, something opposite to what is observed for IR5 where a change in the power of tens for

$K_1(Q2R5)$ and $K_1(Q2L5)$ is obtained (see Table 8-12).

In addition, Table 8-14 contains the reported corrections established by the team of experts at the CERN. These corrections labeled by *OMC Correction* were calculated by the OMC team using the same experimental data, although with different filters, [57]. In the table, the value reported in parenthesis corresponds to the magnetic errors measurements where more magnets were involved in the same IR (the other magnet has the variable `dktx1.r1` and value of -3.31×10^{-5}).

In the experiment on May 11th, 2011, some corrections in the LHC were performed in IR2, IR5 and IR8. In particular for IR5 they are:

- at MQXB2.R5, 1.9×10^{-5}
- at MQXB2.L5, -0.09×10^{-5}
- at MQXA1.R5, -2×10^{-5}
- at MQXA1.L5, 2×10^{-5}

The corrections performed at LHC, for IR5, are only for normal quadrupole magnetic errors. More than one magnet is modified by the change in the variables MQXA1.R5 and MQXA1.L5, but because the symmetry of the triplets at the left and right of IP5, there are not expected greater variations in the predicted corrections without taking into account this modification. The values for the OMC corrections presented in the Table 8-14 does not report a change in the quadrupoles given by the variables MQXA1.R5 and MQXA1.L5.

It is clear that most of the values obtained using the Action and Phase method are similar to the values of the corrections installed in the LHC on May 11th, 2015. Also, there are some cases where the corrections are similar to the obtained using SBS. The values reported in the table are obtained from the first iteration with the SbS (as performed with the simulated orbits), these values are labeled by *SBS calc.*, and the calculation were made from the *Linux terminal* and do not from the *GUI*. As mentioned in the analysis of the simulated data, the SbS program have been taken with the option SUSSIX, and other options, like SVD, are available. It is possible that some other option in SbS would imply a closer value do not only to the Action and Phase Method values but also closer to the other corrections reported in the LHC with this same data.

Once the magnetic errors are measured and the corrections are determined, plots for the Phase Advance Difference are constructed for each beam and transverse plane. For the above analysis of the LHC experimental orbits (Table 8-14), the average of the obtained corrections at the several configurations are taken. This last means that for the APJ method the average

was taken without taking into account if the measurement was done with Beam 1 or Beam 2.

The results for IR5 are presented in Figure 8-11.left and Figure 8-11.right, for the phase advances ϕ_x and ϕ_y , respectively, while the results for IR1 are in Figure 8-12.left and Figure 8-12.right. The reported plots are for the measurements of Beam 2.

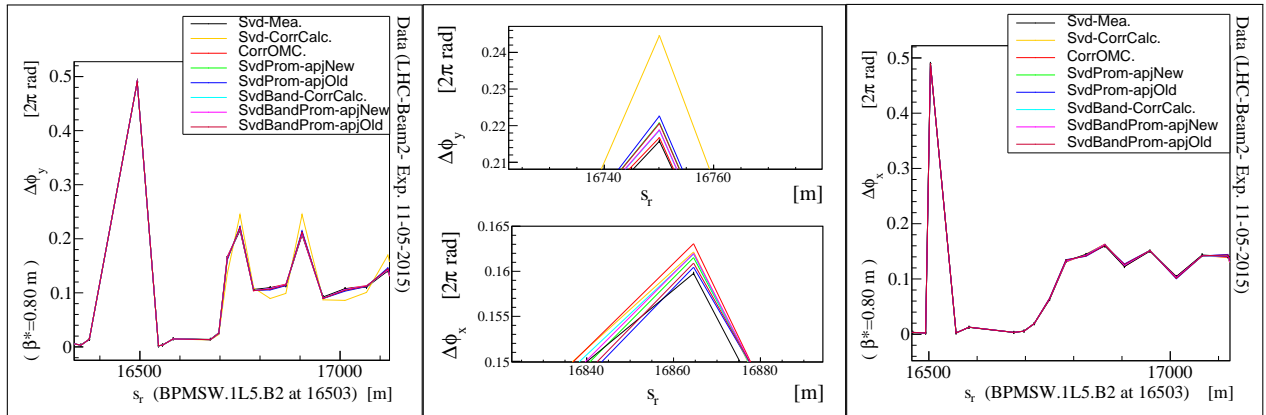


Figure 8-11.: Phase Advance Difference segment by segment at IR5, for the calculated corrections with the different methods, measured and propagated in planes Y (left) and X (right). A close-up (center) for the approximations to the data points (with error bars, 11-05-2015's Experimental Orbits) is presented. The same LHC model is used in all cases therefore the plots overlaps at the start.

These plots are obtained when SbS adds the corrections to the LHC model in the simulator. Therefore, it is expected that the line corresponding to the measurement, denoted by *Svd-Mea.* be overlapped by the lines corresponding to the corrections. In the plots the measurement line are for the orbits after filtering using *Svd*. The labels are: *Svd-CorrCalc.* for the correction calculated using SbS after filtering with *Svd*, *CorrOMC.* for the correction given by the OMC team at CERN with the orbits treated as they usually do, *SvdProm-apjNew* for the correction given by the Reformulation of APJ, *SvdProm-apjOld* for the correction using the previous version of APJ, *SvdBand-CorrCalc.* for the correction given by SBS when the orbits are also filtering using *Band*, *SvdBandProm-apjNew* for the correction given by the APJ Reformulation on the orbits including *Band*, and *SvdBandProm-apjOld* for the correction given by the previous APJ on the orbits including *Band*.

In general for the two IRs, it is visually observed that the results using SBS for the orbits filtered using *Svd* gives the furthest results from the experimental line. Additionally, although it might not be clear from the values on the tables, there is a consistency between the results obtained using SBS and using APJ. For a better appreciation of the similarities and differences in the results from the different methods, in upper left corner of the plots, a

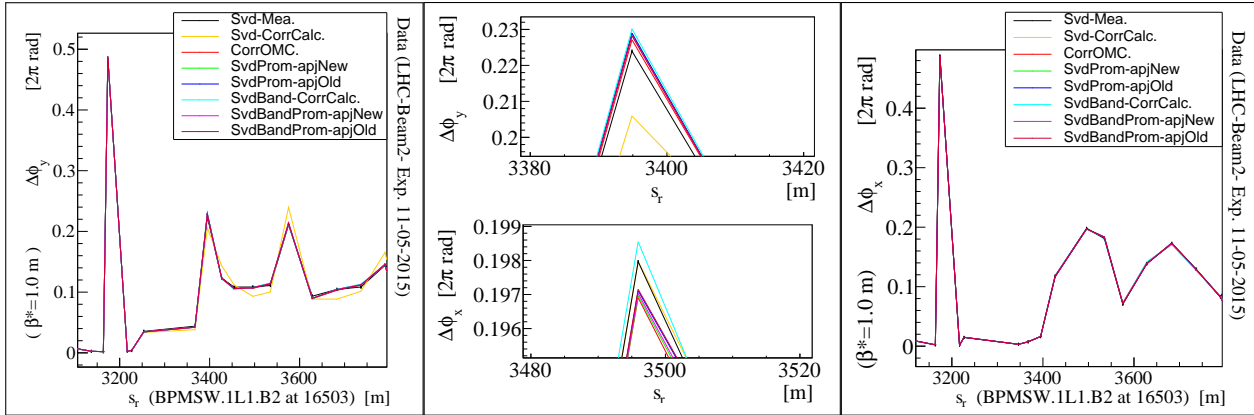


Figure 8-12.: Phase Advance Difference segment by segment at IR1, for the calculated corrections with the different methods, measured and propagated in planes Y (left) and X (right). A close-up (center) for the approximations to the data points (with error bars, 11-05-2015's Experimental Orbits) is presented. The same LHC model is used in all cases therefore the plots overlaps at the start.

close-up of the main peaks is presented (the peaks corresponds to the magnetic errors). In the close-up it is clear to see that none of the calculated corrections are totally effective, in the sense that there is not a line that overlapped the measured one.

From the results for IR5 all the corrections seems to be equally effective, except for the calculations obtained as *Svd-CorrCalc.*, while for IR1, the results obtained from both transverse planes are compensate, and the best correction will be with *SvdBandProm-apjNew*. These results are similar to what it is obtained using Beam 1 (see Appendix in [44]).

To remark, the corrections given by SBS using *SvdBand* are not only much closer to the APJ results compared to *Svd*, but also their corresponding line is the closest to the experiment measurement one.

For the skew quadrupole errors a different comparison analysis is presented. As mentioned before, the RDT method is used in this case. In Table 8-15, the corrections from the measured magnetic errors for the 2015's experimental orbits are presented. For this type of errors there were not a correction performed at LHC in May 11th, 2015.

The results from IR1 seems to be more precise than the results for IR5, according to the numbers in the table. This might be because the presence of sextupole errors or higher multiple magnetic errors in IR5 compared to the non-linear errors in IR1.

From a first sight on the values in the Table 8-15, without taking into account the optics or

the beam involved, there is a similarity in the results obtained from APJ using the traditional configuration and the results obtained from SBS.

Something that it is very evident in this Table **8-15**, and it is noticed in the previous corresponding tables, is the larger difference between the results obtained for MQSL5 when $\beta^* = 1.0 m$ and the Beam is 1 using the Old formulation compared to the results for the others β and Beams using both APJ and SBS. The corresponding value $0.547 \times 10^{-5} m^{-2}$ is obtained from the measurements on 8 orbits, these are: _05_11. Orbit 1 at 11_23_36, orbit 2 at 11_24_45, orbit 3 at 11_26_12, orbit 4 at 11_30_19, orbit 5 at 11_31_33, orbit 6 at 11_32_37, orbit 7 at 11_33_47, and orbit 8 at 11_35_02. For the filter *SvdProm*, the values of the first 6 orbits are consistent with is other given an average of $1.44 \times 10^{-6} m^{-2}$ (std $6.78 \times 10^{-8} m^{-2}$) while the last two orbits give an average of $-4.62 \times 10^{-6} m^{-2}$ (std $1.40 \times 10^{-7} m^{-2}$).

The above described differences are not observed for the new formulation of APJ, meaning that this an evidence of the expected consequences when using one formulation or the other. Taking a further look on the BPMs measurements in the orbits, it is obtained that the measurements from BPMSY.4L5.B1 (the corresponding central BPM to obtain the magnetic errors at IR5) are not available for some orbits, in fact, for $\beta^* = 1.0 m$ there is not measurements for Plane Y in orbit 2, and for Plane X in orbits 7 and 8. Also, for the others β^* , the measurements are available in both planes for $\beta^* = 0.40 m$, $\beta^* = 0.65 m$, and with exception of one orbit out of six orbits in Plane Y, the measurements are available in both planes for $\beta^* = 0.80 m$. Therefore, these results are a proof that the Old formulation is very sensitive when there is not data for the central BPM in plane X, although, it is an unusual case in the experiments. This evidence is strong for MQSL5 but the same behavior is expected for the other magnetic errors obtained for $\beta^* = 1.0 m$ and Beam 1, and the other cases without the complete measurements.

Also, some other missing measurements could explained why the measurements obtained for $\beta^* = 1.0 m$ has the highest uncertainty, without matter the method used.

Comparing the results for both IRs, the strength of the magnetic errors at IR5 seems to be stronger than for IR1, as observed for the normal quadrupole errors.

The obtained plots for skew magnetic corrections are presented in the following paragraphs. The sequence of the plots is same as presented in Figure 5.21 and Figure 5.22 in [50] for the 2010 measurements. The notation used is the same as given for the normal quadrupole corrections in this dissertation. In this case the vertical axis corresponds to a superimpose of the resonance driving term f_{1001} amplitude, its real part and imaginary part.

Figure **8-13** contains the results for the LHC region IR5 and the 2015's experimental orbits.

It seems that the fit from Beam 1 is better compared to the one for Beam 2. These plots are just for the case $\beta^* = 0.65 m$, after the BBQ data were filtered using *Svd*. The plots for the other optics can be consulted in the appendix of [44].

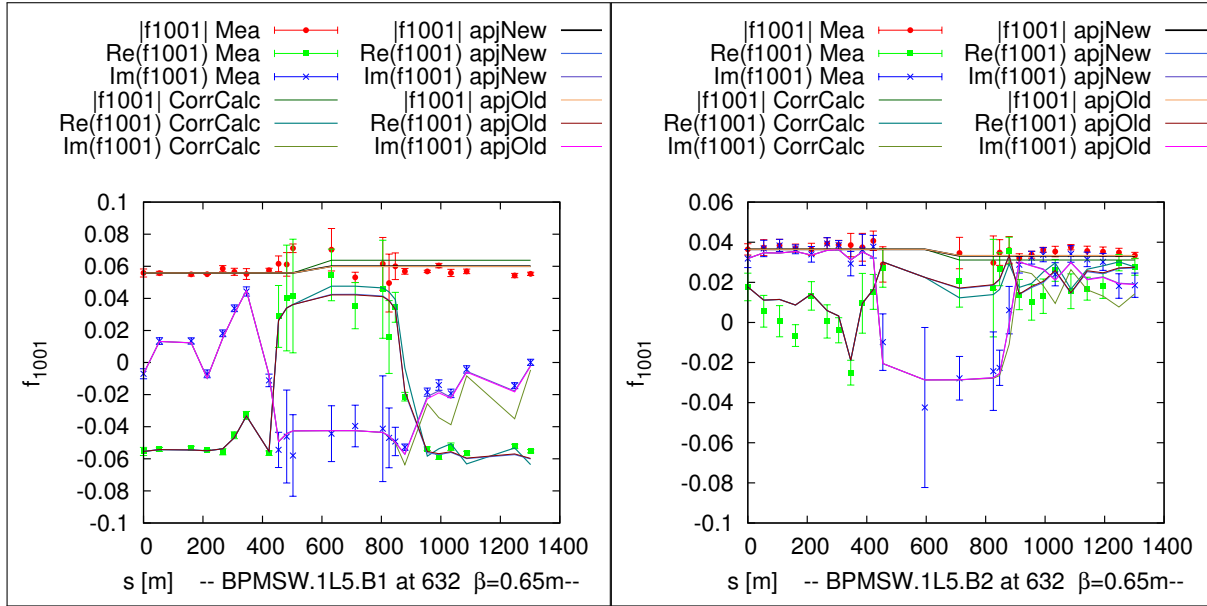


Figure 8-13.: Results for the calculated corrections using the different methods for LHC region IR5. In the plots the real part (Re), the imaginary part (Im) and the absolute value f_{1001} are shown. (left) Using Beam 1 and (right) using Beam 2. 11-05-2015's Experimental Orbits.

For IR1 also, the fit for Beam 1 looks better than the fit for Beam 2. The results are in Figure 8-14. In these cases the results are shown for the case $\beta^* = 0.8 m$. The plots for the other optics can be consulted in the appendix of [44].

Finally, just to remember, the magnetic errors which are corrected using the Action and Phase method or the SBS method are really a very small quantity, even for the scales that the LHC handles, but the changes produced in the optical properties by these magnetic errors could have a big significance because of the precision expected by the physics experiments in the accelerator.

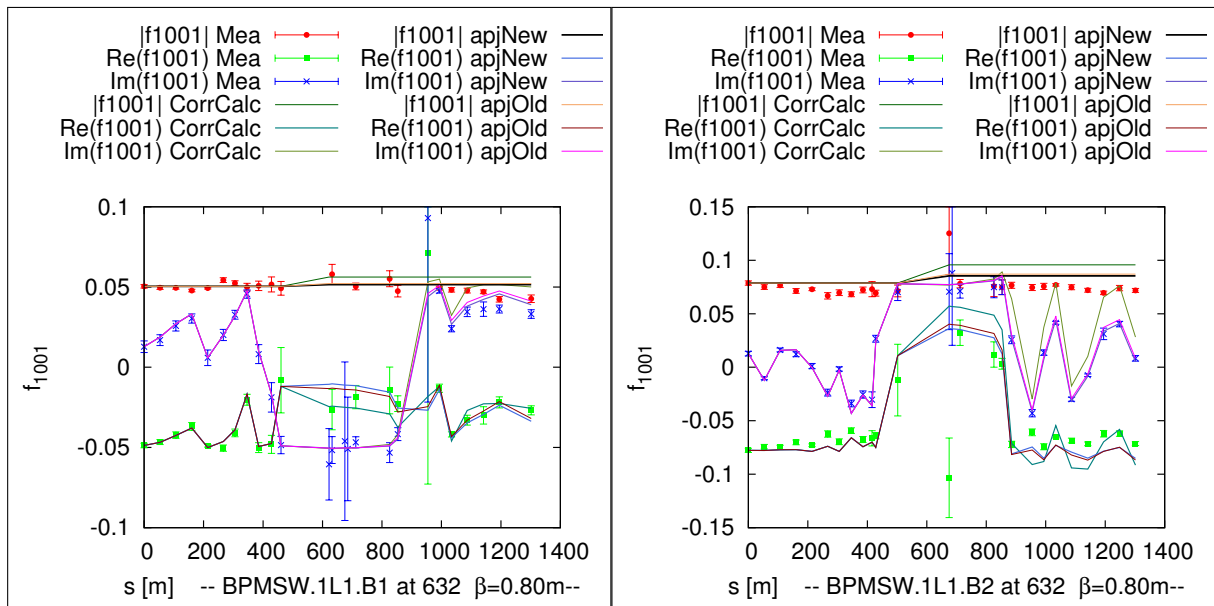


Figure 8-14.: Results for the calculated corrections using the different methods for LHC region IR1. In the plots the real part (Re), the imaginary part (Im) and the absolute value f_{1001} are shown. Using Beam 1 (at left) and using Beam 2 (at right) . 11-05-2015's Experimental Orbits.

Table 8-14.: Comparison for the Normal Quadrupole Corrections Results, obtained using the different Methods in IR1 and IR5. LHC-2015's Experimental Orbits.

LHC Data			IR5	IR1	
Run II	β^*	Beam	$K_1(\mathbf{Q2R5})$	$K_1(\mathbf{Q2L1})$	$K_1(\mathbf{Q2R1})$
May11/15	[m]		$10^{-5} [\text{m}^{-2}]$	$10^{-6} [\text{m}^{-2}]$	$10^{-6} [\text{m}^{-2}]$
SvdProm-New	0.4	1	1.81	2.69	-7.33
SvdProm-Old	0.4	1	1.87	2.85	-7.72
SvdProm-New	0.4	2	1.79	2.65	-7.05
SvdProm-Old	0.4	2	1.86	2.79	-7.44
Svd-SBS calc.	0.4		1.81	3.60	-7.46
SvdBand-SBS calc.	0.4		1.82	3.92	-7.23
SvdProm-New	0.65	1	1.84	2.87	-7.25
SvdProm-Old	0.65	1	1.89	3.03	-7.63
SvdProm-New	0.65	2	1.86	2.94	-6.90
SvdProm-Old	0.65	2	1.92	3.04	-7.33
Svd-SBS calc.	0.65		1.72	6.25	-8.46
SvdBand-SBS calc.	0.65		1.84	2.85	-6.99
SvdProm-New	0.8	1	1.84	2.83	-7.09
SvdProm-Old	0.8	1	1.89	2.98	-7.48
SvdProm-New	0.8	2	1.90	3.16	-6.99
SvdProm-Old	0.8	2	1.95	3.21	-7.39
Svd-SBS calc.	0.8		1.18	15.9	-11.7
SvdBand-SBS calc.	0.8		1.82	1.85	-6.94
SvdProm-New	1.0	1	1.84	2.93	-7.05
SvdProm-Old	1.0	1	1.84	3.07	-7.44
SvdProm-New	1.0	2	1.93	3.10	-7.04
SvdProm-Old	1.0	2	1.97	3.17	-7.47
Svd-SBS calc.	1.0		1.33	18.4	-12.5
SvdBand-SBS calc.	1.0		1.83	4.02	-7.52
OMC Correction [57]	0.4		1.778		(-12.5)
			1.8	3.5	-7.0
			1.9		
			1.75		
Corrections† in LHC			1.9		

Table 8-15.: Comparison for the Skew Quadrupole Corrections Results, obtained using the different Methods in IR1 and IR5. LHC-2015's Experimental Orbits.

LHC Data			K_{1s} (MQSL5)		K_{1s} (MQSL1)	
Run II	β^*	Beam	Svd	SvdBand	Svd	SvdBand
May11/15	[m]		10^{-5} [m ⁻²]	10^{-5} [m ⁻²]	10^{-4} [m ⁻²]	10^{-4} [m ⁻²]
APJ-New	0.4	1	-2.24	3.11	1.80	1.89
APJ-Old	0.4	1	-2.03	3.74	1.90	1.96
APJ-New	0.4	2	-7.66	-6.79	1.54	1.40
APJ-Old	0.4	2	-8.82	-8.11	1.60	1.47
Svd-SBS calc.	0.4		-11.5	-8.83	4.84	5.30
APJ-New	0.65	1	-2.43	6.15	2.28	2.32
APJ-Old	0.65	1	-2.69	6.32	2.39	2.42
APJ-New	0.65	2	-8.18	-6.78	1.82	1.75
APJ-Old	0.65	2	-6.98	-5.58	1.86	1.78
Svd-SBS calc.	0.65		-7.24	-5.30	3.11	3.00
APJ-New	0.8	1	-2.40	5.73	2.38	2.32
APJ-Old	0.8	1	-2.66	5.79	2.49	2.42
APJ-New	0.8	2	-6.61	-4.28	2.12	2.25
APJ-Old	0.8	2	-5.00	-2.58	2.16	2.30
Svd-SBS calc.	0.8		-5.18	-5.39	3.67	2.93
APJ-New	1.0	1	-2.06	7.88	2.44	2.41
APJ-Old	1.0	1	0.547	11.4	2.54	2.50
APJ-New	1.0	2	-6.02	-2.98	2.29	2.43
APJ-Old	1.0	2	-4.02	-0.855	2.33	2.48
Svd-SBS calc.	1.0		-6.46	-6.08	2.15	1.11

9. Conclusion and Future Direction

Up to now, all the proposed objectives for this dissertation have been developed, and the main results have been presented. These studies were made from August 2010 to November 2015 without interruption. In this chapter the conclusions encountered during the development of this dissertation are summarized and further suggestions as future direction are presented.

9.1. Conclusions

A reformulation of the Action and Phase Jump (APJ) Analysis Method have been introduced during this dissertation, in order to obtain and estimate the magnetic errors presented at the LHC region IR5 and IR1, using simulated turn-by-turn orbits from the LHC simulator in MAD-x and experimental orbits from the LHC.

Theoretical equations have been established where the central BPM dependency measurement is removed. An implementation of the equations (in Python) were developed as an extension of the already tested software for the APJ analysis on LHC orbits. Simulated and experimental orbits were analyzed to test and to evaluate the reformulation. Results show an initial contradiction for the effectiveness of the reformulation compared to the previous formulation, this is when the measurements from the 2010's orbits and the corresponding simulated orbits are taken into account. Nevertheless, for the 2015's orbits an improvement in the uncertainty values of the measurement is obtained. Even more, taking into account BPMs experimental issues, an advantage of the reformulation over the previous formulation is directly observed using simulations; for instance, the relative error in the recovered measurement of a single magnetic error is 3.896 % using the old formulation with an orbit without the measurements of the BPMs at the corresponding triplet, while the relative error using the reformulation with this same orbit is 0.1734 %. Certainly, if it is expected to get the magnetic corrections without paying attention of missing measurements from the BPMs, the reformulation is the best choice.

All the experimental LHC data analyzed during this dissertation is obtained using an AC Dipole, and its effect on the magnetic error measurements have been studied in this dissertation from the APJ analysis point of view. Results show that the measurements of the magnetic errors are not affected when the AC Dipole is included in the model of the accelerator, or, when the measurements are done without taking the AC Dipole into account. As

long as the AC Dipole or any other kicker is far away from the location of the magnetic errors that are measured, and betatron oscillations are provided, the APJ method can measure the magnetic errors successfully.

An additional aspect have been considered in the reformulation of the APJ method presented in this dissertation. This is, to include the possibility of having different phase advances in the quadrupoles at the LHC triplets. Results for the measurement of two normal quadrupole errors, using orbits from simulations, leads to a significant reduction in the relative errors, when using the reformulation compare to the previous formulation, from a relative error of 10% to around 1%; but for other trials the relative error is around 4% which is greater than 1%, the acceptable value for the relative errors using the APJ for other configurations. Therefore, the discussed results about the reformulation are understood to be from the formulation that eliminates the BPM measurement at the IR assuming a very small change in the phase advances at the quadrupoles.

The contributions of this dissertation are involved also in the reduction of noise using digital filters on the orbits. In this sense, an exploration of the possible ways to reduce the noise of the orbit data, presented at the LHC, by testing digital filters have been performed. Trials were made initially using simulated orbits obtained as the ideal orbits from the LHC simulator plus some random values as the noise presented, and then the trials are made on experimental orbits. A design of a *band-pass* filter was developed and results show that the best configuration is using a dual-band, otherwise a higher uncertainty in the recovery of the magnetic errors is reached, when the simulation is done for two magnetic errors with the thin lens approximation. Also, the corresponding signal-to-noise ratio for the filter was obtained and studied in simulated orbits, and its results show that the filter does not change the main jumps expected in the Action and Phase variables, and that the characteristic ratio does not change between the APJ regions, before and after the error, which are analyzed. The designed filter was combined with the other proven effective filters in the LHC. In total seven combinations of filters were studied and the filters that imply the least uncertainty were presented together, for each magnetic error measurement. A proposal of the curves to obtain the optimal bandwidth was also introduced in this dissertation, although a different bandwidth $\Delta\omega$ is obtained for each magnetic error. According to the simulated orbits with noise, the best combination of filters is the *SvdBandProm* which reduce the uncertainty further than the previous filter *Prom* when $\Delta\omega < 0.02 \ 2\pi$ rad, but this result is not obvious when using experimental orbits.

During the development of this dissertation a study of the alternative methods to estimate the magnetic errors at the LHC have been performed. Analysis on simulated and experimental orbits using the technique Segment-by-Segment (SBS) and Resonance Driving Terms (RDT) method were made. Although some initial implementation of the RDT method were

made [53], all the analysis presented in this dissertation were done using the CERN software written and used at the LHC by the OMC team. Following the indications provided for the use of the software and the options presented in the code, the magnetic errors at the same locations studied for the APJ method were obtained, and a comparison of the results for the same orbits were made. Results show that similar magnetic error measurements are obtained using all the methods, including APJ, in the 2015's orbits analysis. For the normal quadrupole magnetic errors, plots for the difference in phase advance $\Delta\phi$ for the studied cases were obtained, while plots for f_{1001} were obtained for the skew quadrupole error. In the graphs the difference between the fits given by the different methods is almost imperceptible despite the fact of a perceptible change in the observed averages. This last might imply that a broad range uncertainty is accepted in the measurements judging from the used tools, although as already mentioned, the results from the methods are similar.

Also, it has been found that the use of the filter *SvdBand* favors more the results given by the SBS technique in the experimental data, than the results given by the APJ method. In the SBS procedure, it is also available the module *Tune Cleaning* which can give similar results than the *band-pass* filter and that was not used in this dissertation. A deeper analysis can be performed to confirm this last, and it might be relevant because the observed reduction in the uncertainty is significant.

Although the obtained results for the magnetic error measurements can be interpreted in a subjective way due to the small quantities that are handled, there is one last remark on the results using experimental orbits. For the comparison between the APJ formulations, it have been obtained that the filter *SvdProm* is enough to have lesser values of uncertainty, when comparing to other filters and keeping into account the results for both LHC beams. In general, the biggest difference between the APJ formulations are obtained in the skew magnetic error measurement. Also, in summary, the uncertainty in the IR5 measurements with the 2015's orbits for the quadrupole magnetic errors have a total average ($\langle \sigma K_1 \rangle$ obtained from the two magnetic errors measurements) of $7.41 \times 10^{-7} m^{-2}$ using the previous formulation, and $2.48 \times 10^{-7} m^{-2}$ using the reformulation, while the uncertainty for the skew quadrupole error changes in average from $10.7 \times 10^{-6} m^{-2}$ given by the previous formulation to $3.74 \times 10^{-6} m^{-2}$ using the reformulation. Therefore an experimental evidence that supports the reformulation of the APJ have been obtained.

9.2. Future Direction

The studies reported along this dissertation on magnetic errors measurements in an accelerator like the LHC, ensures that the beams have a good quality and are focused on the expected points of collision. In this way damages in the accelerator components are forewar-

ned and the analysis of physical events recorded are improved. For future research, it is left to obtain what happens in the other IRs LHC wherever possible to apply the APJ method, this can be done with the same experimental data or with new ones; Also, more detailed studies can be developed, for example, to find explanations to discard orbits that are already selected under the method conditions, in order to improve the accuracy and precision of the APJ method and also in the results of the already analyzed data.

A. The Best A_1, B_1, B_1 Combination

In the LHC, to obtain more fine beams, magnetic error measurements and corrections are done, and as discussed during this dissertation the Action and Phase Jump Method is one of the techniques available to obtain the magnetic errors. Nevertheless, during this process it is not convenient to move all the magnets, from an operative point of view in the machine and also because new errors might be introduced.

From the nature of the LHC triplets at the regions IR5 and IR1, description discussed in section 3.3.1, using the collision LHC optics, it is possible to assume that the magnetic errors at all quadrupoles of one triplet can be summarized to one normal quadrupole and one skew quadrupole error. This means that for each IR, all the magnetic quadrupole errors can be summarized into two normal quadrupole correctors, one at the left and one at the right of the IP, and one skew quadrupole corrector.

According to the number and type of quadrupoles in the two triplets for each region of the LHC, see Table **3-1**, there are 30 combinations of correctors to obtain the specific set of three quadrupoles, called in here $A_1 B_1 B_1$, one skew quadrupole error and two normal quadrupole errors. The combinations are organized from 1 to 15 for the sets that include the left skew quadrupole while the combinations from 16 to 30 corresponds to sets that include the right skew quadrupole.

The explicit combinations are written in the generic way in Table **A-1**, where the number of the combination between 1 and 30 is reported in the first column according to the skew quadrupole Q3 in last column. To keep the table in a short size, each row contains two combinations. Each quadrupole Q1, Q2 or Q3 corresponds to the LHC quadrupoles as given in **3-1**.

Using the LHC simulator in MAD-x [5], small magnetic errors were installed in the triplets' quadrupoles at each side of the IP 1 and IP 5. With the traditional configuration of the APJ the magnetic errors are recovered and then corrected using three quadrupoles, two normal quadrupole correctors and one skew quadrupole corrector, for each of the 30 combinations.

The magnetic errors installed in the quadrupoles are $4.0 \times 10^{-5} m^2$ for the normal quadrupole magnets and $2.0 \times 10^{-4} m^2$ for the skew quadrupole magnets. For each IR, a total of eight magnetic errors are installed in ten magnets.

Table A-1.: Generic Combinations $A_1 B_1 B_1$ of Quadrupoles from Two LHC Triplets

Num , Num Comb.	Q1	Q2	Q3 , Q3
1 , 16	3L	2L	SQ.L , SQ.R
2 , 17	3L	1L	SQ.L , SQ.R
3 , 18	3L	1R	SQ.L , SQ.R
4 , 19	3L	2R	SQ.L , SQ.R
5 , 20	3L	3R	SQ.L , SQ.R
6 , 21	2L	1L	SQ.L , SQ.R
7 , 22	2L	1R	SQ.L , SQ.R
8 , 23	2L	2R	SQ.L , SQ.R
9 , 24	2L	3R	SQ.L , SQ.R
10 , 25	1L	1R	SQ.L , SQ.R
11 , 26	1L	2R	SQ.L , SQ.R
12 , 27	1L	3R	SQ.L , SQ.R
13 , 28	1R	2R	SQ.L , SQ.R
14 , 29	1R	3R	SQ.L , SQ.R
15 , 30	2R	3R	SQ.L , SQ.R

Using the APJ method for Beam 1 the corrections are obtained for each combination of three correctors. The optics used for the LHC is the injection (V.6.5) with $\beta^* = 2 \text{ m}$ and tunes of $Q_x = 64.284$ and $Q_y = 59.274$, after the magnetic error are installed.

The quantity of merit given to the magnetic corrections is giving by the β -beating. This quantity is a measurement of the relative errors obtained, point by point, for the β -function along the accelerator, it is the difference between the expected and observed value divided by the expected value.

Theoretically, the β -beating can be related with the magnetic errors presented in the accelerator. After taking the root-mean-squared RMS along the accelerator, it can be shown that ([19]):

$$\left(\frac{\Delta\beta}{\beta}\right)_{RMS} = \frac{1}{2\sqrt{2}|\sin(2\pi\nu)|} \left(\sum_i q_i^2 \beta_i^2\right)^{0.5} \quad (\text{A-1})$$

where ν is the decimal part of the accelerator tune in the transverse plane which are been analyzed, while q_i are the magnetic strengths for the magnet i with magnetic error in the accelerator, and β_i are the corresponding β function. To obtain this relation it is assumed that the quadrupole length is approximately zero. From the table of the LHC triplets (Table **3-1**), it is observed that the distances between the quadrupoles are very small compare to the 27 Km of the ring, and at the same time, the length of the quadrupoles can be consider to be zero so the above approximation holds.

In Figure **A-1** the results for the β -beating for some representative cases are presented. In Figure **A-1**.left the results for the plane X are shown while in Figure **A-1**.right the results for plane Y are shown. From the results it is clear that the β -beating for the combination 3 is much larger compared to the other combinations.

Therefore, although all the quadrupoles have the same amount of magnetic error, the β -beating results show that do not all the combinations are equally effective to obtain the magnetic error corrections.

Also, as seen in the plots, there is a combination that decrease the β -beating almost to zero in both planes. This means that it is possible to correct all the errors at two triples in one IR using just three magnets.

Previous studies reported in [34], show the ability of the APJ to decrease the β -beating after the corrections of the magnetic errors. Nevertheless those studies were done without

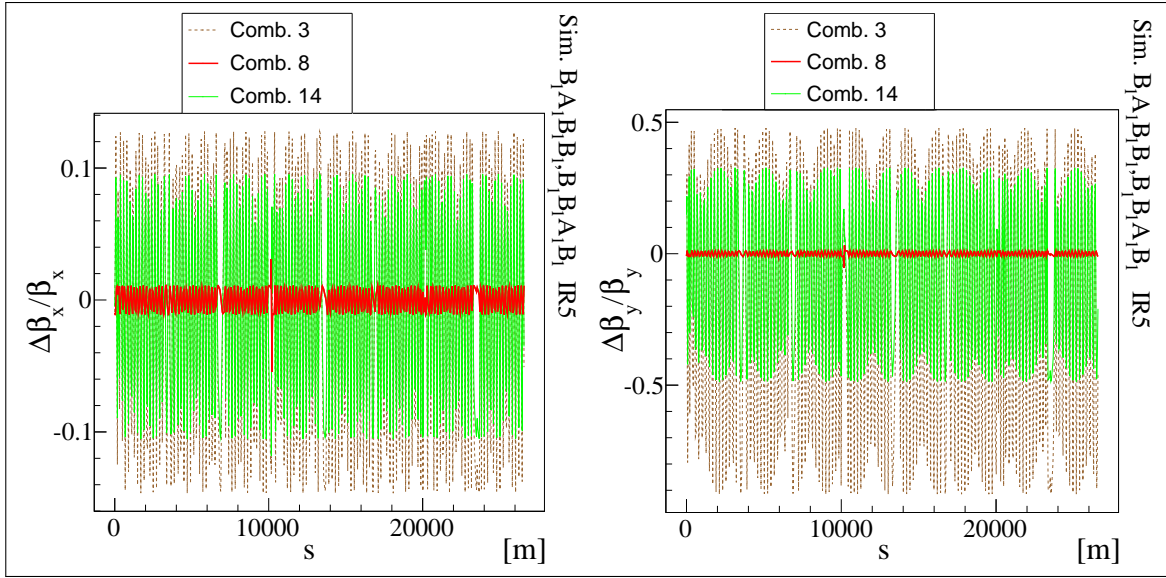


Figure A-1.: Beta-beating after Corrections along the LHC for some combinations $A_1B_1B_1$, in IR5 transverse planes X (left) and Y (right)

taking into account the skew quadrupole error, and only the result from one plane is reported.

To establish the best combinations, the additions of the β -beating RMS in each plane is obtained, and in here this quantity is called Σ . After the calculations, the combinations are organized according to their $\Sigma = RMS_{(\Delta\beta_y/\beta_y)} + RMS_{(\Delta\beta_x/\beta_x)}$ from the highest to the lowest. It is understood that the lower the quantity Σ is, the better magnetic corrections are made.

In Figure **A-2** the results for both IRs are presented. From the plots it is evident that the best combinations of quadrupoles are the ones that have the quadrupoles 2L and 2R with any of the skew correctors, for both IR5 and IR1.

The lowest value for Σ in IR5 is 0.4009 while in IR1 the lowest is 0.3676. These corresponds to the combination 23 in IR5, and the combination 8 in IR1. Nevertheless, both combinations 23 and 8 are the best two combinations for any of the IRs, this implies that the best combination $A_1B_1B_1$ for both IRs is always when the quadrupoles Q2L and Q2R are involved, as presented along this dissertation.

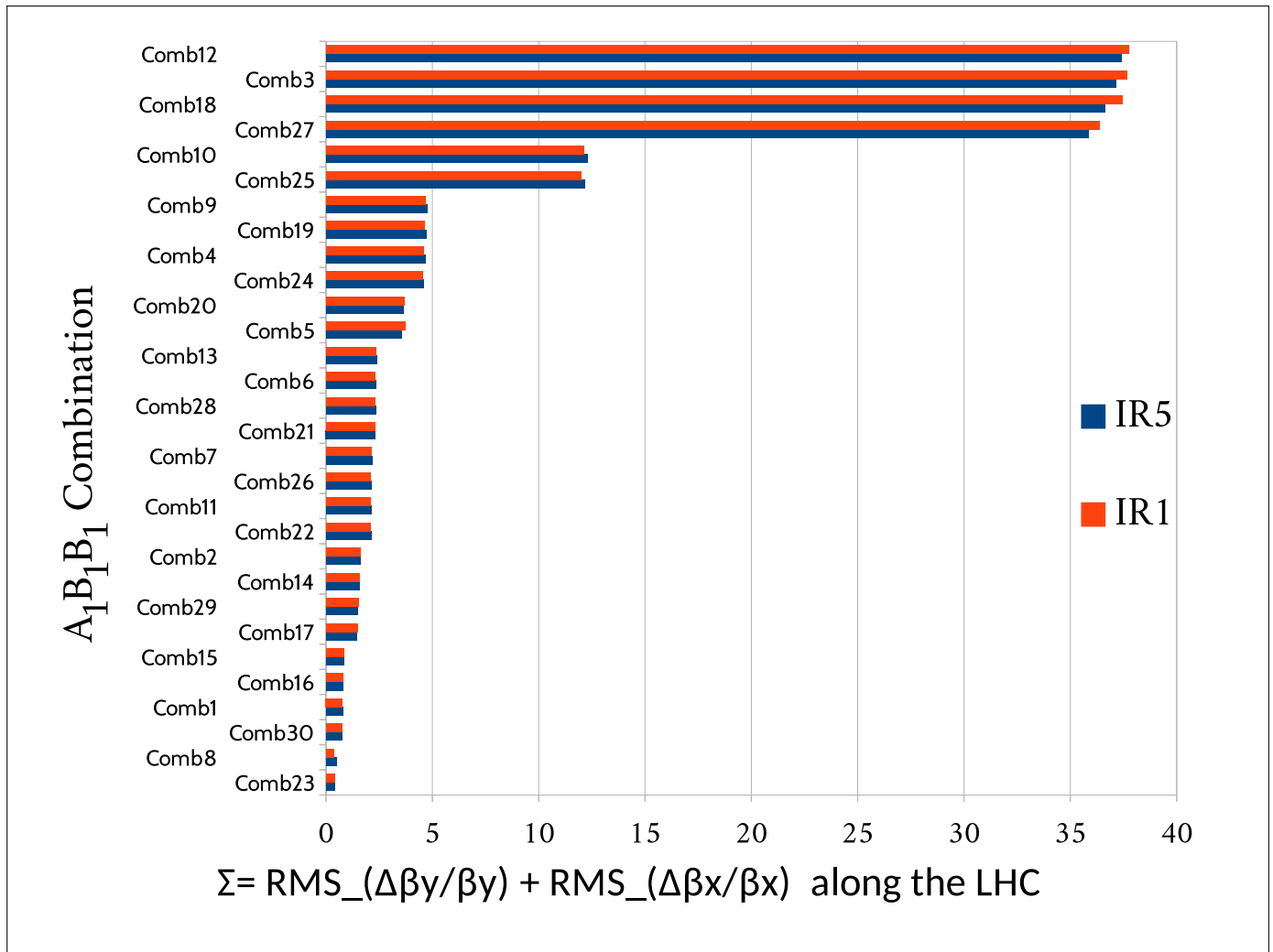


Figure A-2.: RMS for the Beta-beating obtained for the Different Combinations of Quadrupoles $A_1 B_1 B_1$, as given in Table A-1, for regions IR5 and IR1.

B. APJ on Uniform Noised Orbits

If in some way the measurement of the positions, which are obtained with the LHC BPM system, can be restricted to have a more accurately measurement, in the sense that the final normal (Gaussian) distribution of the measurements are within the experimental $\pm\sigma/4$ range or with a very small σ , or just that the presented noise in the orbits could be approximately to have an uniform distribution, a slightly different results are obtained. Additional results comparing the two ways to simulate the noise are reported in [41], for the filter *Band* case alone and as part for this dissertation.

In this section, the results for the magnetic errors from the LHC simulator using the Action and Phase Method, and orbits with noise from a uniform distribution between ± 0.3 mm are presented. The analysis for the orbits were made in a similar way than the presented for normal distribution during this dissertation. First, the plots for the different ways to reduce noise, using digital filters are presented, then the corresponding summarized tables for the best combinations are presented.

The simulation used is the similar to the experimental data from 2010, when the tunes were adjusted to be same as the experimental orbits generated by the AC dipole for Beam 1, in the case of injection orbits with *V6.5.seq* and the modifiers to have $\beta^* = 2$ m at IR1 and IR5 (Initial position of the orbits at $x=0.001$, $y=0.001$ in the PTC_TRACK), and the model is taken as the modified one with the new tunes, as performed previously for the normal noise.

A first look in the frequency plots of some orbits gives the view for the amount of noise that is reduced using just the filter *Band*, designed for this dissertation, and presented in Chapter 5. In the same plots there are presented the case for the simulation without noise (labeled by *nom*).

In Figure **B-1** it is observe that in the horizontal plane X, the amount of noise in the data from 2010 experiment (*dat*) has almost same quantities that the simulation case (*sim2*), with a better representation that what it is observed for the simulated normal distribution (*sim*).

In Figure **B-1**, for the vertical plane it is observed that each case of noise distribution implies a small amount of noise compare to what it is presented in the experimental data.

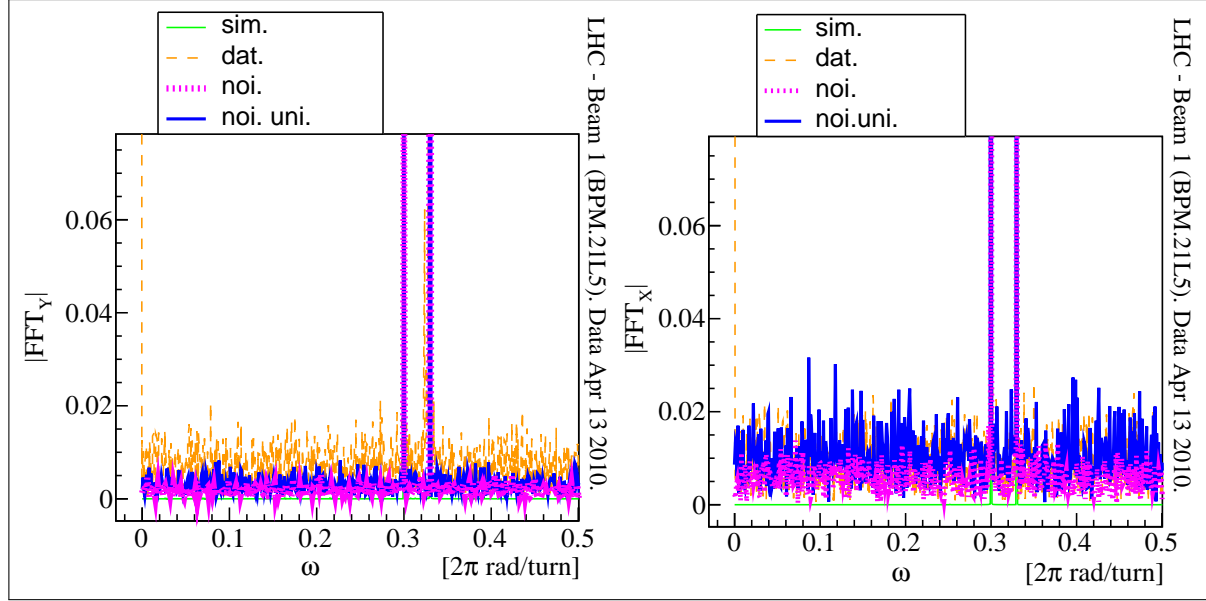


Figure B-1.: Frequency Space for the Transverse Position in the LHC Arcs. The simulated orbit close to the experimental data is denoted by *sim.*, while the experimental orbits taken at 12:54:09 (Apr. 13th, 2010) are denoted by *dat.* Simulated orbits with noise are also presented and they are denoted by *noi.* when using a normal distribution and *noi.uni.* when using an uniform distribution.

The plots for the different ways to reduce noise with uniform distribution against the bandwidth, for the magnetic error measurements, using the new formulation of the Action and Phase Jump Method are in Figure **B-2**, Figure **B-3** and Figure **B-4**.

In a similar way, the plots for the several ways to reduce noise with uniform distribution, using the previous formulation of the Action and Phase Jump Method are in Figure **B-5**, Figure **B-6**, and Figure **B-9**.

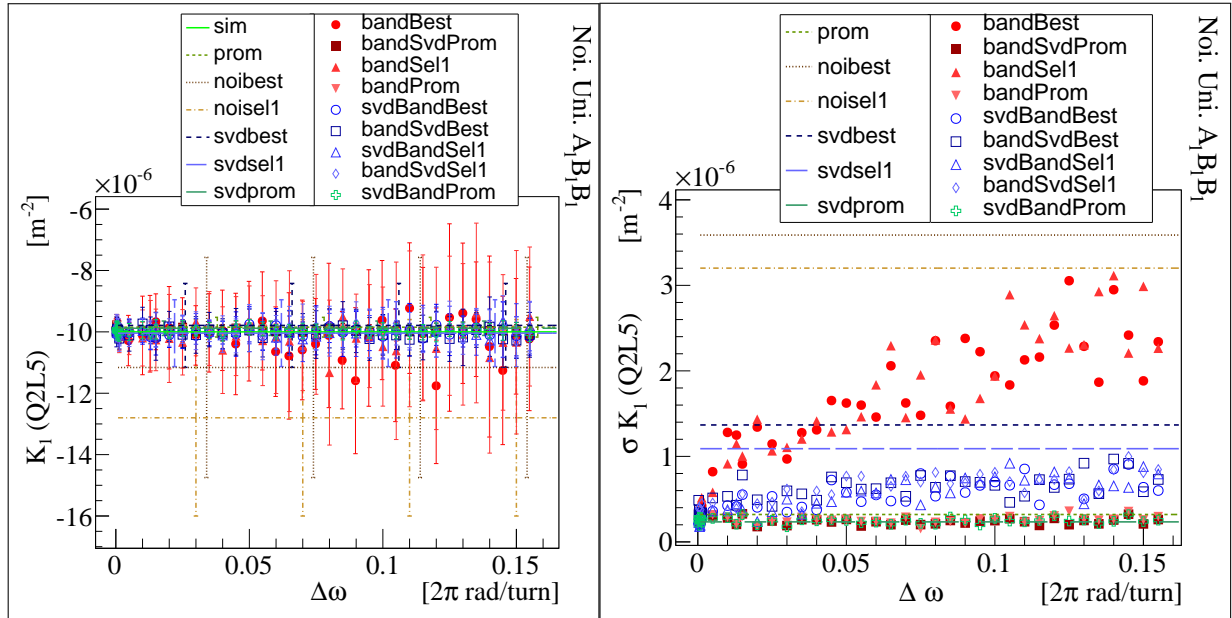


Figure B-2.: Comparison between the filters measurements for K_1 (Q2L5) (left) and its uncertainty (right). Results for the simulation including three magnetic errors and noise from Uniform distribution, using the New Formulation of APJ.

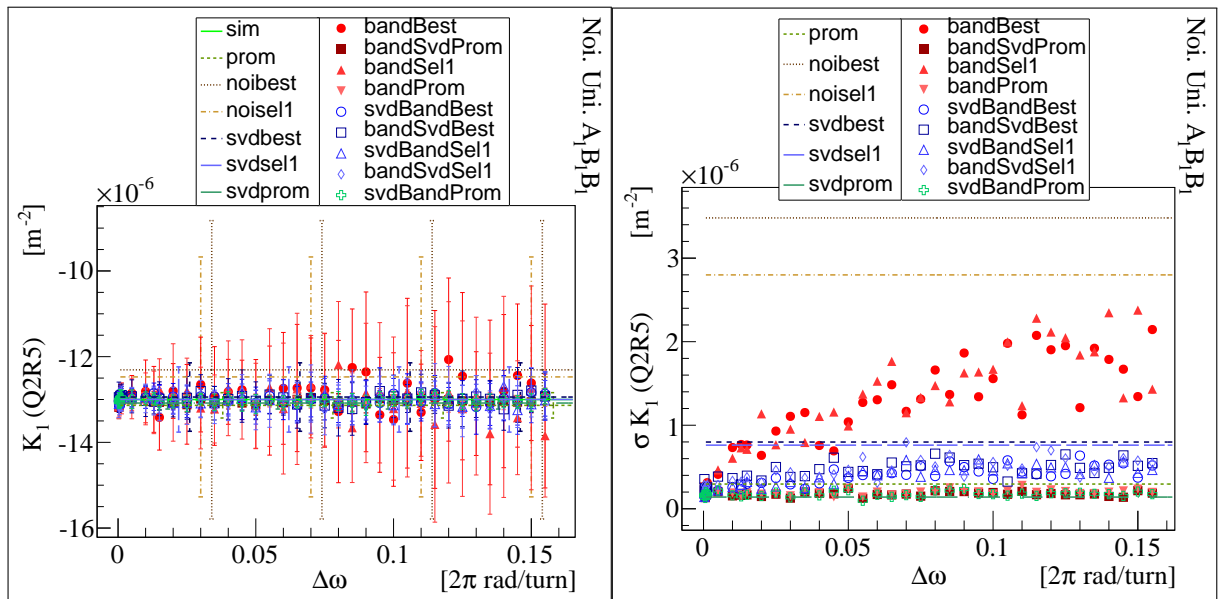


Figure B-3.: Comparison between the filters measurements for K_1 (Q2R5) (left) and its uncertainty (right). Results for the simulation including three magnetic errors and noise from Uniform distribution, using the New Formulation of APJ.

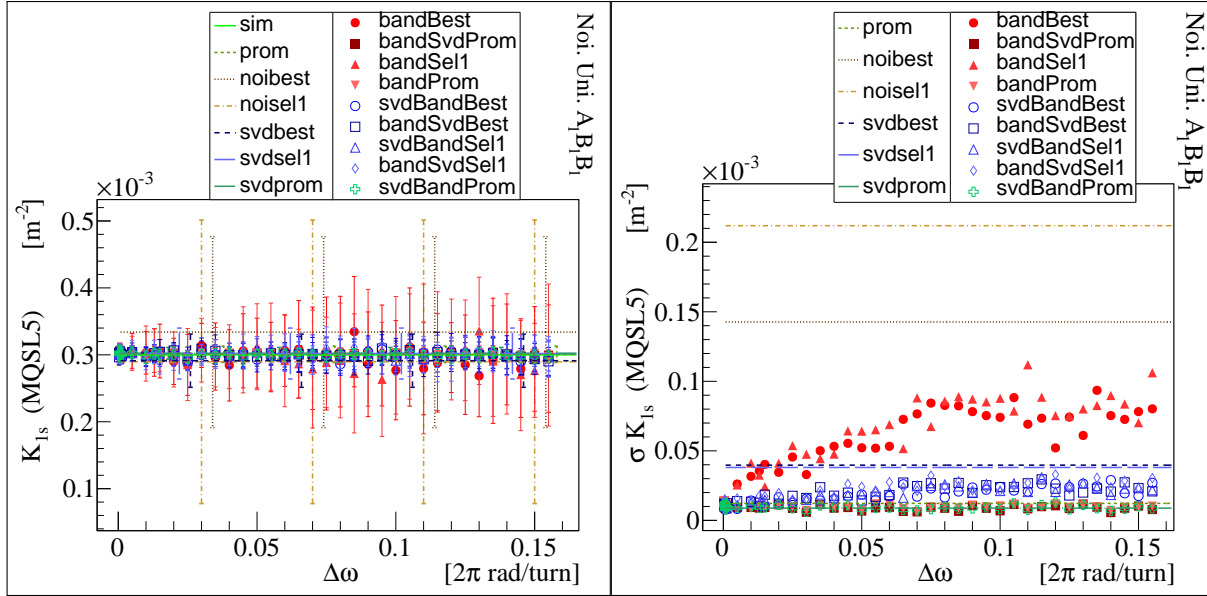


Figure B-4.: Comparison between the filters measurements for K_{1s} (MQSL5) (left) and its uncertainty (right). Results for the simulation including three magnetic errors and noise from Uniform distribution, using the New Formulation of APJ.

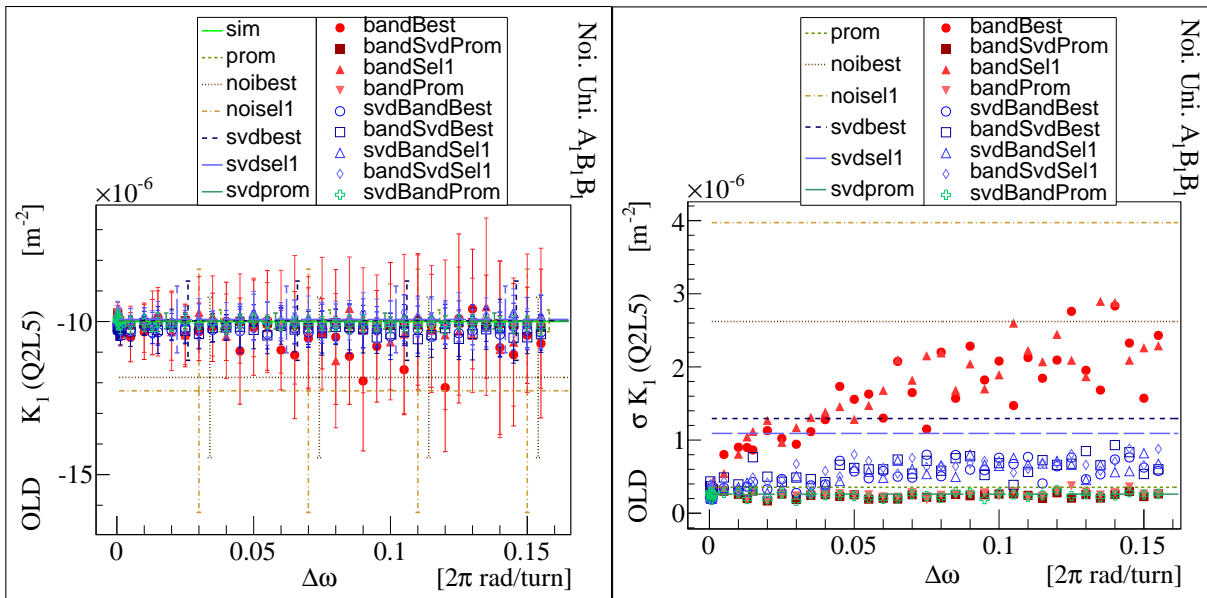


Figure B-5.: Comparison between the filters measurements for K_1 (Q2L5) (left) and its uncertainty (right). Results for the simulation including three magnetic errors and noise from Uniform distribution, using the **Old** Formulation of APJ.

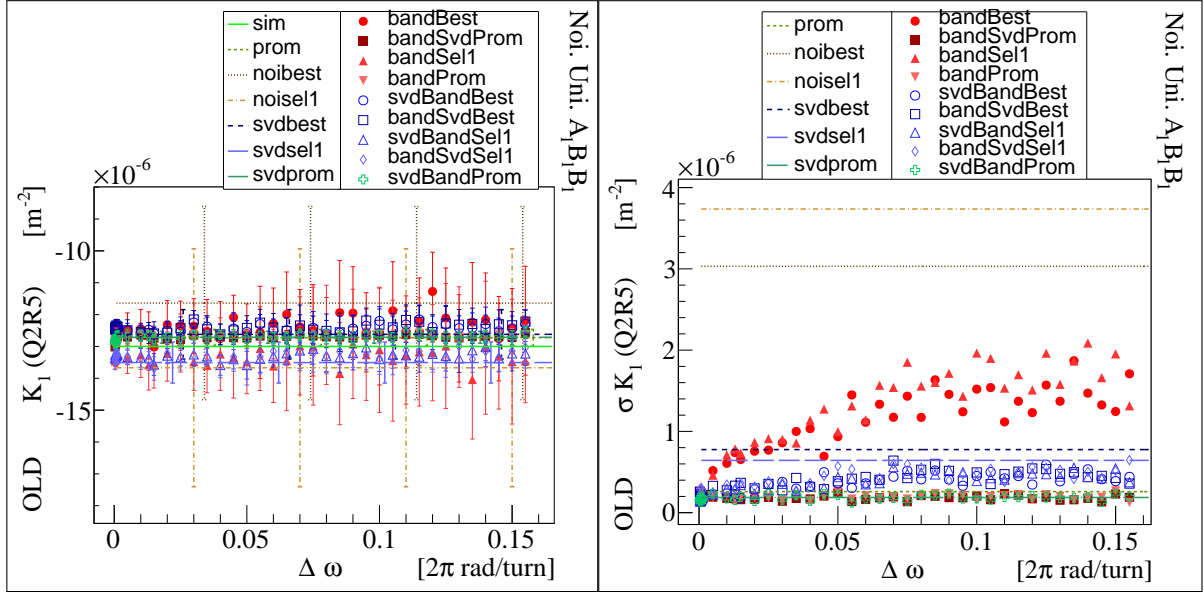


Figure B-6.: Comparison between the filters measurements for K_1 (Q2R5) (left) and its uncertainty (right). Results for the simulation including three magnetic errors and noise from Uniform distribution, using the **Old** Formulation of APJ.

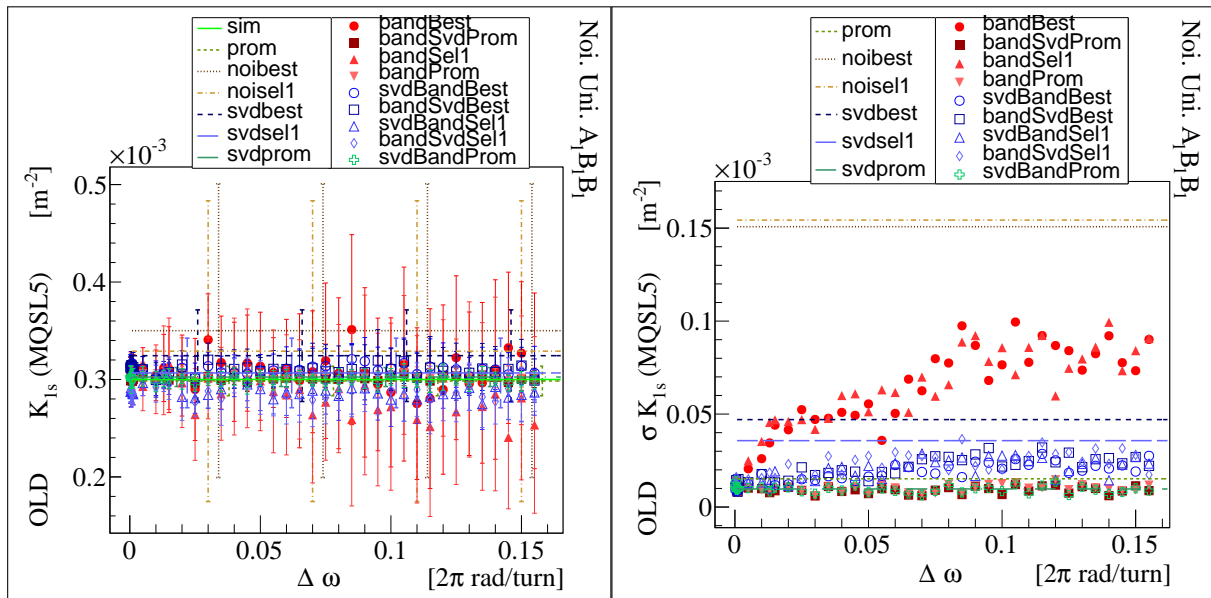


Figure B-7.: Comparison between the filters measurements for K_{1s} (MQSL5) (left) and its uncertainty (right). Results for the simulation including three magnetic errors and noise from Uniform distribution, using the **Old** Formulation of APJ.

B.1. Best Combinations of Filters for the Simulation with Uniform Noise.

Table **B-1** presents the summary for the best ways to reduce noise, ranked according to the lesser value of uncertainty. The measurement of the magnetic errors were made using the Action and Phase Method as given in the labels.

New Formulation sim. Uniform	σK_1 (Q2L5)	σK_1 (Q2R5)	σK_{1s} (MQSL5)
Best combination	BandSvdProm	SvdProm	SvdProm
2nd best combination	SvdBandProm	SvdBandProm	SvdBandProm
3rd best combination	SvdProm	BandSvdProm	BandSvdProm
4th best combination	BandProm	BandProm	BandProm
5th best combination	Prom or SvdBandBest $\Delta\omega < 0.001$	SvdBandBest $\Delta\omega < 0.025$	SvdBandBest $\Delta\omega < 0.01$ or Prom
Old Formulation sim. Uniform	σK_1 (Q2L5)	σK_1 (Q2R5)	σK_{1s} (MQSL5)
Best combination	SvdBandProm	BandSvdProm	BandSvdProm
2nd best combination	BandSvdProm	SvdBandProm	SvdProm
3rd best combination	SvdProm	BandProm	BandProm
4th best combination	BandProm	SvdProm	SvdBandProm
5th best combination	SvdBandBest $\Delta\omega < 0.01$	SvdBandBest $\Delta\omega < 0.015$	SvdBandBest $\Delta\omega < 0.003$

Table B-1.: Uncertainty for the Magnetic Errors Measurements using the New and Old Formulation of APJ

These results (Table **B-1**) , and their corresponding plots from the previous section, imply that the statistical uncertainty is highly reduced in principle with any of the reported combinations to reduce noise, but, the fact that all filters gives similar results could means that there is a limit in the reduction of the uniform noise (compare to the normal case).

The plots for the individual filters and the best filters, using the new formulation compare to the best one obtained using the old formulation case are presented in Figure **B-8** so forth to Figure **B-11**, for the magnetic errors measurement.

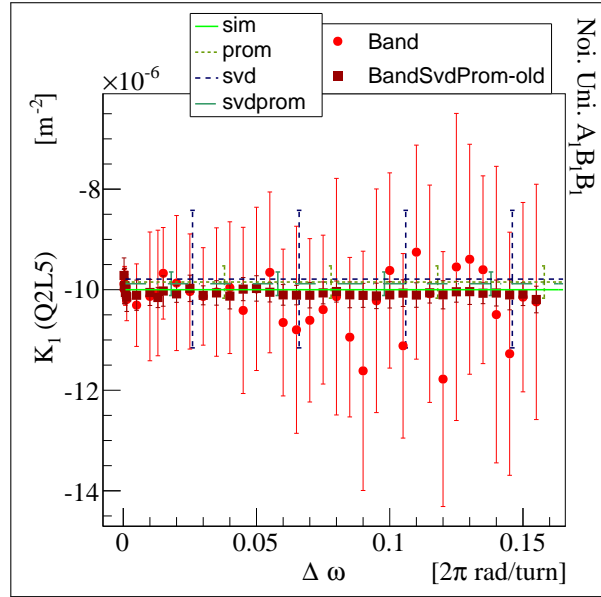


Figure B-8.: Comparison including *Band*, for $K_1(Q2L5)$, between individual filters (orbits selected using *Best*) and the best combinations of Filters, using the New and Old (-old) formulations of APJ. Orbits from the simulation of 3 magnetic errors and noise from uniform distribution.

Figure **B-8**, the first one, presents the results for $K_1(Q2L5)$ with all the different ways to reduce noise, including the *Band* filter. And for a better appreciation the plots, the ones corresponding to the statistical average are plotted without the *Band* filter, in a similar way as previously did for the normal noise analysis results.

For each magnetic measurement the plot with the results for the statistical average is followed by the plot with the statistical uncertainty for each magnetic error. First the results for $K_1(Q2L5)$ are given in Figure **B-9**, then, in Figure **B-10** the plots for $K_1(Q2R5)$ are presented and finally the plots for the skew quadrupole error are in Figure **B-11**.

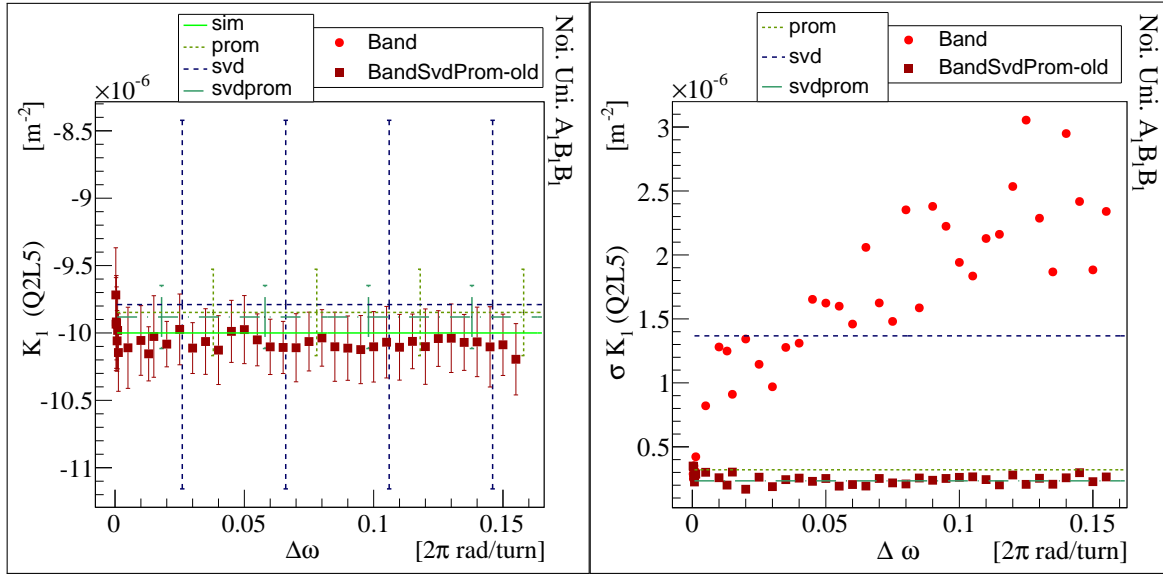


Figure B-9.: Comparison between the formulations when the filters and their combinations are applied, for K_1 (Q2L5) (left) and its uncertainty (right) calculation. Results for simulation including three magnetic errors and noise from Uniform distribution, using the New Formulation and the best case using the **Old** Formulation.

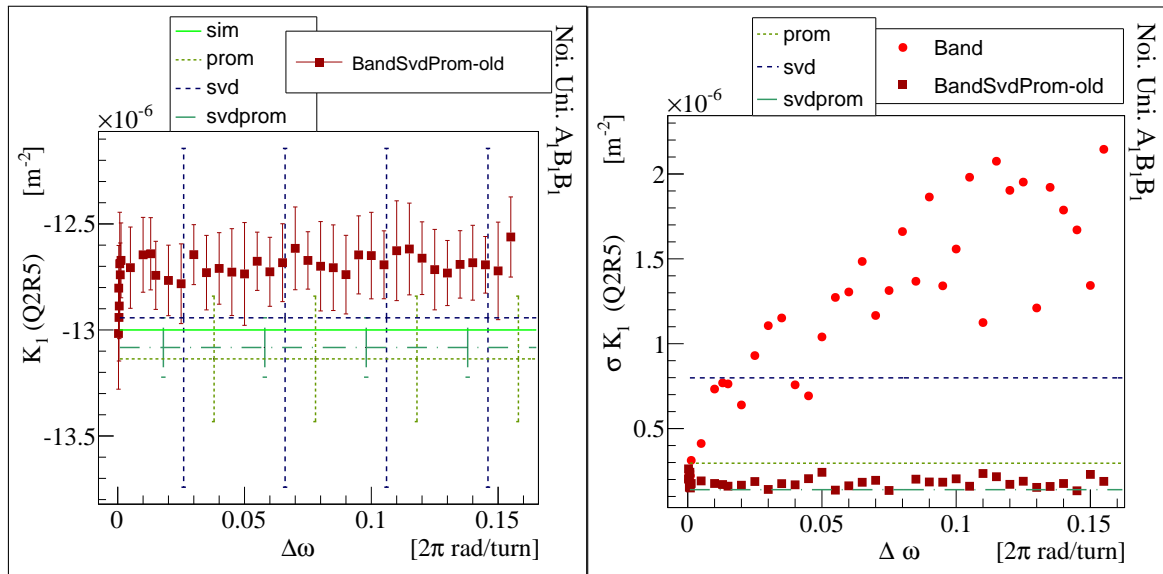


Figure B-10.: Comparison between the formulations when the filters and their combinations are applied, for K_1 (Q2R5) (left) and its uncertainty (right) calculation. Results for simulation including three magnetic errors and noise from Uniform distribution, using the New Formulation and the best case using the **Old** Formulation.

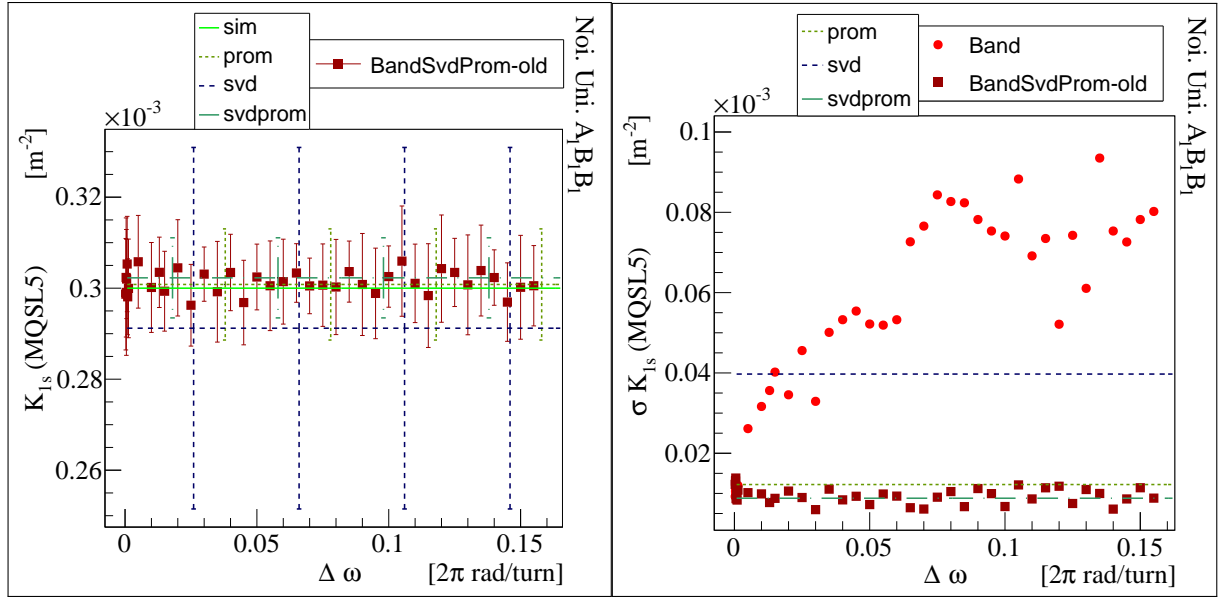


Figure B-11.: Comparison between the formulations when the filters and their combinations are applied, for K_{1s} (MQSL5) (left) and its uncertainty (right) calculation. Results for simulation including three magnetic errors and noise from Uniform distribution, using the New Formulation and the best case using the **Old** Formulation.

Taking the best five band-widths, from the best combination of filters, when using each of the two Action and Phase formulations, Table **B-2**, Table **B-3** and Table **B-5**, are constructed. Similar tables were obtained when analyzing experimental data of 2010 and the simulated orbits with noise from normal distribution. This process is the previous step to get Table **6-7** so forth and Table **8-2** so forth.

$\Delta\omega$ [2π rad]	$K_1(\text{Q2L5})$ $10^{-5} [m^{-2}]$	$\sigma K_1(\text{Q2L5})$ $10^{-7} [m^{-2}]$	$\Delta\omega$ [2π rad]	$K_1(\text{Q2L5})\text{-old}$ $10^{-5} [m^{-2}]$	$\sigma K_1(\text{Q2L5})\text{-old}$ $10^{-7} [m^{-2}]$
0.0750	-1.00	1.55	0.0200	-1.01	1.72
0.0200	-0.999	1.80	0.0750	-1.01	1.82
0.0130	-1.01	2.06	0.0130	-1.02	1.95
0.0900	-0.993	2.19	0.0650	-1.01	2.18
0.0650	-1.01	2.19	0.1100	-1.01	2.21
$\Delta\omega$ [2π rad]	$K_1(\text{Q2R5})$ $10^{-5} [m^{-2}]$	$\sigma K_1(\text{Q2R5})$ $10^{-7} [m^{-2}]$	$\Delta\omega$ [2π rad]	$K_1(\text{Q2R5})\text{-old}$ $10^{-5} [m^{-2}]$	$\sigma K_1(\text{Q2R5})\text{-old}$ $10^{-7} [m^{-2}]$
0.0006	-1.31	1.35	0.1550	-1.26	1.26
0.0550	-1.30	1.40	0.0400	-1.27	1.49
0.0450	-1.30	1.42	0.1350	-1.27	1.55
0.0300	-1.30	1.55	0.0300	-1.26	1.55
0.0130	-1.30	1.57	0.0006	-1.29	1.55
$\Delta\omega$ [2π rad]	$K_{1s}(\text{MQSL5})$ $10^{-4} [m^{-2}]$	$\sigma K_{1s}(\text{MQSL5})$ $10^{-6} [m^{-2}]$	$\Delta\omega$ [2π rad]	$K_{1s}(\text{MQSL5})\text{-old}$ $10^{-3} [m^{-2}]$	$\sigma K_{1s}(\text{MQSL5})\text{-old}$ $10^{-6} [m^{-2}]$
0.0700	3.01	5.94	0.0300	3.02	6.07
0.1400	3.01	7.04	0.0500	3.02	7.12
0.0300	3.03	7.13	0.0700	3.01	7.13
0.0500	3.01	7.14	0.0750	3.02	7.45
0.0650	3.02	8.53	0.0850	3.02	7.66

Table B-2.: Results for the First Five (the ones with the least statistical uncertainty) bandwidths using the Filter Combination *BandProm*. Simulated Orbits with Noise from Uniform Distribution.

$\Delta\omega$	$K_1(\text{Q2L5})$	$\sigma K_1(\text{Q2L5})$	$\Delta\omega$	$K_1(\text{Q2L5})\text{-old}$	$\sigma K_1(\text{Q2L5})\text{-old}$
$[2\pi \text{ rad}]$	$10^{-6} [m^{-2}]$	$10^{-7} [m^{-2}]$	$[2\pi \text{ rad}]$	$10^{-5} [m^{-2}]$	$10^{-7} [m^{-2}]$
0.0200	-9.99	1.79	0.0200	-1.01	1.69
0.0550	-9.93	1.86	0.0300	-1.01	1.89
0.0300	-9.99	1.91	0.0550	-1.01	1.93
0.1150	-9.97	1.93	0.0650	-1.01	1.93
0.1250	-9.94	2.01	0.0130	-1.02	2.01
$\Delta\omega$	$K_1(\text{Q2R5})$	$\sigma K_1(\text{Q2R5})$	$\Delta\omega$	$K_1(\text{Q2R5})\text{-old}$	$\sigma K_1(\text{Q2R5})\text{-old}$
$[2\pi \text{ rad}]$	$10^{-5} [m^{-2}]$	$10^{-7} [m^{-2}]$	$[2\pi \text{ rad}]$	$10^{-5} [m^{-2}]$	$10^{-7} [m^{-2}]$
0.0550	-1.30	1.26	0.1450	-1.27	1.33
0.0300	-1.30	1.28	0.0750	-1.27	1.35
0.0006	-1.31	1.34	0.0550	-1.27	1.37
0.1450	-1.31	1.38	0.0300	-1.26	1.41
0.0200	-1.31	1.47	0.0010	-1.27	1.50
$\Delta\omega$	$K_{1s}(\text{MQSL5})$	$\sigma K_{1s}(\text{MQSL5})$	$\Delta\omega$	$K_{1s}(\text{MQSL5})\text{-old}$	$\sigma K_{1s}(\text{MQSL5})\text{-old}$
$[2\pi \text{ rad}]$	$10^{-4} [m^{-2}]$	$10^{-6} [m^{-2}]$	$[2\pi \text{ rad}]$	$10^{-3} [m^{-2}]$	$10^{-6} [m^{-2}]$
0.1400	3.00	5.60	0.0300	3.03	5.96
0.0300	3.03	5.83	0.1400	3.02	6.09
0.0700	3.00	6.15	0.0700	3.00	6.11
0.0650	3.03	6.46	0.0650	3.03	6.44
0.0850	3.02	6.55	0.0850	3.04	6.71

Table B-3.: Results for the First Five (the ones with the least statistical uncertainty) bandwidths using the Filter Combination *BandSvdProm*. Simulated Orbits with Noise from Uniform Distribution.

Simulation	$K_1(\text{Q2L5})$	$\sigma K_1(\text{Q2L5})$	$K_1(\text{Q2L5})$ -old	$\sigma K_1(\text{Q2L5})$ -old
Unif. Noise	$10^{-6} [m^{-2}]$	$10^{-7} [m^{-2}]$	$10^{-6} [m^{-2}]$	$10^{-7} [m^{-2}]$
Noise Level	-11.2	35.9	-11.8	26.2
Prom	-9.85	3.21	-9.98	3.54
SvdProm	-9.88	2.34	-9.98	2.61
	-10.0	1.55	-10.1	1.72
BandProm	-10.1	2.06	-10.2	1.95
	-9.99	1.79	-10.1	1.69
BandSvdProm	”	”	”	”
	-9.96	1.77	-10.1	1.69
SvdBandProm	-9.93	1.94	-9.97	1.87

Table B-4.: Summary of Results for the Best Combinations of Digital Filters for $K_1(\text{Q2L5})$.
Simulated Orbits with noise from Uniform Distribution

$\Delta\omega$ [2 π rad]	$K_1(\text{Q2L5})$ $10^{-6} [m^{-2}]$	$\sigma K_1(\text{Q2L5})$ $10^{-7} [m^{-2}]$	$\Delta\omega$ [2 π rad]	$K_1(\text{Q2L5})\text{-old}$ $10^{-5} [m^{-2}]$	$\sigma K_1(\text{Q2L5})\text{-old}$ $10^{-7} [m^{-2}]$
0.0300	-9.96	1.77	0.0300	-1.01	1.69
0.0006	-9.93	1.94	0.0006	-0.997	1.87
0.0950	-10.0	1.98	0.0950	-1.01	1.92
0.0200	-10.0	2.01	0.0200	-1.01	1.92
0.0650	-9.97	2.06	0.0130	-1.01	1.94
$\Delta\omega$ [2 π rad]	$K_1(\text{Q2R5})$ $10^{-5} [m^{-2}]$	$\sigma K_1(\text{Q2R5})$ $10^{-7} [m^{-2}]$	$\Delta\omega$ [2 π rad]	$K_1(\text{Q2R5})\text{-old}$ $10^{-5} [m^{-2}]$	$\sigma K_1(\text{Q2R5})\text{-old}$ $10^{-7} [m^{-2}]$
0.0550	-1.30	0.966	0.0550	-1.27	1.24
0.0006	-1.31	1.30	0.0006	-1.28	1.29
0.0300	-1.30	1.37	0.1450	-1.27	1.33
0.0750	-1.30	1.43	0.0200	-1.27	1.45
0.0650	-1.31	1.43	0.0400	-1.26	1.46
$\Delta\omega$ [2 π rad]	$K_{1s}(\text{MQSL5})$ $10^{-4} [m^{-2}]$	$\sigma K_{1s}(\text{MQSL5})$ $10^{-6} [m^{-2}]$	$\Delta\omega$ [2 π rad]	$K_{1s}(\text{MQSL5})\text{-old}$ $10^{-3} [m^{-2}]$	$\sigma K_{1s}(\text{MQSL5})\text{-old}$ $10^{-6} [m^{-2}]$
0.0300	3.02	6.16	0.0700	2.99	6.36
0.1400	3.00	6.92	0.1250	3.01	6.49
0.0700	3.00	7.20	0.1400	2.99	6.36
0.0650	3.02	7.48	0.0300	3.01	7.16
0.0500	3.00	7.64	0.0650	3.02	7.27

Table B-5.: Results for the First Five (the ones with the least statistical uncertainty) Bandwidths using the Filter Combination *SvdBandProm*. Simulated Orbits with Noise from Uniform Distribution.

Simulation	$K_1(\text{Q2R5})$	$\sigma K_1(\text{Q2R5})$	$K_1(\text{Q2R5})$ -old	$\sigma K_1(\text{Q2R5})$ -old
Unif. Noise	$10^{-5} [m^{-2}]$	$10^{-7} [m^{-2}]$	$10^{-5} [m^{-2}]$	$10^{-7} [m^{-2}]$
w/o Filter	-1.23	34.8	-1.16	30.3
Prom	-1.31	2.96	-1.27	2.59
SvdProm	-1.31	1.40	-1.27	1.87
BandProm	-1.31	1.35	-1.26	1.26
	”	”	-1.29	1.55
BandSvdProm	-1.30	1.26	-1.27	1.33
	-1.30	1.28	-1.26	1.41
SvdBandProm	-1.30	0.966	-1.27	1.24
	-1.31	1.30	-1.28	1.29

Table B-6.: Summary of Results for the Best Combinations of Digital Filters for $K_1(\text{Q2R5})$. Simulated Orbits with noise from Uniform Distribution

Simulation	$K_{1s}(\text{MQSL5})$	$\sigma K_{1s}(\text{MQSL5})$	$K_{1s}(\text{MQSL5})$ -old	$\sigma K_{1s}(\text{MQSL5})$ -old
Unif. Noise	$10^{-4} [m^{-2}]$	$10^{-6} [m^{-2}]$	$10^{-3} [m^{-2}]$	$10^{-6} [m^{-2}]$
w/o Filter	3.34	143	3.50	151
Prom	3.01	12.2	2.98	15.2
SvdProm	3.02	8.80	3.02	9.73
BandProm	3.01	5.94	3.02	6.07
	3.03	7.13	”	”
BandSvdProm	3.00	5.60	3.03	5.96
	3.03	5.83	”	”
SvdBandProm	3.02	6.16	2.99	6.36
	”	”	3.01	7.16

Table B-7.: Summary of Results for the Best Combinations of Digital Filters for $K_{1s}(\text{MQSL5})$. Simulated Orbits with noise from Uniform Distribution

References

- [1] J. Cardona and S. Peggs and F. Pilat and V. Ptitsyn, *Measuring Local Gradient and Skew Quadrupole Errors in RHIC IRs*, in *Proceedings of EPAC 2004, Lucerne, Switzerland, 2004*, edited by J. Chrin and Ch. Petit-Jean-Genaz and J. Poole and C. Prior and H.A. Synal (PSI and CERN and ASTeC CCLRC RAL and Trinity College Oxford and ETH, 2004), (EPS-AG), pp. 1553–1555.
- [2] Javier F. Cardona and Stephen G. Peggs, *Linear and Nonlinear Magnetic Error Measurements using Action and Phase Jump Analysis*, *Phys. Rev. ST Accel. Beams* **12**(014002 and 059901(E)(2010)), 014002 (2009).
- [3] J. Cardona and R. Calaga and R. Miyamoto and R. Tomás and G. Vanbavinckhove, *Comparison of the Action and Phase Analysis on LHC Orbits with Other Techniques*, in *Proceedings of IPAC2011, San Sebastián, Spain, 2011*, edited by C. Petit-Jean-Genaz and A. Blanco and I. Etxebarria and F. Perez and A. Wolski and V. Schaa, (CERN and ESS and CELLS and U. Liverpool and Cockcroft Institute and GSI, 2011), (EPS-AG), pp. 2004–2006.
- [4] O.R. Blanco and J.F. Cardona, *Action and Phase Jump Analysis for LHC Orbits*, in *Proceedings of 2011 Particle Accelerator Conference, New York, NY, USA*, edited by T. Satogata and K. Brown (2011), (IEEE), vol. Beam Dynamics and EM Fields, pp. 1–3.
- [5] BE/ABP, *MAD-X is the successor of MAD-8 and was first released in June 2002*, Tech. rep., CERN, Accelerator Beam Physics Group. MAD - Methodical Accelerator Design (Consulted inclusive on 29-09-2015), <http://mad.web.cern.ch/mad/>.
- [6] S.Y. Lee, *Accelerator Physics* (World Scientific, 2004), pp. 26,46,173,100,100,137, 3rd ed.
- [7] CERN, *LHC Achieves 2011 Data Milestone*, in *CERN COURIER, News* (International Journal of High-Energy Physics, 2011), vol. 51, p. 6.
- [8] LHC, *LHC Performance and Statistics*, Tech. rep., CERN, <http://lhc-statistics.web.cern.ch/LHC-Statistics> (2011).
- [9] W. Scandale, *LHC Luminosity and Energy Upgrade*, in *Proceedings of EPAC 2006, Edinburgh, Scotland, 2006*, edited by C. Biscari and H. Owen and Ch. Petit-Jean-Genaz

and J. Poole and J. Thomason (INFN-LNF and CCLRC DL and CERN and CCLRC RAL, 2006), (EPS-AG), no. TUXPA03 in *Circular Colliders*, pp. 910–914.

- [10] R. Assmann and J.P. Koutchouck and M.Placidi and E. Tsismelis, *On the Measurement of the Relative Luminosity at the LHC*, in *LHC Project Document*, CERN, Switzerland (April 2004), vol. rev 1.1, p. 7 of 24.
- [11] LHC NEWS, *The LHC Gets Set for More Luminosity*, in *CERN COURIER, news* (International Journal of High-Energy Physics, 2010), vol. 50, p. 6.
- [12] LHC, *Design Report*, Tech. rep., CERN, <http://lhc.web.cern.ch/lhc/LHC-DesignReport.html> (2009).
- [13] R. Tomás and O. Brüning and M. Giovannozzi and P. Hagen and M. Lamont and F. Schimdt and G. Vanbavinckhove and M. Aiba and R. Calaga and R. Miyamoto, *CERN Large Hadron Collider Optics Model, Measurements, and Corrections*, *Phys. Rev. ST Accel. Beams* **13**(12), 121004 (Dec 2010).
- [14] Javier Fernando Cardona, *Linear and Non Linear Studies at RHIC Interaction Regions and Optical Design of the Rapid Cycling Medical Synchrotron*, Ph.D. thesis, University of New York at Stony Brook (2003).
- [15] Martin Reiser, *Theory and Design of Charged Particle Beams* (2008).
- [16] Helmut Wiedemman, *Accelerator Physics* (Springer, 2007), p. 75, 3rd ed.
- [17] Yohani Rodríguez G., *Deducción de términos Resonantes a partir de Hamiltonianos y Álgebras de Lie*, Trabajo de grado (físico), Universidad Nacional de Colombia. Sede Bogotá. Facultad de Ciencias. Departamento de Física. (2007).
- [18] Animesh K. Jain, *Basic Theory of Magnets*, in *CERN Accelerator School on Measurement and Alignment of Accelerator and Detector Magnets*, Anacapri, Italy (1997).
- [19] D.A. Edwards and M.J. Syphers, *An Introduction to the Physics of High Energy Accelerators*. (Wiley Vch. Verlag GmbH and Co KgaA, 2004), pp. 67,56,105.
- [20] Michiko G. Minty and Frank Zimmermann, *Beam Techniques - Beam Control and Manipulation*, Tech. rep., University of Chicago and Argonne National Laboratory, USPAS (June 1999).
- [21] E.D. Courant and H.S. Snyder, *Theory of the Alternating-Gradient Synchrotron*, *Annals of Physics* **281**(1-2), 360 (2000), received 15 July 1957, Available online 27 March 2002.
- [22] Yinton T. Yan, *The Use of Lie Algebra Methods to Analyze and Design Accelerator Beamlines*, Tech. rep., USPAS (2001).

- [23] R. Tomas, *Direct Measurement of Resonance Driving Terms in the Super Proton Synchrotron (SPS) of Cern using Beam Position Monitors*, Ph.D. thesis, Universitat de Valencia. Dep. Física Atòmica Molecular i Nuclear., Geneva (2003).
- [24] CERN press office, *CERN experiments observe particle consistent with long-sought Higgs boson*, in *press.web.cern.ch* (04 Jul 2012), consulted inclusive on April 2016, <http://press.web.cern.ch/press-releases/2012/07/cern-experiments-observe-particle-consistent-long-sought-higgs-boson>.
- [25] ATLAS Collaboration and CMS Collaboration, *Combined Measurement of the Higgs Boson Mass in pp Collisions at $\sqrt{s} = 7$ and 8 TeV with the ATLAS and CMS Experiments*, Physical Review Letters **114**(191803) (2015).
- [26] EDMS, *Naming and Conventions. (LHC webpage)*, Tech. rep., CERN (2011).
- [27] Velev, G.V. and Bossert, R. and Carcagno, R. and DiMarco, J. and Feher, S. and Kashikhin, V.V. and Kerby, J. and Lamm, M. and Orris, D. and Schlabach, P. and Strait, J. and Sylvester, C. and Tartaglia, M. and Tompkins, J.C. and Zlobin, A.V., *Magnetic Field Measurements of LHC Inner Triplet Quadrupoles Fabricated at Fermilab*, IEEE Transactions on Applied Superconductivity **17**, 1109 (June 2007).
- [28] V. Ptitsyn and J. Cardona and F. Pilat and J.-P. Koutchouk, *Measurement and Correction of Linear Effects in the RHIC Interaction Regions*, in *Proceedings of the 2001 Particle Accelerator Conference, Chicago, Illinois U.S.A., 2001*, edited by P. Lucas, S. Webber (2001), (IEEE), pp. 3132–3134.
- [29] J. Cardona and S. Peggs and T. Satogata and F. Pilat and V. Ptitsyn, *Determination of Linear and Non Linear Components in RHIC Interaction Regions from Difference Orbit Measurements*, in *Proceedings of EPAC 2002, Paris, France, 2002*, edited by T. Garvey and P. Le Roux and C. Petit-Jean-Genaz and J. Poole (LAL and CERN 2002), (EPS-IGA and CERN), pp. 311–313.
- [30] Javier Cardona and Steve Peggs and Todd Satogata and Rogelio Tomas, *Action and Phase Analysis to Determine Sextupole Errors in RHIC and the SPS*, in *Proceedings of the 2003 Particle Accelerator Conference, Portland, Oregon U.S.A., 2003*, edited by J. Chew and P. Lucas and S. Webber (2003), (IEEE), pp. 2901–2903.
- [31] J. Cardona and R. Tomas Garcia, *Non Linear Error Analysis from Orbit Measurements in SPS and RHIC*, in *Proceedings of 2005 Particle Accelerator Conference, Knoxville, Tennessee, 2005*, edited by C. Horak (ORNL and SNS, 2005), (IEEE), pp. 2012–2014.
- [32] J. Cardona, *Local Magnetic Error Estimation Using Action and Phase Jump Analysis of Orbit Data*, in *Proceedings of PAC07, Albuquerque, New Mexico, USA, 2007*, edited

- by C. Petit-Jean-Genaz (CERN, August 2007), (IEEE), Beam Dynamics and Electromagnetic Fields, pp. 3244–3246.
- [33] Javier Cardona, *Action and Phase Jump Analysis on Orbit Data* (LAP LAMBERT Academic Publishing, 2010).
- [34] Javier Fernando Cardona, *Optics Measurements, Corrections and Modeling for High-Performance Storage Rings*, Action-Phase analysis (Unpublished. Talk in CERN Workshop. June 2011), <https://indico.cern.ch/event/132526>.
- [35] A.C. García B. , J.F. Cardona., *Filtro Digital para Reducir Ruido en la Medición de un Error Magnético en el Acelerador LHC.*, (Unpublished, available in <https://posterscarolinag.files.wordpress.com/2016/04/posterb1.pdf>), Armenia, Colombia (2013), abstract in *Libro de Resúmenes. XXV Congreso Nacional de Física.* (Ministerio de Cultura. Colombia. 2013) pp. 149.
- [36] R.W. Hamming, *Digital Filters* (Prentice-Hall, 1977).
- [37] M. Aiba and S. Fartoukh and A. Franchi and M. Giovannozzi and V. Kain and M. Lamont and R. Tomás and G. Vanbavinckhovea and J. Wenninger and F. Zimmermann and R. Calaga and A. Morita, *First β -beating Measurement and Optics Analysis for the CERN Large Hadron Collider*, Phys. Rev. ST Accel. Beams **12**(081002) (2009).
- [38] R. Tomás, *Normal Form of Particle Motion under the Influence of an AC-Dipole*, Phys. Rev. ST Accel. Beams **5**(054001), 054001 (May 2002).
- [39] R. Miyamoto and S.E. Kopp and A. Jansson and M.J. Syphers, *Parametrization of the Driven Betatron Oscillation*, Phys. Rev. ST Accel. Beams **11**(084002), 084002 (2008).
- [40] E. Forest and F. Schimdt and E. McIntosh, *Introduction to the Polymorphic Tracking Code*, Tech. Rep. CERN-SL-2002-044 (AP), CERN (2002).
- [41] A.C. García B. , J.F. Cardona, *Noise Reduction using Filters on Turn-by-Turn LHC Orbits to Obtain Magnetic Errors with The Action and Phase Jump Analysis Method*, in *Proceedings of PAC2013, Pasadena, CA, USA, 2015*, edited by Todd Satogata and Christine Petit-Jean-Genaz and Volker Schaa (Jefferson Lab and CERN and GSI, 2013), (JACoW), 084002, pp. 883–885.
- [42] *The Python Software Foundation*, www.python.org.
- [43] T. Persson , R. Tomas., *Improved Control of the Betatron Coupling in the Large Hadron Collider*, Phys. Rev. ST Accel. Beams **17**(051004), 051004 (May 2014), the 8 values is ratify to be the best SVD clean configuration.

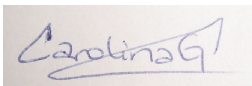
- [44] J.F. Cardona , A.C. García B., *Proyecto: Reformulación del método de acción y fase para obtener errores magnéticos en el LHC, No. 3.396.*, in *Proyectos, Fundación Para la Promoción de la Investigación y la Tecnología (propuesta del 4 de julio de 2013)* (Catálogo Biblioteca Luis Angel Arango.), p. Proyecto: Reformulación del método de acción y fase para obtener errores magnéticos en el LHC, (Unpublished).
- [45] A.C. Garcia B. , J.F. Cardona, *Reformulation of the Action and Phase Method to Obtain Magnetic Errors in the LHC*, in *Proceedings of IPAC2015, Richmond, VA, USA, 2015*, edited by S. Henderson and E. Akers and T. Satogata and V. RW Schaa (ANL and J. Lab and GSI, 2015), (JACoW, 2015), Beam Dynamics and EM Fields, pp. 80–82.
- [46] A.C. García B. , J.F. Cardona, *Comparison between Digital Filters and Singular Value Decomposition to Reduce Noise in LHC Orbits used for Action and Phase Jump Analysis*, in *Proceedings of IPAC2015, Richmond, VA, USA, 2015*, edited by S. Henderson and E. Akers and T. Satogata and V. RW Schaa (ANL and J. Lab and GSI, 2015), (JACoW), Beam Dynamics and EM Fields, pp. 83–85.
- [47] A. Franchi and R. Tomas and F. Schmidt, *Magnet Strength Measurement in Circular Accelerators from Beam Position Monitor Data*, Phys. Rev. ST Accel. Beams **10**(074001), 074001 (2007).
- [48] R. Bartolini and F. Schmidt, *Normal Form via Tracking or Beam Data*, Particle Accelerators **59**, 93 (1998).
- [49] Rogelio Tomás, *Optimizing the global coupling knobs for the LHC*, Tech. Rep. ATSNote-2012-019 MD, CERN (2014).
- [50] Glenn Vanbavinckhove, *Optics Measurements and Corrections for Colliders and Other Storage Rings*, Ph.D. thesis, Universiteit van Amsterdam (2012).
- [51] Thomas Bach and Rogelio Tomás, *Improvements for Optics Measurement and Corrections Software*, Tech. Rep. ACC-NOTE-2013-0010, CERN (2013).
- [52] A. Franchi and R. Tomás and G. Vanbavinckhove, *Computation of the Coupling Resonance Driving term f_{1001} and Coupling Coefficient C from Turn-by-Turn single-BPM Data*, CERN - Internal Note- AB Department (2008).
- [53] A.C. García B. , J.F. Cardona, *Estimación de errores magnéticos a partir del análisis espectral de las órbitas de las partículas en aceleradores de altas energías*, RCF, Revista Colombiana de Física **46**(1), 21 (2014).
- [54] R. Tomás and M. Bai and R. Calaga and W. Fischer and A. Franchi and G. Rumolo, *Measurement of Global and Local Resonance Terms*, Phys. Rev. ST Accel. Beams **8**(024001), 024001 (Feb 2005).

-
- [55] BEABP, OMC, <https://twiki.cern.ch/twiki/bin/view/BEABP/SourceCode>, Tech. rep., CERN (Consulted inclusive on November 17th, 2015).
- [56] J. F. Cardona, (personal communication) (Dec 2014).
- [57] Piotr Skowronski and Ewen Maclean and Andy Langner and Lukas Malina, *OMC Team Meeting*, (Unpublished.), <https://indico.cern.ch/event/392537/>, <https://indico.cern.ch/event/394801/> (May 2015).

Declaración

Me permito afirmar que he realizado la presente tesis de manera autónoma y con la única ayuda de los medios permitidos y no diferentes a los mencionados en la propia tesis. Todos los pasajes que se han tomado de manera textual o figurativa de textos publicados y no publicados, los he reconocido en el presente trabajo. Ninguna parte del presente trabajo se ha empleado en ningún otro tipo de tesis.

Bogotá, D.C., 01.11.2015

A rectangular box containing a handwritten signature in blue ink. The signature appears to be 'Carolina G.' with a stylized flourish at the end.

A.C. García B.